UNIVERSITY OF BELGRADE

FACULTY OF MECHANICAL ENGINEERING

Abdasalam M. Eramah

FRICTION STIR WELDING PARAMETERS INFLUENCING THE FRACTURE RESISTANCE OF AN AL 5083 ALLOY WELDED JOINT

Doctoral Dissertation

Belgrade, 2013

UNIVERZITET U BEOGRADU
MAŠINSKI FAKULTET

Abdasalam M. Eramah

UTICAJ PARAMETARA FRIKCIONOG ZAVARIVANJA MEŠANJEM NA OTPORNOST NA LOM ZAVARENOG SPOJA LEGURE AL 5083

Doktorska Disertacija

Beograd, 2013

DEDICATION

To my Parents, Wife, Teachers and Staff of Faculty of Mechanical Engineering

MENTOR:

Dr Aleksandar Sedmak, full professor
University of Belgrade, Faculty of Mechanical Engineering

MEMBERS OF COMMISSION:

Dr Zoran Radaković, associate professor
University of Belgrade, Faculty of Mechanical Engineering

Dr Marko Rakin, associate professor
University of Belgrade, Faculty of Technology and Metallurgy

Dr Aleksandar Saljnikov, associate professor
University of Belgrade, Faculty of Mechanical Engineering

Dr Srđan Tadić, Research Associate,
University of Belgrade, Faculty of Mechanical Engineering, Innovation Center

Date of defense:

ACKNOWLEDGEMENTS

I wish to express his gratitude to Prof**. Dr. Aleksandar Sedmak** for his kind support, encouragement and valuable guidance throughout the research, showing the trust and giving me an opportunity to present my work at various meetings, which assisted me to envisage my good ad motivated me, also wish to express his gratitude to Dr**. Srdjan Tadic** for his meticulous suggestion during the discussions at various meeting and encouragement throughout the research and endless support. I would also like to thanks to **Dr. Aleksandar Zivkovic**, **GOSA FOM** for donations of time to prepared material alloys and welded alloys by friction stir welding, also thanks is given to **Technical Military Institute, Zarkovo** for experimental charpy impact test. Sincere personal thanks go to **Prof. Dr. Katarina Gevic**, University of Novi Sad for help to get SEM analysis that used in investigated surface fracture.

And

Dedicated to my family for their encouragement……..

My wife her endless a love and support……

It would have been just impossible, without you

ABSTRACT

Friction stir welded is relatively new- solid-states joining process for welded several material such as aluminum, copper, titanium and magnesium. Also FSW technique is preformed in solid state without melting hence avoiding hot cracking. In this research selected aluminum 5083 alloy, it is widely used in applications in which the combination of strength and low weight is attractive. In friction stir welding (FSW) pin connected to a shoulder in rotated and slowly plunged into the joint line between two pieces of plats. When the shoulder tools rotation and contact the material surface, it generated friction heating between the welding tool and the material of the work pieces. This heat causes the latter soften without reaching the melting point and allows traversing of tool along the welding. Friction stir welding presents several benefit for joining of various alloys, specially of aluminum alloy one of the significant advantage of FSW is the heat inputs are small relative to fusion welding techniques and due to the low temperature of the process, material such as Al, Cu, Mg alloys that cannot be welded by fusion processes are easily weld by FSW. On the other hand, FSW has some drawback is often slower traverse rate then some fusion welding and exit hole left when tool is withdrawn.

Friction stir welding process generates three distinct microstructural zones that result from the welding process as following: nugget zone also known as the dynamically recrystallized zone (DRZ) where the tool piece pin passes into this zone and by experience, it has high deformation and high heat, generally consists of fine equated grains due to recrystallisation, the thermo mechanically affected zone (TMAZ) and the heat affected zone (HAZ), all zones together are called welding zone. After welded aluminum alloy tested specimens alloy by charpy impact test to evaluate absorbed energy caused the fracture material and toughness of material. Also obtained high resolution images by macro-photographs and by scanning electron microscope (SEM) to evaluate type of surface fracture and detected fracture and micro void in material then analysis material by energy dispersive x-ray spectroscopy (EDX) to shown distribution elements of chemical compound in aluminum alloy after heating and cooling precipitation. Finally, selection the optimized FSW parameters for welded aluminum 5083 alloy, it achieved higher fracture resistance in welded zone of alloy.

Keywords: Friction stir welding, aluminum 5083 alloy, charpy impact test, microstructural fracture analysis, absorbed energy, fracture resistance, ductile fracture.

Scientific field:

Material Science Engineering

Sub scientific field:

Structural Integrity of Welded Joints

UDK 621.791.052:620.179.2:[669.71(043.3)]

Абстракт

Фрикционо заваривање мешањем представља релативно нов, савремен поступак заваривања великог броја материјала, као што су легуре алуминијума, бакра, титанијума, магнезијума итд. Јединствена особина овог поступка је да се одвија у чврстом стању, без појаве топљења. У овој дисертацији, испитивана је Al-Mg легура 5083, коју одликује добра комбинација чврстоће, жилавости и отпорности на корозију. Током фрикционог заваривања мешањем, специјално дизајниран алат, који се ротира, продире у материјал, управо у линији спајања две плоче које се заварују. На контактној површини ослобађа се топлота која омекшава материјал, олакшава кретање алата уз истовремено мешање материјала. Овако заврени спојеви имају читав низ предности у односу на класично заварене спојеве – укупна потрошња енергије далеко је мања, нема појаве течних фаза, чврстоћа споја често буде већа него код основног материјала и, коначно, нема штетних утицаја на природну околину. Постоје, наравно, и недостаци ове технологије, пре свега повезани са дужином заварених спојева која зависи од димензија машине на којој се поступак изводи.

Током овог поступка заваривања, у зони заварених спојева јављају се јасно дефинисане зоне утицаја топлоте, као и код поступка класичног заваривања. Међутим, код фрикционог заваривања мешањем, појављује се и зона термо-механичког утицаја под симултаног дејства топлоте и пластичне деформације материјала. У овој дисертацији, испитиван је утицај процесних параметара фрикционог заваривања на чврстоћу заварених спојева. Испитиван је утицај (i) ротационе брзине заваривања (у опсегу 500 до 800 обртаја у минути), (ii) утицај транслационе брзине (75-150 mm/min) и, (iii) утицај нападног угла алата (1^o-4^o). Сви заварени спојеви испитивани су на отпорност према ударној жилавости. Нумеричком обрадом експерименталних резултата, одређена је ударна жилавост заварених спојева као и брзина и енергија лома. Поред механичких испитивања, извршена су опсежна микроструктурна испитивања применом оптичког и скенинг електронског микроскопа (SEM). Ова испитивања омогућила су бољи увид у механизам и кинетику дуктилног лома заварених спојева. Коначно, на основу

анализе механичких и микроструктурних испитивања, одређени су оптимални параметри фрикционог заваривања испитиване легуре.

Кључне речи: фрикционо заваривање мешањем, легура алуминијума 5083, ударна жилавост, микроструктурна анализа лома, енергија лома, дуктилни лом.

Научна област: Инжењерство материјала

Ужа научна област: Интегритет заварених спојева

УДК 621.791.052:620.179.2 : [669.71 (043.3)]

TABLE OF CONTENTS

Chapter 3: Experimental Work

Chapter 4: Results

Chapter 5: Discussion

LIST OF FIGURES

LIST OF TABLES

NOMENCLATURE

Item	*Description*
A_S	Shoulder Contact Area (m^2)
AAxxx	Aluminium Association Alloy Designation
AS	Advancing Side
DRX	Dynamic Recrystallisation; Dynamically Recrystallised
ε	Strain
E_1 , E_2	Energy (J)
EDX	Energy-Dispersive X-ray Spectroscopy
f	Feed (Traverse) Speed (mm/min)
Fe	Iron Element
F_N , F_P	Normal and Traverse Force (N)
F_V	Particles Volume Fraction
FSW	Friction Stir Welding; Weld
G	Shear Modulus
H	Sheet Thickness (m)
H_P	Pin Height (m)
HAZ	Heat Affected Zone
K	Potassium Element
KHN	Knoop Hardness Number
k	Thermal Conductivity (W/m.°C)
k_y	Hall-Petch Slope/Constant (MPa $\mu m^{1/2}$)
Mg	Magnesium Element
Mn	Manganese Element
MIG	Metal Inert Gas
ms	Millisecond
O	Oxygen Element
P	Normal Pressure (Pa)
Q	Heat Generation (W)
Q	Heat Flux (W/m^2)
q_v	Volumetric Heat Source (W/m^3)
R_S, R_P	Tool Shoulder and Pin Radii (m)
RS	Retreating Side
R^*	Ratio between Shoulder and Pin Diameter

Item	*Description*
σ	Stress (Pa)
Y	Yield Stress (Pa)
SEM	Scanning Electron Microscope
Si	Silicon Element
STZ	Stirred Zone
τ	Shear Stress (Pa)
μ	Friction Coefficient
t	Temperature (°C)
T_m	Melting Temperature (^{0}C)
T	Torque (N.m)
TWI	Techanical Welding Institute
TIG	Tungsten Inert Gas
TMAZ	Thermo-mechanically Affected Zone
VHN	Vicker's Hardness Number
ω	Rotation Speed (rad/s), (rpm)
v	Welding Speed (mm/min)
Θ,α	Angles
WN	Weld Nugget
W_f	Final Lateral Dimension
W_i	Initial Lateral Dimension
ΔW	Lateral Expansion
x, y, z	Space Coordinates (m)

CHAPTER 1 : INTRODUCTION

1.1 Friction Stir Welding (FSW):

Friction stir welding (FSW) is a relatively new solid- states joining process that was invented in 1991 at the Welding Institute (TWI) in the united kingdom (Thomos, 1994) and is very energy efficient environment friendly, and versatile, being considered to be the most significant development in metal joining in a decade. Since its invention, a large amount of research was carried out in several fields and different materials. Aluminum alloys are the material more often studied and where this technology has shown a better performance.[1]

FSW is a technique which to able aluminum, lead, magnesium, titanium, steel and copper to be welded. FSW can used to join aluminum sheets and plates without filler wire or shielding gas, material thickness from 0.8 to 65 mm can be welded from one side at full penetration and without porosity or internal voids, material that have been successfully friction stir welded to data include all aluminum alloys, copper, magnesium, lead and zinc.[10] Despite the practical application of the FSW technique has been successful, there is still a lack of design data and understanding of the failure mechanisms.[2]

Friction stir welding is a method for joining of metals; it is a technique, which allows aluminum, load, magnesium, titanium, steel and copper to weld continuously with a non-consumable tool. In friction stir welding a pin connected to a shoulder is rotated and slowly plunged into the joint line between two pieces of sheet or plate material, which are butted together (Fig.1-1). The parts of be jointed have to be firmly clamped in a manner to prevent the abutting joint faces from being forced a part.

Frictional heat is generated between the wear resistant welding tool (Fig. 1-2) and the material of the work pieces. This heat causes the latter to soften without reaching the melting point and allows traversing of the tool along the weld line. The plastically deformed material is transferred from the leading edge of the tool to the trailing edge of the tool probe and is forged by the intimate contact of the tool shoulder and the pin profile. It leaves a solid phase bond between the two pieces.[3]

Friction stir welding presents several benefits for joining of various alloys, especially of aluminum alloys. One of the significant advantages of FSW is that the process is entirely solid state. The heat inputs are small relative to fusion welding techniques such as metal inert gas(MIG), tungsten inert gas (TIG), laser beam and resistance welding. Joining is done at low temperature that eliminates the major problem of conventional welding

processes, which must be performed under inter gas to prevent the dissolution of atmospheric gases in the melted material of the joint. The elimination of cracking in the weld fusion and heat affected zones (HAZ), weld porosity, filler material and costly weld preparation are further important advantages of friction stir welding. Due to the low temperature of the process, materials such as Al- Cu- Mg alloys that con not be welded by fusion processes are easily weld by FSW.[3]

On the other hand, FSW has some drawback is often slower traverse rate than some fusion welding and exit hole left when tool is withdrawn, FSW imposes exacting requirements on the construction of welding machines, clamping of jointed parts and design of tools.

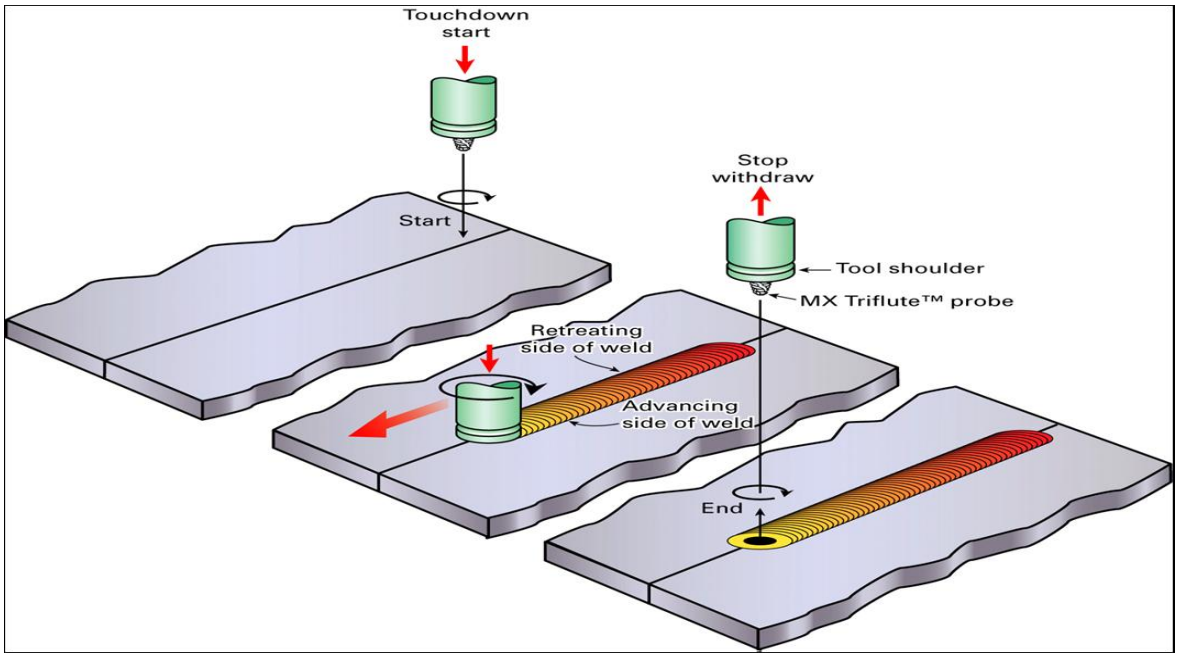

Figure 1-1. Explanation of the Friction Stir Welding Process.[4]

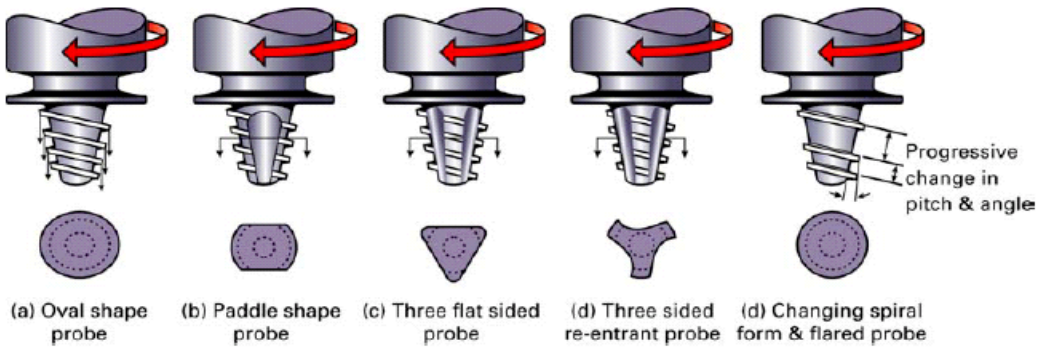

Figure 1-2. Tools of Various Geometry Used in FSW.(c) TWI[4]

Friction stir welding (FSW) a technique is performed in solid state without melting hence avoiding hot cracking. Fig.1-3 shows FSW process where weld joint is obtained by inserting a rotating pin into the adjoining edges of the plates to be welded.

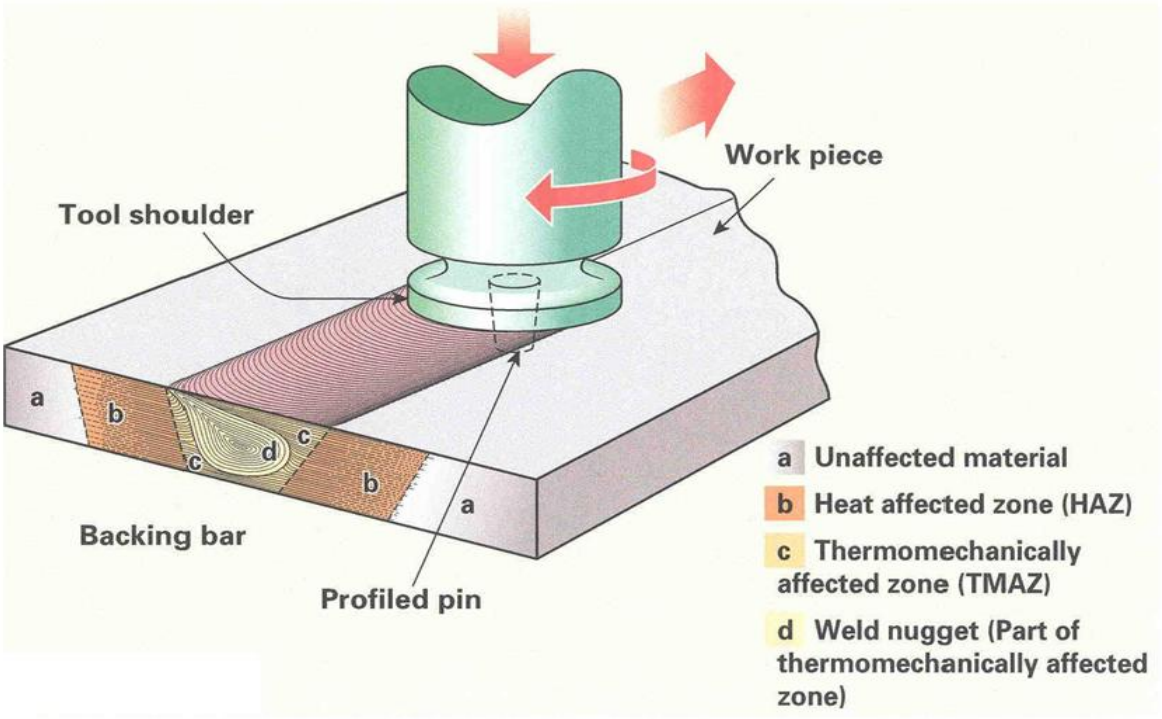

Figure1-3. Micro-structural feature of FSW.[13]

Friction stir welding (FSW) process generates three distinct microstructureal zones that result from the welding process, shown in Figure (1-3) (Mishra and Mahoney, 2007).

A – The nugget zone, also known as the dynamically recrystallized zone,

B – The thermo- mechanically affected zone (TMAZ),

C – The heat affected zone (HAZ).

D – The nugget zone is the region through which the tool piece pin passes, and thus experience high deformation and high heat. It generally consists of fine equated grains due to full recrystallisation.

1.2 Aluminum alloys:

Aluminum is the third most abundant element in the earth's crust, comprising over 8% of its weight. Yet, until about 150 years ago aluminum in its metallic from was unknown to man. The reason, aluminum unlike iron or copper does not exist as a metal in nature. Because of its chemical activity and its affinity for oxygen, aluminum is always found combined with other elements, mainly as aluminum oxide, as such it is found in nearly all clays and many minerals. Aluminum is widely used in applications of it is light in weight, yet some of its alloys have high strength comparable to mild steel. Also it has high resistance to corrosion and is not toxic, aluminum has good conductivity, good ductility at sub zero temperature, it is non sparking and non magnetic. While commercially pure aluminum (defined as at least 99% aluminum) close find application in electrical conductors, chemical equipment, and sheet metal work, it is a relatively weak material, and its use is restricted to applications where strength is not important factor.[8]

However, much greater strengthening is obtained through alloying with other metals, and the alloys themselves can be further strengthened through strain hardening or heat treating other properties, such as castability and machinability, are also improved by alloying. Thus aluminum alloys are much more widely used than is the pure metal the principal alloying additions to aluminum are copper, manganese, silicon, magnesium, and zinc, other element are also added in smaller amounts for metallurgical purposes. Therefore, aluminum alloys are used in many applications in which the combination of high strength and low weight is attractive. The main alloying element in the 5xxx series is magnesium. A magnesium content of around 5% provides good strength and high corrosion resistance in salt water. In fact, the first aluminum boat was built in 1891 and the first welded aluminum ship in 1953 [9].

Furthermore, pure aluminum melts at 660 ^{0}C. Aluminum alloys have an approximate melting range from 482 ^{0}C to 660 ^{0}C, depending upon alloy. There is no colour change in aluminum when heated to the welding or brazing range.[1]

Aluminum 5083 alloy was selected to study in this research, its alloy that is commonly used in the manufacturing of pressure vessels, marine, vessels armoured vehicles, aircraft

cryogenics, drilling rigs, miming, structures and even in missile components etc. this alloy is considered as a one of the beast weldable aluminum alloys and exhibits a slight reduction of the strength of the heat affected zone (HAZ) comparatively to the most of other aluminum alloys. In the tempered condition, it is strong, and retains good formability due to excellent ductility. [5]

This study presents the results of an experimental setup in which the aluminum 5083 alloy was FS Welded, by using various combinations of process parameters (rotational, travel speed and tilt angle). Also measured the mechanical properties of the weld joint were assessed by absorbed energy in charpy impact test, and describe the fracture mechanism of aluminum 5083 alloy by scanning electron microscope.

1.3 The Aims of Study:

The first aim of this research is to create quality friction stir welds of aluminum 5083 alloy by various welding speed and rotational speed. The second aim is to tested mechanical properties of aluminum alloys by charpy test that objective is to evaluate absorbed energy that caused fracture material alloy, also using Scanning Electron Microscope (SEM) to describe the microstructure of surface fracture. Finally, focus the optimized welding parameters in order to establish the excellent weld parameters for welded AA5xxx regarding to results of study.

To achieve these aims set out above a series of objective must be met. Used different FSW parameters in order to establish the best possible welding conditions for the aluminum 5083 alloy; this requires mechanical property testing at room temperature and comparisons drawn against the parent materials and previous studies from the literature review. The next objective is to evaluate the fracture surface microstructure, using scanning electron microscope (SEM) to describe the fracture mechanism; once again these findings are compared with materials covered in the literature review in order to continuously improve the weld properties and to create the optimized welds for aluminum 5083 alloy.

1.4 Chapter Abstracts:

Chapter 2 Literature Review: describe friction stir welding process and details the friction stir welding tool and its fundamental role in producing the join. Some different aspects of tool and it design are described, material flow, process requirements are explained, this includes details of the microstructure around the FSW tool, involved details of weld affected zone, also explain the advantages and drawbacks of the FSW process. Furthermore, describe the heat generation during friction stir welding [5]

Also describe the aluminum 5083 alloy that is overview some information about the order and when the human know the aluminum in the earth. Firstly, that is important explain the designation systems of classification aluminum alloys, also describe temper designation system and explain chemical analysis , mechanical properties of aluminum alloy that will be used for friction stir welding.

Chapter 3 describes the experimental study involved preparation material specimens for welding joint and lists the various experimental setups used to create the welds and subsequently test mechanical properties as charpy test, also using scanning electron microscope to investigate the fracture mechanism.

Chapter 4 provides the results of all the mechanical properties coupled with the microstructural observations in order to present a clear understanding of mechanisms fracture at work during forming of friction stir welded materials.[5]

Chapter 5 provides the discussion results of mechanical properties and microstructural observations of surface fracture.

Conclusion contains all the conclusions drawn from this research including the observations mode from the mechanical testing, microstructural investigations.[5]

CHAPTER 2: LITERATURE REVIEW

2.1 Friction Stir Welding (FSW):

In FSW a cylindrical tool (consisting of shoulder with a profiled threaded/unthreaded probe (nip or pin) assembly) is rotated with high rotation constant speed and plunged at a constant traverse rate into the joint line between the two pieces of sheet or plate material to be welded together. The parts have to be clamped rigidly on to a backing bar in a manner that prevents the abutting joint faces from being forced apart. The pin is slightly less than the weld depth required and the tool shoulder should be in intimate contact with the surface, shown Fig (2-1).

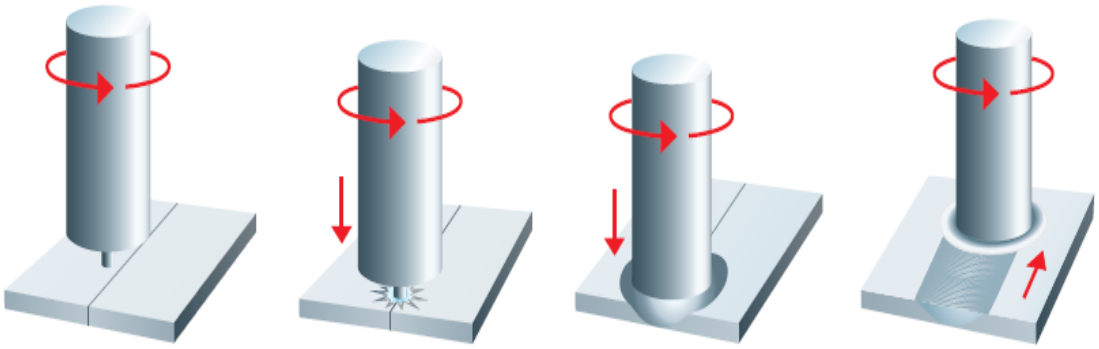

Figure 2-1. Friction stir welding operation.[11]

The frictional heat generated by the welding tool makes the surrounding material softer and allows the tool to move along the joint line. The softened material starts to flow around probe; it is allowing the traversing of the tool along the weld line in a plasticized tubular shaft of metal. It's the pin is moved in the direction of welding the leading face of the pin, assisted by a special pin profile, forces plasticized material to the back of the pin whilst applying a substantial forging force to consolidate the weld metal. This easily stirring action by the rotating tool yields a heavily deformed region in the material.

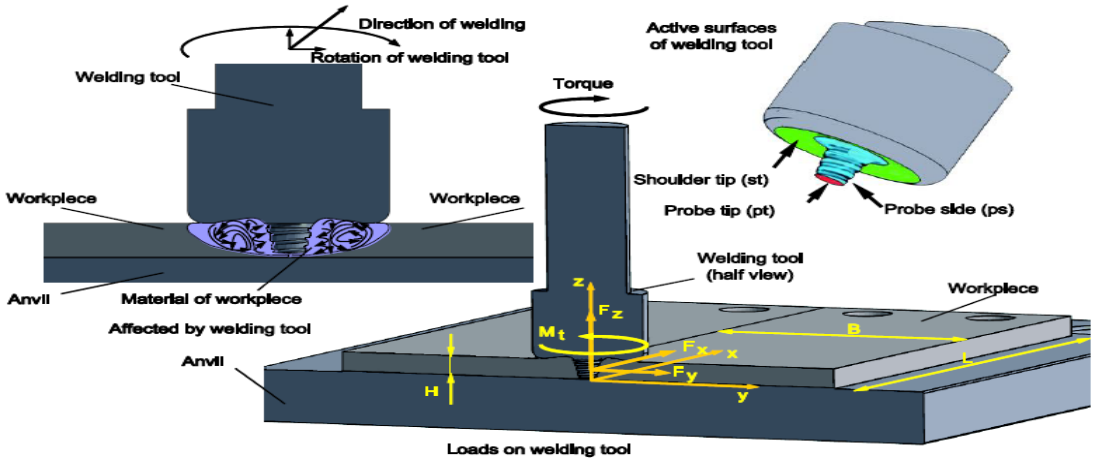

Figure 2-2. Friction Stir Welding: Principle of Operation [14]

2.1.1 Heat Generations during FSW of Al 5083:

Heat generation process at FSW was investigated at the beginning of 2002 for the first time. This happened 11 years after the invention of FSW. Heat generation is a complex process of transformation of a specific type of energy into heat. During friction stir welding, one part of mechanical energy delivered to the welding tool is consumed in the welding process, another is used for deformational processes etc. and rest of the energy is transformed into heat. The analytical procedure for the estimation of heat generated during FSW is very complex because it includes a significant number of variables and parameters. The heat generation in FSW can be divided in to two parts: frictional heat generated by the tool and heat generated by material deformation near the pin and the tool shoulder region.[14]

Furthermore, by referred to frictional heat, it is difficult to estimate the temperature inside the weld affected zone during the welding, but it can be estimated probably maximum temperature that will be generated during friction stir welded by using Equation (2-1).

By an Equation (2-1) can be represented frictional heat generated for maximum temperature during FSW that indicated the effects of rotational and welding speeds on the welding temperature.

$$\frac{T}{T_m} = k\left(\frac{\omega^2}{v\times 10^4}\right)^{\alpha} \quad (2\text{-}1)$$

Where:

T is the FSW temperature (C^0),

T_m is the melting temperature of the sheet material (C^0),

α is reported to range from 0.04 to 0.06,

k is constant, it is between 0.65 to 0.75,

ω is the tool rotational,

v is the welding speed

Referred to Eq. (2-1), the FSW process temperature is related to the ω^2/v ratio. It means that increasing the rotational speed at constant welding speed leads to a higher welding temperature. It also indicates that the variations of tool rotational speed have higher effects on the process temperature than the welding speed variations.[6] Table (2-1) shown the results of approximate of maximum temperature during FSW by using variable parameters for applied on each specimens.

As results, Figure (2-3) shows the relationship between the rotational speed and maximum temperature. It seems when increase the rotation speed the temperature will be increased. Also when the traversing speed is increase the maximum temperature will be decreased as shown in Figure (2-4).

Table 2-1. Calculations of Maximum Temperature during FSW.

No. of samples	Thickness (mm)	Length x width (mm)	Rotation speed (rpm)	Welding speed mm/min	ω/v (rev/mm)	Title (dgree)	Max. temp. during FSW (C^0)
1.1	6.2	130 x 90	500	75	6.67	1^0	392
1.2	6.2	130 x 90	600	75	8	1^0	399
1.3	6.2	130 x 90	700	75	9.33	1^0	405
1.4	6.2	130 x 90	800	75	10.67	1^0	410
1.5	6.2	130 x 90	500	100	5	2^0	386
1.6	6.2	130 x 90	600	100	6	2^0	393
1.7	6.2	130 x 90	700	100	7	2^0	399
1.8	6.2	130 x 90	800	100	8	2^0	405
1.9	5.8	130 x 90	500	125	4	3^0	382
1.10	5.8	130 x 90	600	125	4.8	3^0	389
1.11	5.8	130 x 90	700	125	5.6	3^0	395
1.12	5.8	130 x 90	800	125	6.4	3^0	400
1.13	5.5	130 x 90	600	150	4	4^0	385
1.14	5.5	130 x 90	700	150	4.67	4^0	391
1.15	5.5	110 x 90	500	150	3.3	4^0	378

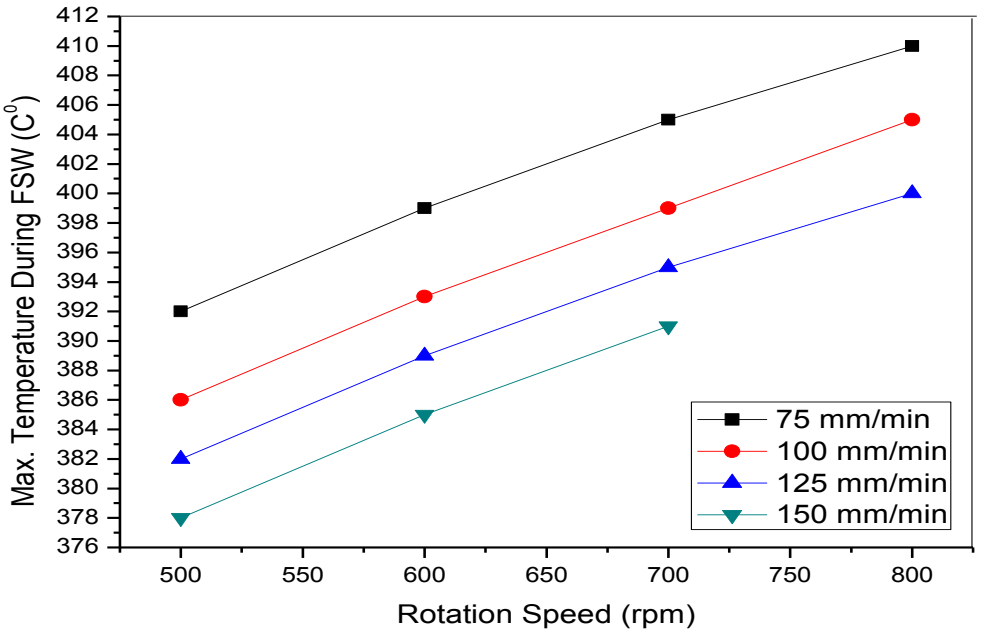

Figure 2-3. Explain relationship between the rotation speed and max. temperature

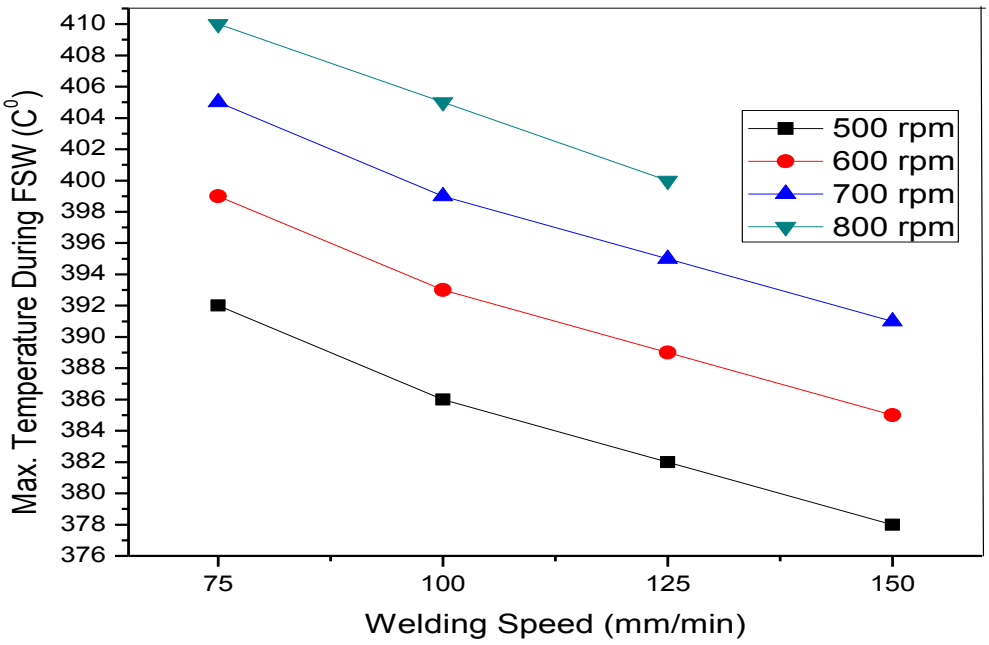

Figure 2-4. Explain relationship between the welding speed and max. temperature.

Generally, temperature measurements during FSW of aluminum alloys have shown that the process is a solid-state welding process, with a T_{max} between 400 and 550 °C for pure aluminum alloy. T_{max} is observed under the shoulder, where the maximum heat flux exists. The temperature increases with an increase in the rotation speed, a decrease in the welding speed, or precisely the pseudo-heat index, and an increase in the plunge depth. Based on the thermocouple measurements, it can be concluded that the temperatures generated do not appear to be strongly influenced by the alloy type in most cases, except when the incipient melting temperature is exceeded, which is in any case undesirable for weld integrity. The difficulty in obtaining reliable thermocouple measurements within the weld emphasizes, it needs for computer models that can predict the temperatures in the weld.[15]

2.1.2 Analytical Estimation of Heat Generation during FSW:

Three different analytical estimations are suggested, all of which are based on a general assumption of uniform contact shear stress $\tau_{contact}$ and further distinguished by assuming a specific contact condition. In the first estimation, a sticking interface condition (δ = 1) is assumed and in the second estimation a pure sliding (δ = 0) interface described by a Coulomb friction condition is assumed. In the case of the sticking condition, the shearing is assumed to occur in a layer very close to the interface and in the sliding condition the shear is assumed to take place at the contact interface. These two types of estimation are distinguished by the assumptions under which the shear stress $\tau_{contact}$ is introduced. The third estimation is used in the case where the partial sliding/sticking condition is assumed.

During the FSW process, heat is generated at or close to the contact surfaces, which have complex geometries according to the tool geometry (seen in Figure 2-5), but for the analytical estimation, a simplified tool design with a conical or horizontal shoulder surface, a vertical cylindrical probe side surface or a horizontal (flat) probe tip surface is assumed. The conical shoulder surface is characterized by the cone angle α, which in the case of a flat shoulder, is zero.

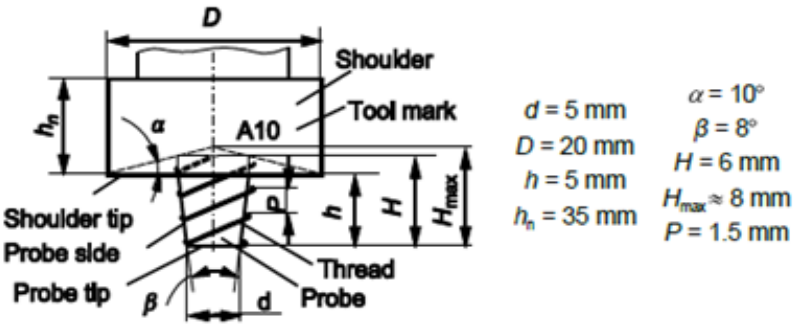

Figure 2-5. Schematic of welding tools [14]

The simplified tool design is presented in figure 2-5, where Q_1 is the heat generated under the tool shoulder, Q_2 at the tool probe side and Q_3 at the tool probe tip, hence the total heat generation, $Q_{total} = Q_1 + Q_2 + Q_3$. To derive the different quantities, the surface

under examination is characterized by either being conical, vertical or horizontal and the surface orientations relative to the rotation axis are decisive for the expressions.

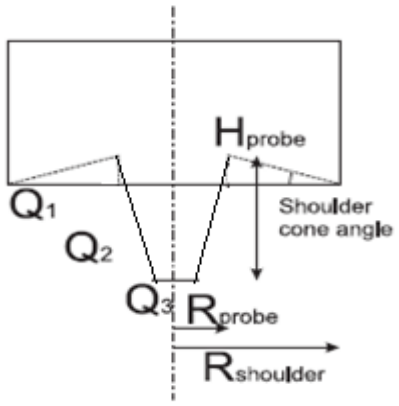

Figure 2-6. Heat generation contributions in analytical estimates. [16]

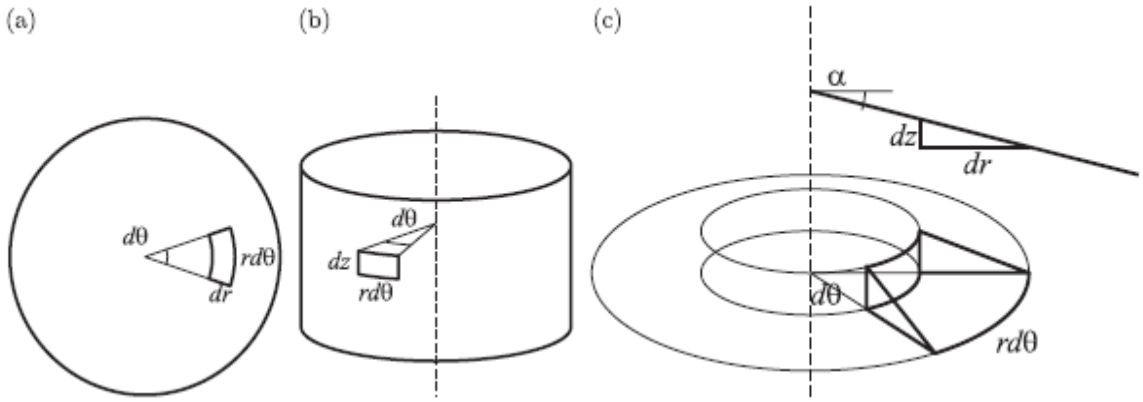

Figure 2-7. Schematic drawing of surface orientations and infinitesimal segment areas. (*a*) Horizontal (seen from above). (*b*) Vertical. (*c*) Conical/tilted. Projection of conical segment area onto horizontal and vertical segments. [16]

The expressions for each surface orientation are different, but are based on the same Equation for heat generation:

$$dQ = \omega\, dM = \omega r dF = \omega r_{\tau contact}\, dA \qquad (2\text{-}2)$$

(a) - Heat Generation, General:

The following derivations are analytical estimations of heat generated at the contact interface between a rotating FSW tool and a stationary weld piece matrix. The mechanical

power due to the traverse movement is not considered, as this quantity is negligible compared to the rotational power.

(i)- Surface orientations. A given surface of the tool in contact with the matrix is characterized by its position and orientation relative to the rotation axis of the tool (Fig. 2-7). If the tool rotation axis is vertical (along the *z*-axis), then a flat shoulder surface would be horizontal or in the θr-plane. A cylindrical surface on the tool would be vertical or in the θz-plane. The following subscripts have been used to characterize the orientation of the surface:

− = Horizontal (perpendicular to the rotation axis, circular surface).

| = Vertical (parallel to the rotation axis, cylindrical surface).

\ = Conical (tilted with respect to rotation axis, conical surface).

Horizontal. In order to calculate the heat generation from a horizontal circular tool surface rotating around the tool centre axis, an infinitesimal segment on that surface is investigated. The infinitesimal segment area $dA- = r\, d\theta\, dr$ is exposed to a uniform contact shear stress $\tau_{contact}$. This segment contributes with an infinitesimal force of $dF- = \tau contact\, dA-$ and torque of $dM- = r\, dF-$. The heat generation from this segment is

$$dQ- = \omega r\, dF- = \omega r 2\tau_{contact}\, d\theta\, dr \qquad (2\text{-}3)$$

where *r* is the distance from the investigated area to the centre of rotation, ω is the angular velocity, and $r\, d\theta$ and dr are the segment dimensions.

Vertical. For a cylindrical surface on the tool, the heat generation from an infinitesimal surface segment with the area of $dA| = d\theta\, dz$ is

$$dQ| = \omega r\, dF| = \omega r 2\tau_{contact}\, d\theta\, dz \qquad (2\text{-}4)$$

where dz is the segment dimension along the rotation axis.

Conical. In the case of a conical surface segment, a similar approach is adopted as in the case of the horizontal and vertical. In fact, the force/torque contribution from the tilted segment is split up into the contribution from a horizontal and a vertical segment, as the tilted segment area is projected onto the main planes relative to the tool rotation axis. The

tilted orientation is characterized by the cone angle α, which is the angle between the horizontal ($r\theta$) plane and the segment orientation in the rz-plane.

$$dF\backslash = dF- + dF| \tag{2-5}$$

The projection of the tilted segment area is given by

$$\begin{aligned} dz &= \tan\alpha\, dr \\ dA| &= r\, d\theta\, dz = r\, d\theta \tan\alpha\, dr \\ dA- &= r\, d\theta\, dr \end{aligned} \tag{2-6}$$

Inserting this into Eq. (2-5) gives

$$dF\backslash = \tau_{contact}\, dA + \tau_{contact}\, dA| = \tau_{contact} r\, d\theta\, dr(1 + \tan\alpha) \tag{2-7}$$

An interpretation of this is that the segment area is enlarged by the fraction of tan α compared to a horizontal segment. The modification of the heat generated at the tilted segment is

$$dQ\backslash = \omega r\, dF\backslash = \omega r 2_{\tau contact}\, d\theta\, dr(1 + \tan\alpha) \tag{2-8}$$

It is possible to characterize a rotation symmetrical FSW tool shoulder and probe surfaces by these three types of surface orientations. The limitation in describing modern FSW tools featuring threads, flutes and facets is recognized.

(ii)- Heat generation from the shoulder. The shoulder surface of a modern FSW tool is in most cases concave or conically shaped. The purpose of this geometric feature is to act as an escape volume as the probe is submerged into the matrix during the plunge operation, secondarily enhancing the extrusion and consolidation of the material during the weld operation. Previous analytical expressions for heat generation include a flat circular shoulder, in some cases omitting the contribution from the probe. This work extends the previous expressions so that conical shoulder and cylindrical probe surfaces are included.

An analytical model for the heat generation, that includes non-uniform pressure distribution or strain rate dependent yield shear stresses, material flow driven by threads or flutes, is not taken into account. Integration of Eq.(2-8) over the shoulder area from R_{probe} to $R_{shoulder}$ gives the shoulder heat generation, Q_1.

$$Q_1 = \int_0^{2\pi} \int_{R_{prode}}^{R_{shoulder}} w\ \tau_{contact} r^2 (1 + tan\ \alpha) dr\ d\theta \qquad (2-9)$$

$$= \frac{2}{3}\pi\ \tau_{contact} w\left(R_{shoulder}^3 - R_{prode}^3\right)(1 + \tan\alpha)$$

(iii)- Heat generation from the probe. The probe is simplified to a cylindrical surface with a radius of R_{probe} and a probe height H_{probe}. The heat generated from the probe consists of two contributions; Q_2 from the side surface and Q_3 from the tip surface. Integrating dQ|, i.e. (2-4), over the probe side area gives

$$Q_2 = \int_0^{2\pi} \int_0^{H_{prode}} w\ \tau_{contact}\ \ R_{probe}^2\ dz\ d\theta$$
$$= 2\pi\tau_{contact}\, w\, R_{probe}^2\, H_{probe} \qquad (2-10)$$

and integrating the heat flux based on Equation (2-3) over the probe tip surface, assuming a flat tip, gives

$$Q_3 = \int_0^{2\pi} \int_0^{R_{prode}} w\ \tau_{contact}\ \ r_{probe}^2\ dr\ d\theta$$
$$= \frac{2}{3}\pi\tau_{contact}\, w\, R_{probe}^3 \qquad (2-11)$$

The three contributions are combined to get the total heat generation estimate Q_{total}

$$Q_{total} = Q_1 + Q_2 + Q_3$$
$$= \frac{2}{3}\pi\ \tau_{contact}\ w\ \left(\left(R_{shoulder}^3 - \ R_{prode}^3\right)(1 + \tan\alpha) + R_{probe}^3 + 3R_{probe}^2\ H_{probe}\right) \ (2-12)$$

In the case of a flat shoulder, the heat generation expression simplifies to

$$Q_{total} = \frac{2}{3}\pi\, \tau_{contact}\, w\left(R_{shoulder}^3 + 3R_{prode}^2 H_{probe}\right) \qquad (2-13)$$

(b) - Contact Shear Stress:

Equation (2-12) is based on the general assumption of a constant contact shear stress as mentioned before, but the mechanisms behind the contact shear stress vary depending on whether the sliding or sticking condition is present.

(i) - Shear stress for sticking condition. If the sticking interfaces condition is assumed, the matrix closest to the tool surface sticks to it. The layer between the stationary material points and the material moving with the tool has to accommodate the velocity difference by shearing. Using the upper limit formulation to calculate the shear stress for this deformation to take place, it follows that the stress is independent of the width of the deformation layer.

This allows the deformation layer, starting at the tool interface and extending further into the weld matrix, to be treated as a shear line/surface. The position of this shear line/surface is very close to the contact interface; therefore, the tool geometry is used to describe it. The yield shear stress τ_{yield} is estimated to be $\sigma_{yield}/\sqrt{3}$, where σ_{yield} is the weld material yield stress. This result is readily obtained by comparing Von Mises yield criterion in uniaxial tension and pure shear. The contact shear stress is then

$$\tau_{contact} = \tau_{yield} = \frac{\sigma_{yield}}{\sqrt{3}} \qquad (2-14)$$

It is well known that the yield stress is independent of pressure, but highly temperature dependent. If the same shear yield stress is applied all over the interface, the assumption of an isothermal interface follows. This gives a modified expression of Eq. (2-12), assuming the sticking condition.

$$Q_{total,sticking} = \pi \frac{\sigma_{yield}}{\sqrt{3}} w \left(\left(R_{shoulder}^3 - R_{prode}^3 \right)(1 + \tan\alpha) + R_{probe}^3 + 3R_{probe}^2 H_{probe} \right) \quad (2-15)$$

(ii)- Shear stress for sliding condition. Assuming friction interface conditions where the tool surface and weld material are sliding against each other, the frictional shear stress $\tau_{friction}$ is introduced in the general Equation (2-12). The choice of Coulomb's friction law to describe the shear stress estimates the critical friction stress necessary for a sliding condition as

$$\tau_{contact} = \tau_{friction} = \mu p = \mu\sigma \quad (2-16)$$

Where μ is the friction coefficient, and p and σ are the contact pressures. Thus, for the sliding condition, the total heat generation is given by

$$Q_{total,sticking} = \frac{2}{3}\pi\mu p w \left(\left(R_{shoulder}^3 - R_{prode}^3 \right)(1 + \tan\alpha) + R_{probe}^3 + 3R_{probe}^2 H_{probe} \right) \quad (2-17)$$

Used Equations 2-15 and 2-17 for calculation heat generation during FSW with different tools pin and shoulder to explain behaviour heat distribution with change that parameters, it shows in Table 2-2 and shows Figure 2-8 .

Table 2-2. Heat generation during FSW by different tools parameters

Tools No.	SD (mm)	PD (mm)	H_{prode} (mm)	μ	α	$Q_{Tatal,sticking}$ (500 rpm)	$Q_{Tatal,sticking}$ (600 rpm)	$Q_{Tatal,sticking}$ (700 rpm)	$Q_{Tatal,sticking}$ (800 rpm)
1	20	5	6	0.41	10^0	667 (W)	785.4 (W)	916.3 (W)	1047.2 (W)
2	26	5.6	5.9	0.41	10^0	753.6 (W)	887.4 (W)	1035.3 (W)	1183.2 (W)
3	13	5	3.19	0.41	10^0	422.9 (W)	498.3 (W)	581.3 (W)	664.3 (W)
4	25.4	5	1.6	0.41	10^0	737.97(W)	868.97(W)	1013.8 (W)	1158 (W)

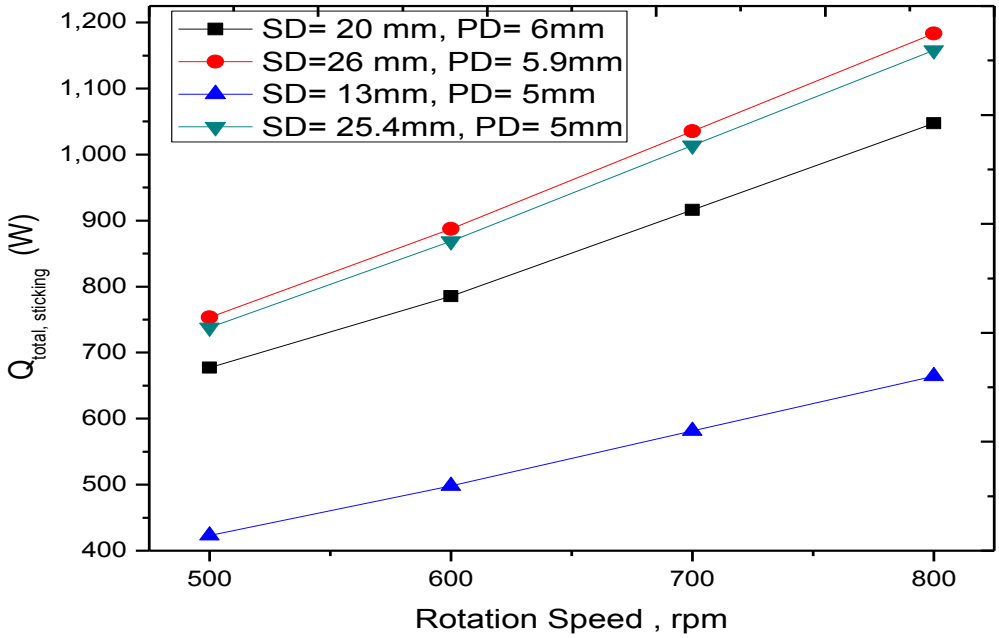

Figure 2-8. Relationship between rotation speed and heat generation

(iii)- Shear stress for partial sliding/sticking condition. The analytical solution of the heat generation for the partial sliding/sticking condition is simply a combination of the two solutions, respectively, with a kind of weighting function. Note that this is only possible because of the assumption of a uniform distribution of the contact state variable δ over the entire contact surface. From the partial sliding/sticking condition follows that the slip rate between the surfaces is a fraction of ωr, lowering the heat generation from sliding friction. This is counterbalanced by the additional plastic dissipation due to material deformation. It is convenient to define the weighting function parameter as identical to the contact condition variable or dimensionless slip rate δ, which is described in this paper. This enables a linear combination of the expressions for sliding and sticking

$$Q_{total} = \delta Q_{total,sticking} + (1-\delta) Q_{total,sliding}$$

$$= \frac{2}{3}\pi \left(\delta \tau_{yield} + (1-\delta)\mu p\right) \times w \left(\left(R_{shoulder}^3 - R_{prode}^3\right)(1+\tan\alpha) + R_{probe}^3 + 3R_{probe}^2 H_{probe}\right) \quad (2-18)$$

where δ is the contact state variable (dimensionless slip rate), τ_{yield} is the material yield shear stress at welding temperature, μ is the friction coefficient, p is the uniform pressure at the contact interface, ω is the angular rotation speed, α is the cone angle, $R_{shoulder}$ is the shoulder radius, R_{probe} is the probe radius and H_{probe} is the probe height. This final expression can estimate the heat generation for $0 \leq \delta \leq 1$, corresponding to sliding when $\delta = 0$, sticking when $\delta = 1$ and partial sliding/sticking when $0 < \delta < 1$.

In a special case where the sliding condition and flat shoulder are assumed, Equation (2-19) is expressed in terms of the plunge force as:

$$Q_{sliding,plunge\ force} = \frac{2}{3}\, w\mu F \left(R_{shoulder} + 3\frac{R_{probe}^2\, H_{probe}}{R_{shoulder}^2} \right) \qquad (2-19)$$

using the relationship that the pressure equals the force divided by the projected area. A similar expression without the last term has been suggested by Frigaard *et al* .

2.1.3 Correlation between Shoulder/Pin and Heat Generation Q_{total}:

During FSW the joining of plates takes place below the melting point of the materials. The maximum temperature reached during the process is 0.8 of the melting temperature of the work pieces. The welds are created by the combined action of frictional heating and mechanical deformation due to a rotating tool. Rotational speed of the tool, tool traverse speed, and vertical pressure on the plates during welding are the main process parameters of FSW (Rajakumar *et al*., 2010). However the tool geometry which involves the geometry of the FSW tool shoulder and tool pin probe profile is also an important characteristic which affects the weld strength. Also involved this research correlation the effectiveness of an FSW joint is strongly affected by several tool parameters; in particular, geometrical parameters such as the height and the shape of the pin and the shoulder surface of the tool have a relevant influence both on the metal flow and on the heat generation due to friction forces.[26]

A dimensionless correlation has been developed based on Buckingham's π-theorem to estimate the peak temperature during friction stir welding (FSW). A relationship is proposed between dimensionless peak temperature and dimensionless shoulder and pin.

Apart from the estimation of peak temperature, it can also be used for the selection of welding conditions to prevent melting of the workpiece during FSW. The correlation includes thermal properties of the material and the tool, the area of the tool shoulder and the rotational speed with neglected welding speeds of the tool.[27]

Furthermore, it can be correlated equations to calculate the maximum heat when used the ratio between diameter of shoulder and pin by used liner equation below during friction stir welding by different rotation speed. (Shown in Figures 3-9, 3-10, 2-9, and 2-12).

$$Q_{Total} = 90.06 + 136.72\ R^{*} \longrightarrow \text{For 500 rpm} \qquad (2-20)$$

$$Q_{Total} = 102.65 + 161.12\ R^{*} \longrightarrow \text{For 600 rpm} \qquad (2-21)$$

$$Q_{Total} = 119.65 + 188.12\ R^{*} \longrightarrow \text{For 700 rpm} \qquad (2-22)$$

$$Q_{Total} = 137.23 + 214.7\ R^{*} \longrightarrow \text{For 800 rpm} \qquad (2-23)$$

Where:

Q_{Total} is heat generation by various rotational speed.

R^{*} is ratio between diameters of shoulder and pin.

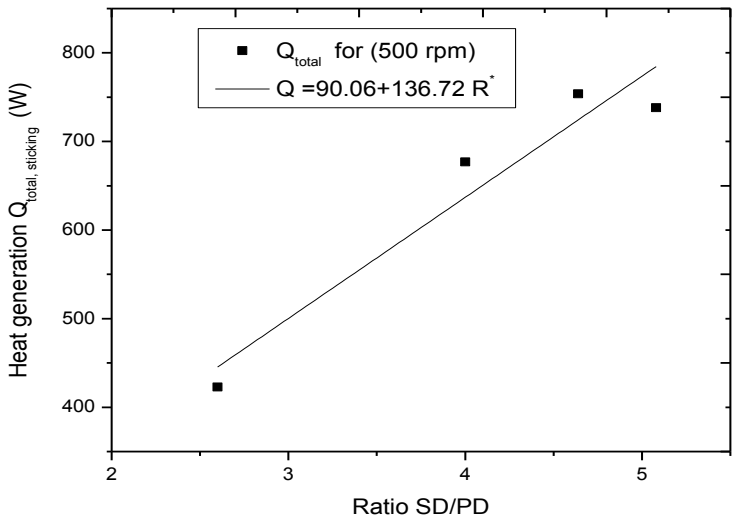

Figure 2-9. Linear relationship between total temperature and dimensionless diameters shoulder and pin for 500 rpm.

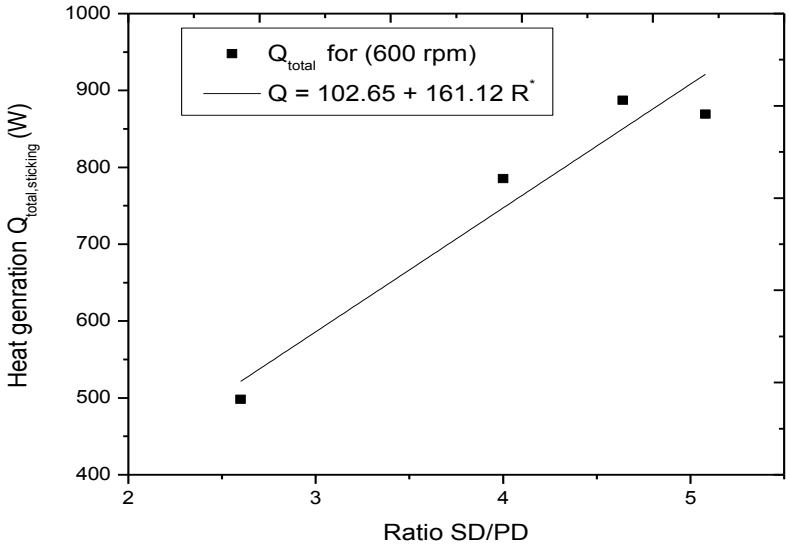

Figure 2-10. Linear relationship between total temperature and dimensionless diameters shoulder and pin for 600 rpm.

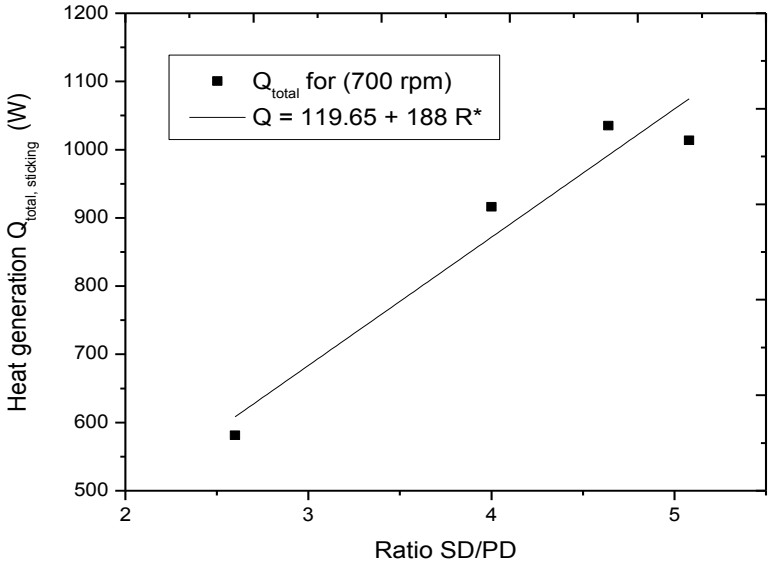

Figure 2-11. Linear relationship between total temperature and dimensionless diameters shoulder and pin for 700 rpm.

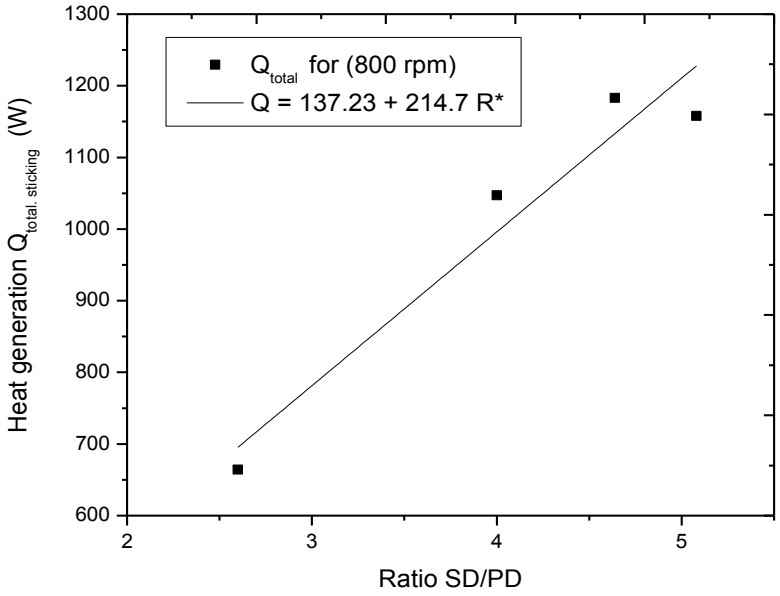

Figure 2-12. Linear relationship between total temperature and dimensionless diameters shoulder and pin for 800 rpm.

2.1.4 Heat Generation Ratios:

Based on the geometry of the tool and independent of the contact condition, the ratio of heat generation, i.e. contributions from the different surfaces compared to the total heat generation, are as follows:

$$f_{shoulder} = \frac{Q_1}{Q_{total}} = \frac{\left(R_{shoulder}^3 - R_{prode}^3\right)(1+\tan\alpha)}{\left(R_{shoulder}^3 - R_{prode}^3\right)(1+\tan\alpha) + R_{probe}^3 + 3R_{probe}^2 H_{probe}}$$

$$f_{shoulder} = \frac{Q_1}{Q_{total}} = \frac{3R_{probe}^2 H_{probe}}{\left(R_{shoulder}^3 - R_{prode}^3\right)(1+\tan\alpha) + R_{probe}^3 + 3R_{probe}^2 H_{probe}}$$

$$f_{shoulder} = \frac{Q_1}{Q_{total}} = \frac{R_{probe}^3}{\left(R_{shoulder}^3 - R_{prode}^3\right)(1+\tan\alpha) + R_{probe}^3 + 3R_{probe}^2 H_{probe}}$$

(2 – 24)

In this research used the tool dimensions are $R_{shoulder}$ = 10mm, R_{probe} = 2.5mm, H_{probe} = 6mm, α = 10°.and by compare the this tools and different tools design to calculate heat generation ratio .shown Table 2-3 and Figure 2-15.

Table 2-3. Heat Generation Ratio With Different Parameters

Tools No.	$f_{shoulder}$ (%)	$f_{prode\ side}$ (%)	$f_{prode\ tip}$ (%)
1	0.9	0.088	0.012
2	0.92	0.07	0.01
3	0.82	0.15	0.04
4	0.97	0.02	0.009

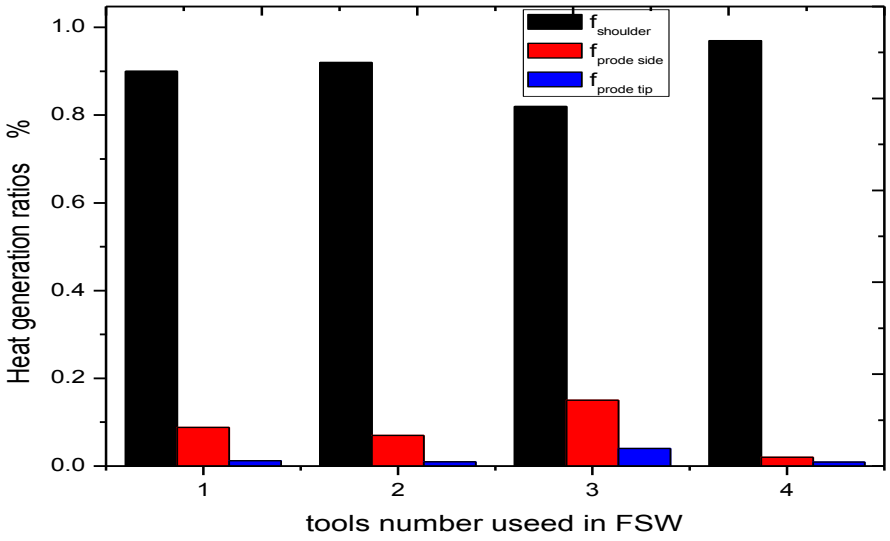

Figure 2-13. Heat generation ratio with different tools

This indicates that, for the specific tool geometry, the shoulder contributes the major fraction of the heat generation and the probe tip heat generation is negligible compared to the total heat generation. This correlates with the results found in [15], noting that the contribution from the probe due to the traverse motion is included in the estimate by Colegrove and Shercliff, which is not the case in the present estimates. [16]

General, heat generation is a complex process of transformation of a specific type of energy into heat. During friction stir welding, one part of mechanical energy delivered to

the welding tool is consumed in the welding process, another is used for deformational processes etc., and the rest of the energy is transformed into heat. The analytical procedure for the estimation of heat generated during friction stir welding is very complex because it includes a significant number of variables and parameters, and many of them cannot be fully mathematically explained. Because of that, the analytical model for the estimation of heat generated during friction stir welding defines variables and parameters that dominantly affect heat generation. These parameters are numerous and some of them, e. g. loads, friction coefficient, torque, temperature, are estimated experimentally. Due to the complex geometry of the friction stir welding process and requirements of the measuring equipment, adequate measuring configurations and specific constructional solutions that provide adequate measuring positions are necessary.[14]

2.1.5 Experimental Measurement of the Torque and Axial Force:

Experimental estimation of the welding force during FSW is difficult when the axis of the welding tool is horizontal (Fig. 2-14) due to the geometry of the FSW process. When the axis of the welding tool is vertical, the estimation of the welding force is less complex than when it is horizontal, however, the estimation of the torque is difficult due to the dimensions and functional demands of the torque sensor (axial force from the welding tool should not reach the torque sensor). The measuring the torque delivered to the welding tool is done by mounting the torque sensor (load cell) on the shaft that transmits power from the machine spindle to the welding tool. The axial force from the contact between the welding tool and workpices should not be delivered to the torque sensor due to its sensitivity to forces. The axial force is measured behind the workpicess and the anvil. Figure 2-14 shows the experimental measuring configuration used for the estimation of experimental torque and axial force. It is an unusual configuration for the FSW process because the axis of the welding tool is horizontal. It is important that the intensity of the axial force is lower when the rotation speed of the tool is higher, while the travel speed of the tool has to no significant influence on the axial force.[14]

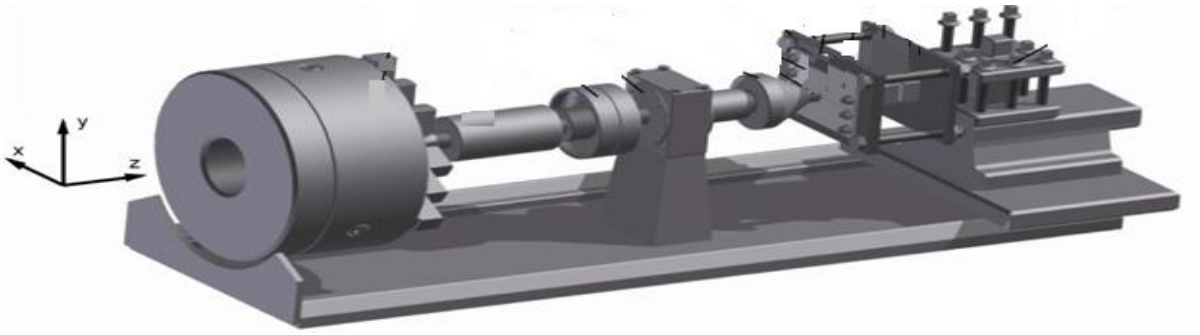

Figure 2-14. Measuring configuration for torque and axial force.[14]

2.1.6 Experimental Estimation of the Friction Coefficient:

The majority of published research on FSW confirms the complexity of the friction processes in FSW. Many of them recognize the problem of the estimation of the friction coefficient, however, they neglect it and consider the friction coefficient to be constant, taking the value of = 0.3 – 0.4. Figure 2-14 shows torque estimation in this measuring configuration is difficult since the configuration has to be vertical. Torque is measured indirectly: electrical power consumption on machine electromotor is measured and transformed into torque. The value of torque is measured only for the comparison with sensor-based values in horizontal configuration and has no influence on the friction coefficient estimation.

To estimate the coefficient of friction at FSW, it is necessary to estimate the momentum of friction and axial force. The momentum of friction is a multiplication of the tangential force F_t and length of the force pole (friction pole) L_t. If the diameter of the welding tool probe in contact is d, friction coefficient μ can be estimated as

$$\mu = \frac{3F_t\, L}{F_Z\, d} \qquad (2-25)$$

The Equation is approximate and due to the design limitations of the FSW process applicable only to plunging, first dwelling and beginning of the welding phases.

2.1.7 Experimental Estimation of the Temperature:

The estimation temperature during FSW, it can be obtained by an infrared camera and/or by thermocouples embedded at specific spots in workpieces. The infrared camera catches thermal images of surfaces captured by the camera frame, but the temperatures in the depth of the workpieces and welding tool, as well as the temperature on their contact, cannot be estimated. Thermocouples provide temperatures in the depth of the material, but they require preparation of workpieces, and it is necessary to have more than one thermocouple for a complete thermal image of the material.

For the purpose of the analytical estimation of the amount of heat generated during FSW, it is important to have the temperature of the material around the welding tool while it travels along the joint line. Satisfactory measuring results applicable in the analytical model can be obtained by the infrared camera shows in Figure (2-17) and there is no need for any preparation of workpieces.

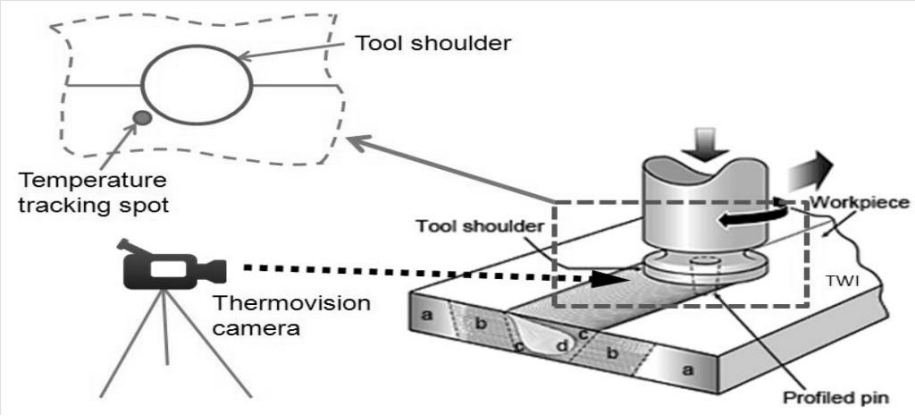

Figure 2-15. Schematic view of the experimental setup for thermovision camera.[16]

2.1. 8 Weld Zones:

The first attempt at classifying FSW microstructures was made by Threadgill. This work was focused solely on aluminum alloys, and was limited to features classification by light microscopy However, work on other metallic materials has demonstrated that the behaviour of aluminum alloys is not typical of most metals and alloys, and this initial classification was inadequate. Consequently, a revised set of terms was suggested and then subsequently revised and adopted in the American Welding Society Standard. These microstructural terms are illustrated in (Figure 1-3), and are defined below along with

alternative terms commonly found in the literature: unaffected material or parent metal: material remote from the weld, which has not deformed and which, although it may have experienced a thermal cycle from the weld, is not affected by heat in terms of detectable changes in microstructure or properties.[31]

(a)- Classification of Weld Zones:

There are two classifications for the weld zones. The first (Threadgill's classification) is based on the microstructural zones, while the second (Arbegast's classification) is based on the processing history of the weld zones during FSW. Both nomenclatures were developed for Al-based alloys; however they are generally applicable to other alloys as well.

(i)- Threadgill's Classification:

Threadgill has classified welds into four microstructural zones, which are: a weld nugget (WN), a thermomechanically affected zone (TMAZ), a heat affected zone (HAZ), beyond which the unaffected base metal (BM exists) as shown in Fig. 2-16. The WN refers to the region previously occupied by the tool pin. In the literature, this region is sometimes referred to as the stirred zone (STZ) . The extent of the TMAZ is the trapezoidal region whose bases are the shoulder diameter and the pin diameter, including regions Nugget and TMAZ in Fig. 2-16. The stirring action experienced within the TMAZ/WN during FSW leads to the formation of dynamically recrystallised grains in WN and plastically deformed or partially recrystallised grains in TMAZ. Beyond the TMAZ, a typically narrow HAZ exists, where only a diminishing thermal-field is experienced until reaching the unaffected BM. Because of the rotation direction of the tool, the weld morphology appears asymmetric between the advancing side (AS) to the retreating side (RS). Towards the AS, where the traverse speed and the tangential velocity component of the rotating tool are in the same direction, the TMAZ/HAZ boundary appears sharper compared to the RS where the boundary is more diffuse. Other features include an extended flow arm from the WN towards the AS, and concentric circles within the WN.

A friction stir welding joint is known have three zones such as weld: a) intensively deformed zone called the stir zone (SZ) , b) thermomechanically affected zone (TMAZ), c) heat affected zone (HAZ),as shown in Fig (2-16).

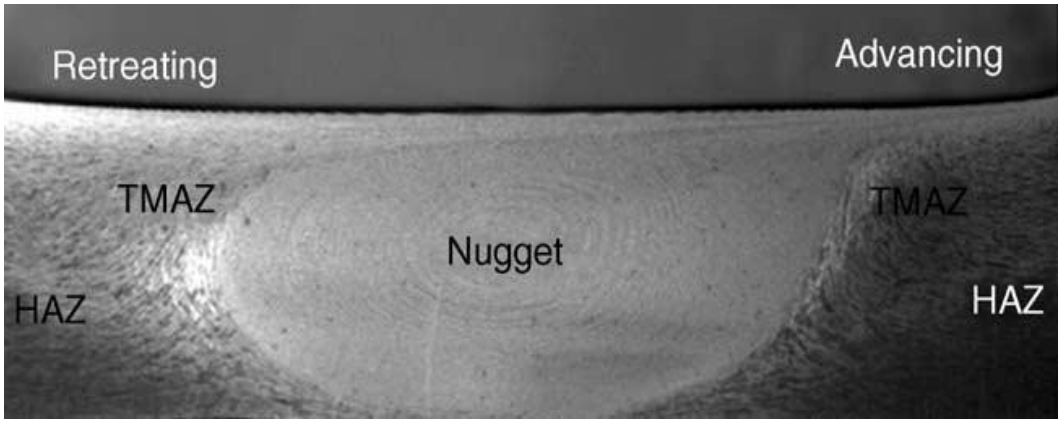

Figure 2-16. Microstructural zone classification in a friction stir welding.[33]

As the results of FSW process generates three zones comprises of commonly referred to weld affected zone (WAZ). The first constituent of the WAZ is the dynamically recrystallized zone (DXZ), also known as the weld nugget, which lies at the centre of the weld along the weld seam. This zone is hardened on either side by the remaining two constituent zones, the thermomechanically affected zone (TMAZ) immediately surrounding the DXZ, and the heat affected zone (HAZ) surrounding the outside characteristics that will be described throughout section, as shown in Figure (2-16).

(i.1) - Dynamically Recrystallized Zone (DXZ) or Nugget Zone:

The DXZ is defined as the area that has direct interaction with the tool probe also referred to as the weld nugget. Dynamic recrystallization is the process by which extreme strain and elevated temperature cause recrystallization of material in the weld nugget as the tool passes through it, resulting in a dispersion of fine, equiaxed grains in this area. Under some FSW conditions, onion ring structure was observed in the nugget zone (Figure 2-16). In the interior of the recrystallized grains, usually there is low dislocation density. However, some investigators reported that the small recrystallized grains of the nugget

zone contain high density of sub-boundaries subgrains, and dislocations. The interface between the recrystallized nugget zone and the parent metal is relatively diffuse on the retreating side of the tool, but quite sharp on the advancing side of the tool .[33]

The DXZ is relatively small, and is characterized by a shape loosely resembling the FSW tool used. The zone is characterisation of all friction stir weld, and has several qualities that are significantly different from the surrounding microstructures. In the DXZ, the dynamically recrystallized grains are frequently an order of magnitude smaller than the grains of the base material (K. V. Sata & Semiath, 2000; Mishra & Ma, 2005; Pouget & Reynold, 2008). The final size of the grains in the DXZ is strongly dependent upon the thermal history of the weld nugget and degree of stirring action, low stirring results in less dynamic recrystallization and larger grains, but higher temperatures from greater stirring also result in larger grains from growth of recrystallized grains. For each alloy, there is a minimum grain size that can be achieved through a balance of minimal thermal input, but great enough stirring action.[12]

(i.1.1) Shape of Nugget Zone:

Depending on processing parameter, tool geometry, temperature of workpiece, and thermal conductivity of the material, various shapes of nugget zone have been observed. Basically, nugget zone can be classified into two types, basin-shaped nugget that widens near the upper surface and elliptical nugget, that the upper surface experiences extreme deformation and frictional heating by contact with a cylindrical-tool shoulder during FSW, thereby resulting in generation of basin-shaped nugget zone. The nugget zone was slightly larger than the pin diameter, except at the bottom of the weld where the pin tapered to a hemispherical termination. Further, it was revealed that as the pin diameter increases, the nugget acquired a more rounded shape with a maximum diameter in the middle of the weld.[33]

(i.2) - Thermo Mechanically Affected Zone (TMAZ):

The TMAZ is a zone that characterized by severe plastic deformation of grains of the base material as well as exposure to raised temperature from proximity to the DXZ. The

grains in this zone have been plastically deformed from shear induced by tool rotation and traverse. The degree of plastic deformation in the TMAZ varies by proximity to the weld and depth in the joint. Grains have a higher degree of plastic deformation closer to the weld and nearer to the tool shoulder, tapering to grains that are less deformed further from the weld centreline (Kwan et al, 2002; Mishra & Ma, 2005). The raised temperature in the TMAZ are significant enough to dissolve strengthening precipitates in areas close to the DXZ and coarsen strengthening precipitates close to the HAZ, causing significant decreases in strength.

The exact line between where precipitates are dissolved and coarsened depends on the welding parameters, thus the resultant precipitate distribution is a function of time – temperature history of the zone (Woo et al., 2006). The TMAZ also has significant differences in the size and sharpness of the transition zone from the DXZ on the advancing and retreating sides of the weld. On the advancing side, the transition is sharp; on the retreating side the TMAZ blends gradually into the DXZ (K. V. Jata &Semiatin, 2000; Mishra & Ma, 2005).[12]

(i.3) - Heat Affected Zone (HAZ):

In friction stir welding, the HAZ is characterized by a microstructure that is not plastically deformed but is still affected by the thermal energy of the FSW process. Similar to precipitate coarsening in the TMAZ, in precipitation strengthened alloys the HAZ is characterized by overaging of precipitates, resulting in degradation of mechanical properties (K.V. Jata, 2000; zekovic, & Kovacevic, 2005; Zhang, 1999). The HAZ is defined by heat input to the work piece, which is a function of the welding parameters. The welding parameters may be very significantly depending on the nature and intent of the process, resulting in a significant variation in corresponding HAZ width and properties (Kwon et al., 2002; Mishra & Ma, 2005). Determining the boundary between the unaffected base material and the HAZ can be difficult even on a micrograph because the variation in properties between a large section of the HAZ and unaffected base material is very small. Measurements of the outer HAZ boundary necessitate the use of thermometers to mark temperature boundaries.

Generally, defining the outer HAZ boundary is unimportant because it is stronger than areas of the HAZ closer to the DXZ, especially in precipitation strengthened alloys (Genevois, 2005; Heinz & Skrotzki, 2002; Ulysse, 2002).[12]

(ii)- Arbegast's Classification

As shown in Fig. 2-17, Arbegast classified the weld along the feed direction into five zones: a) preheat, b) initial deformation, c) extrusion, d) forging, and e) cool down zones. This classification is based on the suggestion that FSW is an extrusion process, as also suggested in several researches. In the preheat zone, the temperature increases due to the moving thermal field surrounding the tool, which is stronger at the top due to shoulder friction. Close to the tool, an initial deformation zone forms because of the stress (*Pmax*) which is caused by the moving tool and the high temperature. The softened material is forced to flow around the tool in the extrusion zone where it gets extruded between the pin threads, with a small amount trapped below the tool in the vortex swirl zone. Behind the tool, the stirred material from the front is deposited in the forging zone, and cools down zone. The widths of the zones depend on the process parameters and thermal and thermomechanical properties of the material being welded [15].

This classification clarifies the influence of the moving thermal field in softening the material in front of the tool prior to stirring, as well as the cooling of the region behind the tool. However, since the characterization of the weld microstructural zones is mostly performed on the weld face, Threadgill's classification will be used in this study, with references to Arbegast's notation when discussing the microstructural development ahead to the moving tool.

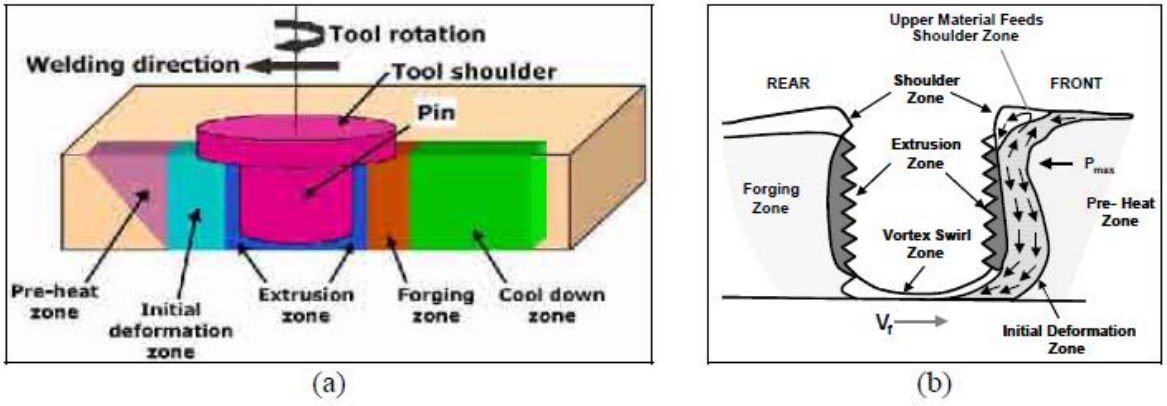

Figure 2-17. a) Processing zone during FSW, b) Deformation zone surrounding a tool moving. [12]

2.1.9 Advantages and drawbacks of FSW:

The solid-state nature of FSW immediately leads to several advantages over fusion welding methods since any problems associated with cooling from the liquid phase are immediately avoided issues such as, porosity, solute redistribution, solidification cracking and liquation cracking are not an issue during FSW. In general, FSW has been found to produce a low concentration of defects and is very tolerant to variations in parameters and materials.

A number of potential benefits of FSW over conventional fusion welding processes have been identified:

- Improved safety due to absence of toxic fumes or the spatter of molten material.
- No consumables conventional steel tools can weld over 1000 m of aluminium and no filler or gas shield is required for aluminium.
- Easily automated on simple milling machines- lower set-up costs and less training.
- Can operate in all positions (horizontal, vertical, etc.) as there is no weld pool.
- Generally good weld appearance and minimal thickness under/over- matching, thus reducing the need for expensive machining after welding.
- Low shrinkage and very small distortion after welding.
- Low environmental impact.

However, some drawbacks of the process have been identified

- Exit hole left when tool is withdrawn.
- Large down forces required with heavy duty clamping necessary to hold the plates together.
- Less flexible than manual and arc processes (difficulties with thickness variations and non-linear welds).
- Often slower traverse rate than some fusion welding techniques although this may be offset if fewer welding passes are required.

2.2 Aluminum alloy [AA5xxx]:

The aluminum 5xxx alloy exhibits good corrosion resistance to seawater and the marine atmosphere, moderate mechanical properties and a high fatigue-fracture resistance. With the growth of aluminum within the welding fabrication industry, and its acceptance as an excellent alternative to steel for many applications, there are increasing requirements for those involved with developing aluminum projects to become more familiar with this group of materials. To fully understand aluminum, it is advisable to start by becoming acquainted with the aluminum identification/designation system, the many aluminum alloys available and their characteristics.

2.2.1 Alloy Designation Systems:

Aluminum alloys are divided into two closes according to how they are produced: wrought and cast. The wrought category is a broad one, since aluminum alloys may be shaped by virtually every known process, including rolling, extruding, drawing, forging, and number of other, more specialized processes. Cast alloys are these that are poured molten into sand (sand casting) or high strength steel molds, and allowed to solidity to produce the desired shape. The wrought and cost alloys are quite different in composition; wrought alloys must be ductile for fabrication, which cast alloys must be fluid for castability. In 1974, the Association published a designation system for wrought aluminum alloys that classifies the alloys by major alloying additions [8]. This system is now recognized worldwide under the international accord for aluminum alloy designations, as a similar system for casting alloys was introduced.

Designation systems, one of advantage in using aluminum alloys and tempers is the universally accepted and easily understood alloy and temper systems by which they are known. It is extremely useful for both secondary fabricators and users of aluminum products and components to have a working knowledge those designation systems.

The alloy system provides a standard of alloy identification that enables the user to understand a great deal about the chemical composition and characteristics of the alloy and similarly, the temper designation system permits are to understand a great deal about the

way in which the product has been fabricated. The alloy and temper designation system in use today for wrought aluminum were adopt by the aluminum industry in about 1955, and the current system for cast system was developed somewhat later.[7].

(a)- Wrought Aluminum Alloy Designation System:

The aluminum association wrought alloy designation system consists of four numerical digits. Sometimes with alphabetic prefixes or suffices, but normally jest four numbers.

- The first digit defines the major alloying class of the series, starting with that number,
- The second digit defines variations in the original basic alloy, that digit is always a Zero (0) for the original composition,
- The third and fourth digits designate the specific alloy with the series, there is no special significance to the values of those digits except in the 1xxx series(see below), nor are they necessarily used in sequence.[7]

Table (2-4) shows the meaning of the first of the four digits in the alloy designation system. The alloy family is identified by that number and the associated main alloying ingredient with three exceptions [7].

Table 2-4. Designation System for Wrought Aluminum Alloys

Series	Main Alloying Element
1xxx	Pure Aluminum, 99% Aluminum
2xxx	Copper
3xxx	Manganese
4xxx	Silicon
5xxx	Magnesium
6xxx	Magnesium and Silicon
7xxx	Zinc
8xxx	Other Element (e.g iron or tin)
9xxx	Unassigned

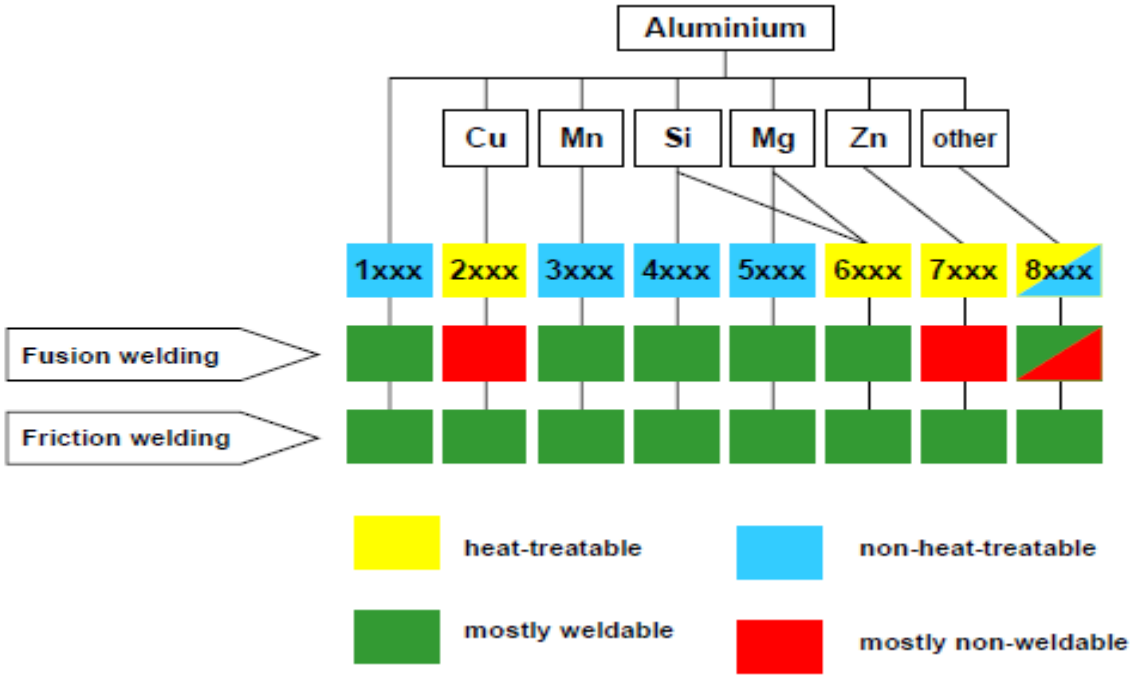

Figure 2-18. Weldability of Various Aluminum alloys.[10]

(b)- Aluminum Alloys Temper Designation System:

The temper designation is always presented immediately following the alloy designation. The specification of an aluminum alloy is not complete without designating the metallurgical condition, or temper, of the alloy. A temper designation system, unique for aluminum alloys, was developed by the aluminum association and is used for all wrought and cast alloys. The temper designation follows the alloy designation, the two being separated by a hyphen, are indicated by are or more digits following the letter. The first character in the temper designation is a capital letter indicating in the temper treatment as follows:

F – *As-Fabricated*. Applies to the products of shaping processes in which no special control over thermal conditions or strain hardening is employed. For wrought products, there are no mechanical property limits,

O – *Annealed*. Applies to wrought products that are annealed to obtain the lowest strength temper, and to cost products that are annealed to improve ductility and dimensional stability the O may be followed by a digit other than Zero,

H – *Strain Hardened (wrought products only)*. Applies to products that have their strength increased by strain hardening, with or without supplementary thermal treatments to produce some reduction in strength, it is always followed by two or more digits.(Table2-5).

W – *Solution Heat Treated*. An unstable temper applicable only to alloys that spontaneously age at room temperature offer solution heat treatment. This designation is specific only when the period of natural aging is indicated; for example W ½ hr,

T – *Thermally Treated to Produce Stable Tempers Other Than F,O or H*. Applies to products that are thermally treated, with or without supplementary strain hardening, to produce stable tempers. The T is always followed by one or more digits.[7]

Table 2-5. Subdivisions of H Temper: Strain Hardened

First digit indicates basic operations:

H1 – Strain hardened only

H2 – Strain hardened and partially annealed,

H3 – Strain hardened and stabilized,

H4 – Strain hardened, lacquered, or pointed

Second digit indicates degree of strain hardening

Hx2 – Quarter hard,

Hx4 – Half hard,

Hx8 – Full hard,

Hx9 – Extra hard.

Third digit indicates variation of two-digit temper.

The most widely used temper designations above are the H and T categories, and always followed by from one to for numeric digit that provide more detail about how the alloy has been fabricated.[7]

2.2.2 Properties of Aluminum Alloys (AA5083):

The properties of representative group of wrought aluminum alloys are generally thought of in two categories: nonheat-treatable and heat-treatable. Nonheat- treatable alloys are these that derive their strength from the hardening effect of elements such as manganese, iron, silicon, magnesium and are further strengthened by strain hardening. The chemical and mechanical properties shown in Table 2-6 and Table 2-7.

Table 2-6. Chemical Composition of the Investigated AA 5083.

Mg	Mn	Cu	Fe	Si	Zn	Cr	Na	Ti	Zr
5.13	0.718	0.013	0.337	0.108	0.513	0.008	0.0005	0.0254	0.0202

Table 2-7. Mechanical Properties of AA5083.

Deformation [%]	Thickness of specimens	Yield strength [MPa]	Ultimate strength [MPa]	Elongation max [%]
16.6	6.02	300.50	369.15	9.79

2.3 Charpy Test:

The charpy impact test was developed in 1905 by the French scientist Georges Charpy (1865 – 1945). The charpy test measures the energy absorbed by a standard notched specimen which braking under an impact load. The charpy impact test continues to be used as an economical quality control method to determine the notch sensitivity and impact toughness of engineering material. The charpy test is commonly used on metals, but is also applied to composites, ceramics and polymers. With the charpy test on most commonly evaluates the relative toughness of material, as such; it is used as a quick and economical quality control device. [19]

The charpy test is the test to determine the resistance of material against shocks; also the test is very important because the resistance of material decrease with decreasing temperature. Furthermore, transition temperature is resistance drop to lower value, which the shifting from ductile to brittle fracture. It is important to know where the transition temperature is located. As a matter of fact, operating below this temperature will increase very mach the risk for fracture.[5]

Charpy impact test is practical for the assessment of brittle fracture of metals and is also used as indicator to determine suitable service temperatures. The charpy test sample has 10 x 6 x 55 mm^3 dimensions, a 45^0 V notch of 2mm depth and 0.25 mm root radius and it is laid horizontally on two supports against an anvil. The sample will be hit by a pendulum at the opposite end of the notch as shown in Figure (2-19). To perform the test, the pendulum set at certain height is released and impact the specimen at the opposite end of the notch to produce a fractured sample. The absorbed energy required to produce two fresh fracture surfaces will be recorded in the unit of Joule. Since this energy depends on the fracture area (excluding the notch area), thus standard specimens are required for a direct comparison of the absorbed energy.[11]

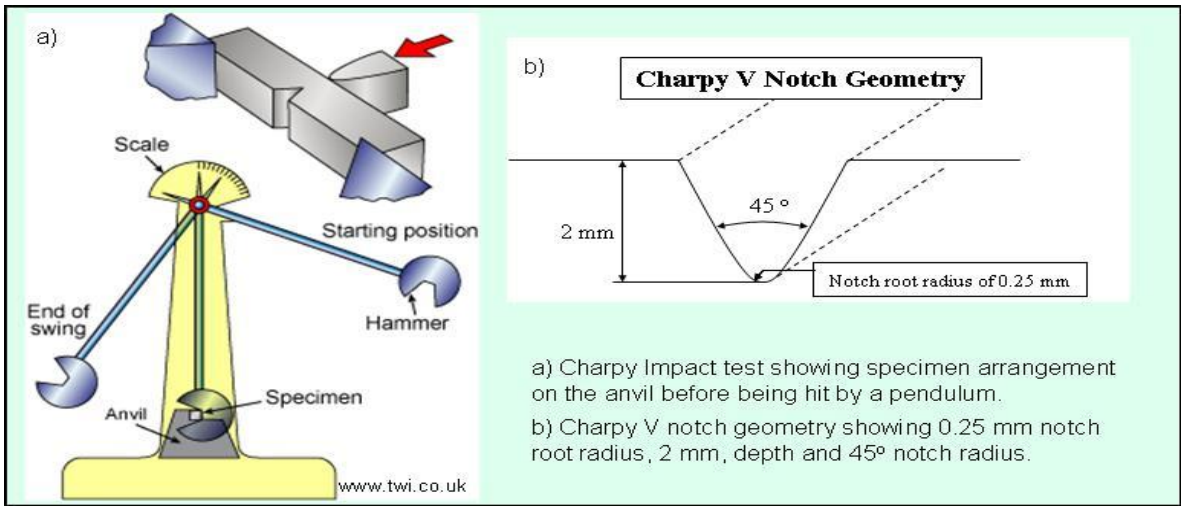

Figure 2-19. Charpy impact test. a) Test method and d) Notch dimensions.[20]

As the pendulum is raised to a specific position, the potential energy (mgh) equal to approximately 300J is stored. The potential energy is converted into the kinetic energy after releasing the pendulum. During specimen impact, some of the kinetic energy is absorbed during specimen fracture and the test of the energy is used to swing the pendulum to the other side of the machine as shown in Figure 2-19(a).

The greater of the high of the pendulum swings to the other side of the machine, the less energy absorbed during the fracture surface. This means the material fractures in a brittle manner. On the other hand, if the absorbed energy is high, ductile fracture will result and the specimen has high toughness. Fracture is caused by the growth of an existing crack (can be few microns in length) to a critical size where a total breakdown of the cracked piece takes place due to the externally applied stresses. Micro-cracks in stressed materials can grow either in a ductile or in a brittle manner.[19]

Microstructural surface fracture shown the kind of fracture as the ductile crack growth involves excessive plastic deformation which consumes a lot of the energy associated with the applied stresses. Fracture due to ductile crack growth is described as ductile fracture. A fracture surface produced by ductile fracture is extremely rough which indicates that a great deal of plastic flow has taken place. On the other hand, brittle crack growth proceeds with little plastic deformation where cracks grow rapidly. Brittle fracture surfaces are flat and do not show evidence of plastic deformation.[19]

CHAPTER 3: EXPERIMENTAL WORK

The applications of FSW process are found in several industries such as aerospace, rail, automotive and marine industries for joining aluminum, magnesium and copper alloys. The FSW process parameters such as rotational speed, welding speed, axial force and attack angle play vital roles in the analysis of weld quality. The goal of this study is to investigate the effects of different rotational speeds, welding speeds and tilt angles on the quality welded in aluminum 5083 alloy. This material alloy has gathered wide acceptance in the fabrication of light weight structures requiring a high strength-to-weight ratio.

3.1 Preparation of material:

The material used in this study was aluminum 5083 alloy. It made in the laboratories of University of Belgrade - faculty of technology by thickness is 7.2 mm, length 1000mm and width 500 mm. First step, it done the hot rolling on the plate samples to reduce the thickness to 6.2 , 5.8 mm and 5.5 mm. second step cuts the work plate to fit size as length to 260mm and width 45mm as two work pieces together as shows in Fig (3-1). The chemical and mechanical properties are given in Tables 2-3 and 2-4.

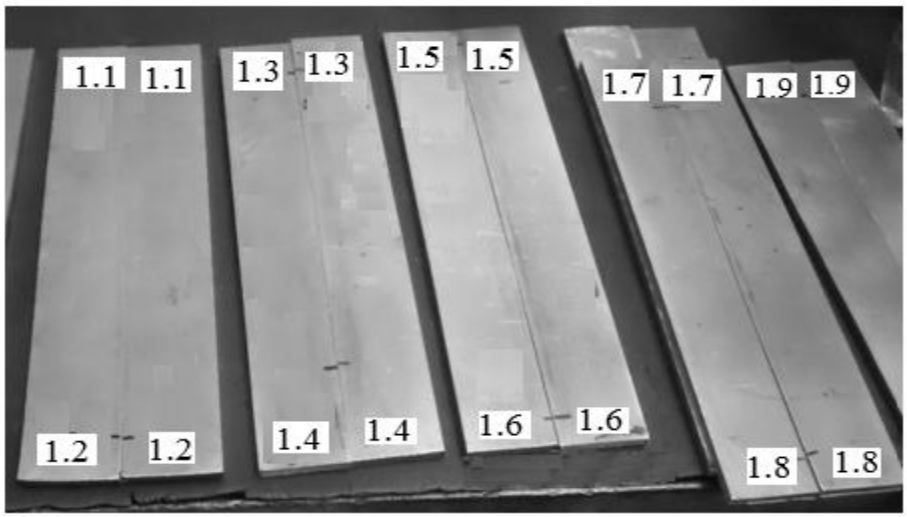

Figure 3-1. spacimens of AA 5083 alloys praperated for FSW.

3.2 Tool shoulder:

The shoulder is designed as a relatively large, when compared to the probe, profiled surface. Although the probe makes the initial contact with the pre-welded material the shoulder has a larger contact area and produces more friction.

(i)- Shoulder Diameter:

A shoulder diameter which is too small could result in insufficient heat being applied to the process through an inadequate contact area between tool and material to be joined and therefore a failed weld or broken tooling. To generate sufficient heat during the process the shoulder diameter should be a minimum of 50% larger than the root diameter of the probe with contact areas up to three times larger deemed to be satisfactory [37]. The diameter of the tooling determines the width of the plasticized region beneath the shoulder and the width of the thermo-mechanically affected zone (TMAZ). The distinct semi-circular trail indentation left in the wake of the tool is evidence of the deformation caused by the shoulder rotation and its width is related to the shoulder diameter. The diameter of the tool shoulder was used to welded aluminum 5083 alloys in this study; it was 20 mm shoulder diameter as shown in Figure 3-2.

Figure 3-2. Tool Shoulder and Tool pin used in FSW

(ii)- Shoulder Profile:

The amount of heat generated by the shoulder contact depends on the profile of this surface. The shoulder profile can be designed to suit the material being joined. This profile can increase or decrease the contact surface area and so increase or decrease the amount of heat supplied. This will also change the amount of deformation experienced by the material at the top of the weld. This enables the tool to be specifically designed for the materials or conditions in which it will be used. As the shoulder profile rotates and makes contact with the material it traps material within any contours of the profile and transports them with the rotation of the tool.[33]

3.3 Tool Probe (Pin):

Protruding from the shoulder profile is a cylindrical probe shown in Figure 3-3. This increases the contact area of the tool and enables heat and deformation to penetrate to the weld root. The probe makes the initial contact with the weld material before being plunged through the material, for a typical butt weld the probe stops when the tool shoulder contacts the material in the region of 0.1mm below the top surface of the material. The probe rotates with the shoulder as it is pulled through the weld material. [33]

Figure 3-3. Tool Probe (Pin) with Tread Right Hand.

(i)- Probe (Pin) Height:

The probe length dimension is 6 mm. For a butt weld the probe must be nearly as long as the material thickness. For example the shoulder penetrates the material by a small amount, approximately 0.1mm; the probe must finish a small amount, approximately 0.1mm, before the bottom surface of the weld material to prevent total penetration of the tool. This means that roughly speaking the tools probe should be designed to be in the region of 0.2mm less than the thickness of the material to be welded [36]. The probe length must be designed for the desired weld depth. The probe must not contact the backing plate as it would cause potential failures in the weld such as root flaws caused by impurities included in the weld from the backing plate, damage to the tool as a result of it being plunged into the backing plate or an unsatisfactory weld root as shown in Figure 3-3.[33]

(ii)- Root and Tip Diameter:

The probe tip and root diameter dimensions are 5mm and 6mm respectively. A simple cylindrical probe would have an equal root and tip diameter of approximately the same length of the probe. A more complex conical shape would have a far larger root diameter than tip diameter and would stand more chance of the probe breaking whilst under process conditions. However a conical shape yields superior welds than a cylindrical probe. Friction stir welding probes are commonly designed as frustums as shown in Figure 3-3.

(iii)- Threaded Probe:

Some probes contain more complex geometry in the form of a helical ridge or external thread. This external thread acts in the same way as any shoulder profile, changing the surface contact and deformation experienced by the weld material. These threads are designed in a specific way. As the tool is rotated the helix would either encourage or resist the plunge into the material depending on the pitch. The pitch of a screw accepts the material when rotated clockwise. This has a right-hand-pitched thread. The thread on an FSW probe is designed to oppose the plunge and push material downwards instead of drawing it upwards. This requires a left-hand-pitched thread (LH thread), when the spindle rotates in a clockwise direction. The helical ridge pushes the weld material towards the

bottom or weld root. This force produces vertical mixing to accompany the rotational mixing. The thread size or pitch will determine how successful the mixing of the weld material is. A small pitch may not produce enough deformation and so bonding of the stirred material is impaired. However too large a pitch will cause the tool to act like a drill and expel weld material before the shoulder makes contact to compresses the material. The probe works as an auger, immersed in the plasticized weld material. Furthermore, the tool was rotated counter-clockwise to force softened material towards the root of the weld and to obtain a full joint at the root of the weld. The butted plates were clamped on steel backing plate as shows in Fig (3-5). The tools are manufactured from wear resistant material with good static and dynamic properties at elevated temperature. The rotation plate tool was fixed to the spindle of milling machine.[33]

3.4 Tilt angle:

A suitable tilt angle of the tool must be selected to ensure optimum efficiency of the tool. It mainly depends on the shoulder geometry. It is usually set to 3° for a plain shoulder, and varied to 1.5° for a concave shoulder and between 0 and 1° for a scroll shoulder. Moreover, the tilt angles used in this research for welded aluminum alloys were 1^0, 2^0, 3^0 and 4^0 respectively away from the spindle's travel path as shows in Figure 3-4. Therefore, tilt angle affects the vertical and horizontal flow of the weld of the weld material. On the other hand, improper tilt angle may cause tunnel and crack-like defects in the welds.

Figure 3-4. Friction stir welding machine, type AG400.

3.5 Operation FSW Process:

In friction stir welding, shoulder tool with profiled probe is rotated and slowly plunged into the joint line between two pieces of plate material, which are butted together. [12] The two plates are clamped on a rigid back plate (shown Figure 3-5). The fixturing prevents the plates from spreading apart or lifting during welding. The tool is slowly plunged into the workpiece material at the butt line, until the shoulder of the tool forcibly contacts the upper surface of the material and the pin is a short distance from the back plate.[2]

Forces are an important part of friction stir welding technology. The force applied parallel to the axis of rotation of the tool (Z- direction) is the down force, and the force applied parallel to the welding direction (X- direction) is the traversing force. The force developed in a direction perpendicular to both X and Z forces in "side force" (Y-direction).[12]

The depth of penetration is controlled by the length of the profiled pin below the shoulder of the tool. The initial plunging friction contact heats the adjacent metal around the probe as well as a small region of material underneath the probe, but the friction between shoulder and material interface generates significant additional heat to the weld region. [2]

Figure 3-5. Clamps of work piece to machine FSW.

In addition, frictional heat is generated between the wear resistant welding tool and the material of the work pieces. This heat causes the latter to soften without reaching the melting point and allows traversing of the tool along the weld line. The plasticized material is transferred from the leading edge of the tool to the trailing edge of the tool probe and is forged by the intimate contact of the tool shoulder and the pin profile [12]. This plasticized material provides a hydrostatic affect as the rotating tool moves along the joint, which helps the plasticized material to flow around the tool [2], it leaves a solid phase bond between the two, shows in Figure (3-5).

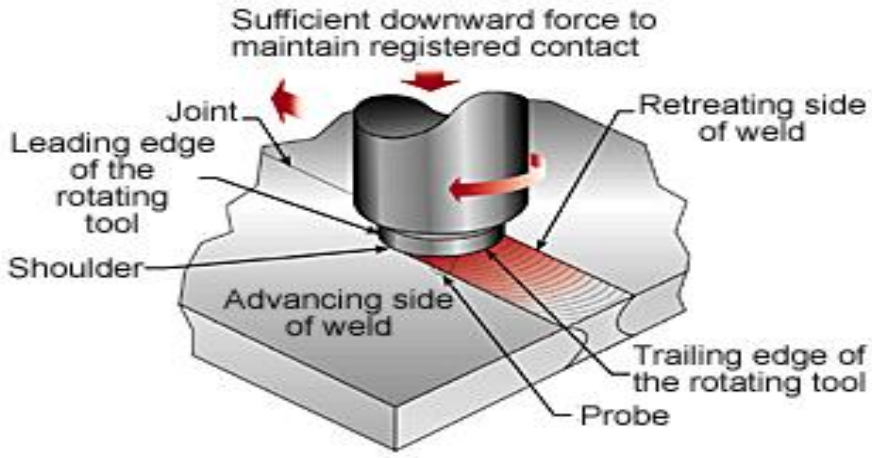

Figure 3-6. Friction stir welding process

The side where the directions are opposite and the local movement of the shoulder is against the traversing direction or side of the weld where direction of travel is opposed to direction of rotation of shoulder is called the retreating side. The total area of the tool on the work piece surface is described as the "tool shoulder footprint" as shown in Fig. 3-6.

In term welding speed is preferred to traversing speed, which is the rate of travel of too along joint line are used 75, 100, 125, and 150 mm/min respectively. The rotation speeds are used 500, 600,700, and 800 rpm respectively. Also the angle of tilt is referred to as the tilt angle. In some instances the tool is tilted sideways, tilt angles are used 1^0, 2^0, 3^0, and 4^0 respectively. [12]

3.6 Microstructure Features of Friction Stir Welded:

In any welding process, the properties and performance of the weld are dictated by the microstructure, which in turn is determined by the thermal cycle of the welding process, which can normally be varied by changing the welding parameters. Therefore welding parameters must be selected that give the best possible microstructure and that allow welds to be made free from defects and other undesirable features. With most materials, it is well understood that welding has some adverse effects on microstructure, properties and thus the 'optimized' weld parameters are often a compromise between making sound welds at economical production rates and producing acceptable, rather than ideal, microstructures and properties.

Friction stir welds in aluminum alloys contain a wide variety of microstructures, which is hardly surprising when the extreme range of strains, strain rates and thermal cycles to which different regions of the weld are exposed is considered. The microstructural variations were first characterized by Threadgill (see Figure.2-16). In the HAZ, remote from the centre of the weld, there is no obvious change to the grain structure, and the HAZ is detected only by a change in hardness and generally by a change in etching response by different rotation speed as shown in Figure 3-7. In precipitation hardened alloys it is widely accepted that some coarsening of precipitates is occurring, and possible dissolution at higher temperatures. In work hardened alloys, dislocation networks may recover, and this may cause some low angle cell boundaries to form. Furthermore as the weld centre is approached, clear evidence of plastic deformation can be seen in the grain structure. In the outer part of the TMAZ, the original grains remain identifiable in the deformed structure, with the formation of subgrain structures and significant associated rotation of the parent grains. Closer to the weld line, the strains will be increased at elevated temperature and allowing the formation of the recrystallised nugget with a fine equiaxed structure. The microstructural characteristics will first be discussed for the nugget region, in which deformation dominates. Evolution of microstructure in the heat affected zone is thermally controlled.[31]

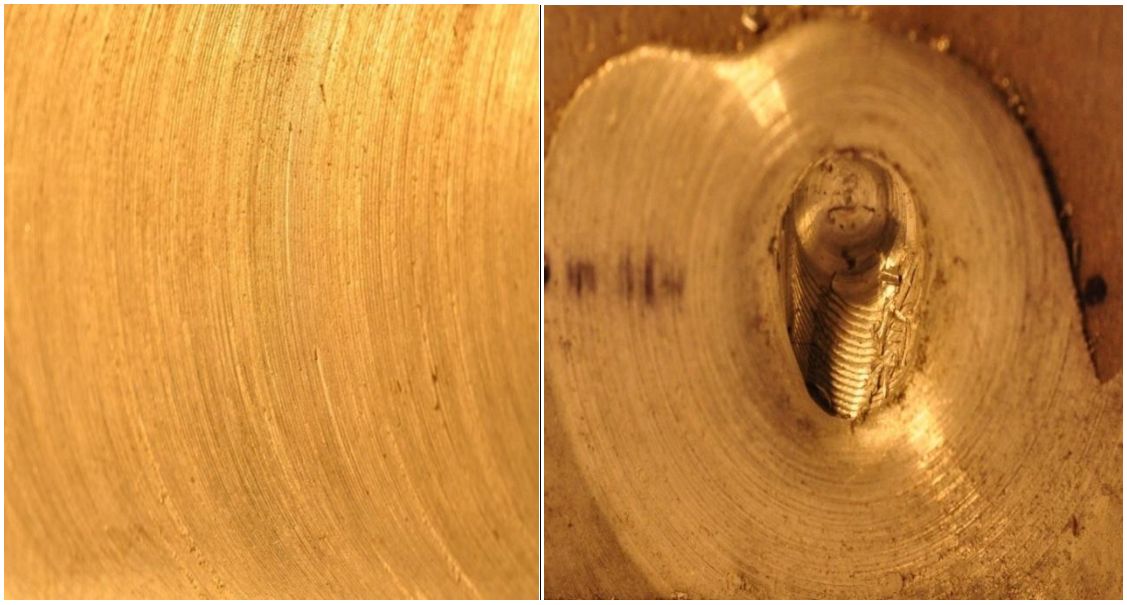

Figure 3-7. View Upper Surface of Material and Top View of Keyhole.

3.7 Deformation Microstructure in Weld Nugget:

(i)- Onion Ring' Structure:

A common observation from the nugget region in FSW is the appearance of a series of circular or elliptical features in etched metallographic sections (seen in Figure.2-16), often termed 'onion rings' (as the sections reveal a slice through a set of nested layers of roughly hemispherical shape, like an onion). The significance of this structure in the weld nugget remains an occasional topic of interest in the literature, that the ring patterns are an etching response to variations in grain size between the rings. Other characteristics of the rings include texture effects and variations in dislocation density. The nugget may also contain fractured constituent particles and the structure has been attributed to a variation in their distribution. This is turn may be a consequence of the banded distribution of the constituent particles present in the base metal, a characteristic that is strongly alloy dependent. These factors primarily relate to the strength of contrast in microstructure observed in the weld nugget, but do not offer a complete explanation of the mechanism of formation, which has not yet been formulated. There seems to be strong argument that

there is a purely kinematic basis for the formation of each ring, associated with one rotation of the tool (or the rotation between positions of tool symmetry. Cyclic fluctuations in the amount of material extruded past the tool and being deposited are to be expected with profiled tools as shown in Figure 3-8. It has therefore been postulated that ring formation may be a function of the tool geometry, tool rotation and forward travel speeds. The practical significance of the phenomenon remains rather limited as the mechanical properties of the nugget are generally good, and the fracture paths in mechanical tests are seldom associated with the onion rings.

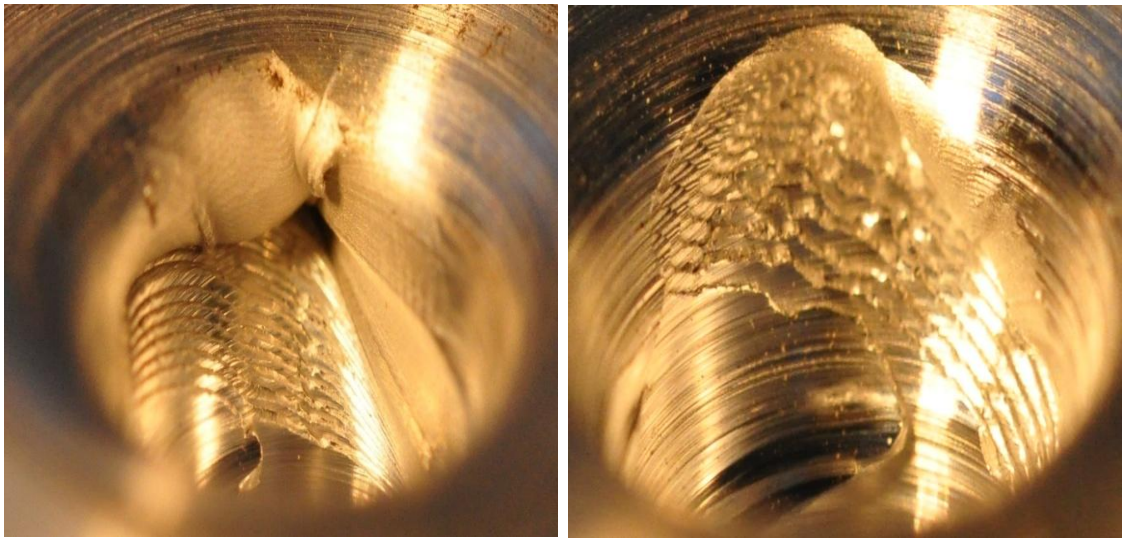

Figure 3-8. Show Thread Formed Material in Keyhole

(ii)- Recovery Versus Recrystallisation :

A feature of the microstructure of friction stir welds in aluminum alloys is the development of a fine grain structure in the centre of the nugget region. On the basis of these observations, it has been concluded that the nugget consists of dynamically recrystallised grains, and not subgrains. High values of forward tool motion per revolution produce harder microstructures, but generally similar grain size. Furthermore, the presence of precipitates as a direct influence on the processes of recovery and recrystallisation. In a study carried out in the region of the tool pin exit hole in a sample of AA5083 alloy as shows in Figure 3-8, it has been argued that the structure of the weld nugget is one of

dynamically recovered subgrains. This postulation, that grain growth is due to the presence of a dynamically recovered subgrain structure in the TMAZ. The microstructural observations may be resolved by considering a mechanism of continuous dynamic recrystallisation in the TMAZ. The deformation process associated with welding introduces a large quantity of dislocations, while at the same time grain growth occurs as the temperature rises. Subgrains, which are very small and exhibit low angle boundaries, begin to form by a process of dynamic recovery. Continuous dynamic recrystallisation then occurs as dislocations are continuously introduced to the subgrains by further deformation. The subgrains grow and rotate as they accommodate more dislocations into their boundaries, forming equiaxed recrystallised grains with high angle grain boundaries. Plastic deformation continues with the repeated introduction of dislocations and the process continues until the end of the thermomechanical cycle, at which point partial recovery takes place.[31]

3.8 Charpy Test:

Charpy impact test is practical for assessment failure of metals that done in laboratories of military institute in Belgrade of 14/11/2012. The charpy test specimens has 10 x 6 x 55 mm^3 dimensions, a 45^0 V notch of 2mm depth and a 0.25 mm root radius that hit by a pendulum at the opposite end of the notch . First of all, tested 30 specimens which the two specimens from the same kind parameters like rotational speed, welding speed, and tilt angle, also the material properties as the same. To perform the test, the pendulum set at a certain height is released and impact the specimen at the opposite end of the notch to produce a fractured sample. The absorbed energy required to produce two fresh fracture surfaces was recorded in the unit of Joule. Since this energy depends on the fracture area (excluding the notch area), thus standard specimens are required for direct comparison of the absorbed energy.

As the pendulum is raised to a specific position, the potential energy equal to approximately 300J is stored. The potential energy is converted into the kinetic energy after releasing the pendulum. During specimen impact, some of the kinetic energy is absorbed during specimen fracture and the rest of the energy is used to swing the

pendulum to the other side of the machine. The greater of the high of the pendulum swings to the other side of the machine, the less energy absorbed during the fracture surface. This means the material fractures in a brittle manner.

3.8.1 Experimental Procedure of Charpy Testing:

1- Examine charpy impact specimens of 10 x 6 x 55 mm^3 dimensions with a notch 45^0 angle and 2 mm depth located in the middle as shown in Figure 2-19 and 3-9.
2- A pair of specimens will be tested at room temperature.
3- Room temperature test is first carried out placing the charpy impact specimen on the anvil and positions it in the middle location using a positioning pin where the opposite site of the notch is destined for the pendulum impact (seen in Figure 3-10).
4- Raise the pendulum to a height corresponding to maximum stored energy of 300J. Release the pendulum to allow specimen impact. Safely stop the movement of the pendulum after swinging back from the opposite side of the machine.
5- When the pendulum is still, safely retrieve the broken specimen without damaging fracture surfaces. Record the absorbed energy in table. Repeat the test at the same test condition using another specimen to average out the obtained values.[20]

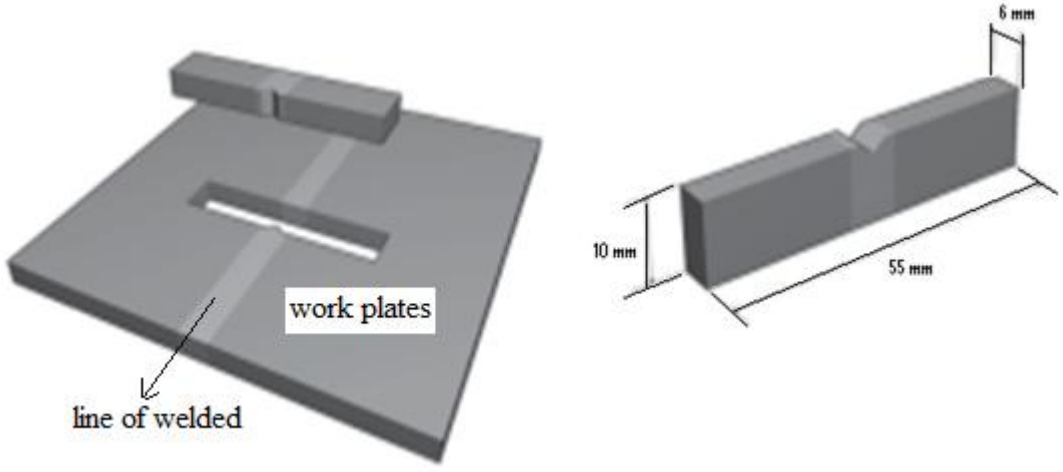

Figure. 3-9. Scheme of the machining of the charpy specimens from the FSW plates and dimensions of the sub-size specimens used for the tests.[21]

The main objective of the impact test is to predict the likelihood of brittle fracture of a given material under impact loading. The test involves measuring the energy consumed in breaking a notched specimen when hammered by a swinging pendulum. The presence of a

notch simulates the pre-existing cracks found in large structures. Note the presence of a notch increase the probability of brittle fracture. The energy absorbed can be calculated by measuring the change in the potential energy of the pendulum before and after breaking the specimen.

In the charpy test, the specimen is supported as simple beam as the square bar specimens with machined notches taking shape of the letter V hence giving other common names for these tests as charpy V-notch. Using an impact machine, the energy absorbed while breaking the specimen is measured. The energy quantities determined are qualitative comparisons on a selected specimen and cannot be converted to energy figures that would serve for engineering design calculations. The purpose of the impact test is to measure the toughness or energy absorption capacity of the materials. It is usually used to test the toughness of metals and this test is quick and inexpensive. The charpy specimens are held such that the specimen rests against two supports on either side of the test notch. The impact location is struck directly behind the test notch such that the specimen undergoes three point bending.[19]

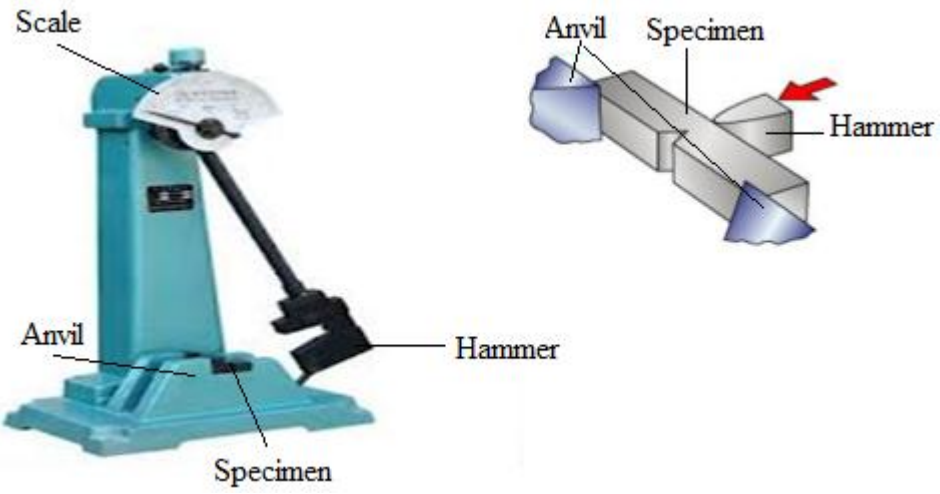

Figure 3-10. Machine of Charpy Test.

Furthermore, the notch size and shape are specified by the test standard, the purpose of the notch is to mimic part-design features that concentrate stress and make crack initiation cosier under impact loads. Notch toughness is the ability that a material processes to absorb energy in the presence of flaw.

3.9 Scanning Electron Microscope (SEM):

Using Scanning Electron Microscope (SEM) to obtain images of surface fracture that done on 22 of May 2013 at University of Novi Sad – Faculty of Technology and takes lot of images for each 12 specimens to get deeper views of fracture surface. Also before done SEM to get images takes macro photographs by high resolution camera to investigated the surface fracture for each charpy specimens (shown in Figures 4-12 (a – o)).

When a material fails by fracture there is complete separation of the two broken halves and a new surface, the fracture surface, is formed. It is often possible to examine the fracture surface and interpret features on it in a manner similar to the examination of a metallographic cross-section specimen. Features on the fracture surface can give us information about the mechanism of crack growth and also about the nature of the crack or defect from which the fracture nucleated. Unlike metallographic cross-sections, fracture surfaces often contain substantial vertical relief and scanning electron microscopy (SEM), with its much greater depth of field, is routinely used for fracture surface investigation, Fractography. It is an important tool of failure analysis and is often used in accident investigation to help pin-point the cause of failure. One part of this practical will use the SEM to study fracture surfaces in order to deduce the causes and mechanisms of fracture. For more details seen the result of work in chapter4.[106]

3.10 Energy Dispersive X-ray Spectroscopy (EDX) Analysis:

Using SEM –EDX analysis to investigate microstructures and chemical composition in aluminum alloyed of fracture surface. In fact, the rapid heat and cooling process introduced a non-equilibrium condition causing changes in the microstructure as well as the chemical composition of the alloyed aluminum surface. However, that is important to do EDX analysis to check the elements in alloy on surface fracture (shows Figures 4-25(a – i) in Chapter 4) and as shown in Table 4-6 and Table 4-7.

CHAPTER 4: RESULTS

The material used in this study was aluminum 5083 alloy has chemical composites in Table (2-1) and 6mm thick plates were welded by the friction stir welding, following the welding were made on the cross-section perpendicular to the welding direction using. Then clean specimens and cut the edges of all samples to prepare samples to charpy test. [21]

Many studies were made on the weldability of aluminum 5083 alloy. Some researchers studied the influence of FSW parameters on fatigue life. They discovered that the rotational speed governs defect occurrence and a strong correlation between the frictional power input, tensile strength and the low cycle fatigue life is obtained, also investigated the optimal conditions for FSW in correlation with welds mechanical properties. These mechanical properties were similar to the base alloy at tool rotations between 500 rpm and 800 rpm at weld- tool travel speeds between 75 mm/min and 150 mm/min also tilt angles between 1^0 - 4^0. [23]

4.1 Charpy V- Notch Impact Tests Results:

Shows in the Table 4-1 average absorbed energy data recorded from charpy test. The lower average absorbed energy was equal 15.22J from specimen that welded by rotational speed was 500 rpm, welding speed was 75 mm/min and tilt angle 1^0 . Also it was 15.23 J from specimen that welded by rotational speed was 800 rpm; welding speed was 125 mm/min and tilt angle 3^0. Additional, the middle average absorbed energy was 19.16 J from specimen that welded by rotational speed 500 rpm, transverse speed 100 mm/min and tilt angle 2^0. Furthermore, the higher average absorbed energy was 23.14 J from specimen that welded by welded rate 800 rpm, transverse speed 100 mm/min and tilt angle 2^0, also it was 23.05 J from specimen that welded by 800 rpm, 75 mm/min and tilt angle 1^0. In fact, if the absorbed energy is high, ductile fracture will result and the specimen has high toughness.

Table 4-1. Average absorbed Energy and Toughness Recorded from Charpy Test.

No. of Sample	Rotation Speed (rpm)	Welding Speed (mm/min)	Tilted Angle (^{0})	Average absorbed Energy (J)	Average Toughness (J/cm^2)
1.1	500	75	1^0	15.22	30.62
1.2	600	75	1^0	16.65	33.57
1.3	700	75	1^0	21.03	42.28
1.4	800	75	1^0	23.05	46.40
1.5	500	100	2^0	19.16	39.42
1.6	600	100	2^0	20.78	41.79
1.7	700	100	2^0	19.84	40.61
1.8	800	100	2^0	23.14	47.69
1.9	500	125	3^0	22.88	51.28
1.10	600	125	3^0	20.43	45.68
1.11	700	125	3^0	16.48	33.94
1.12	800	125	3^0	15.23	32.03
1.13	600	150	4^0	19.93	46.49
1.14	700	150	4^0	21.19	49.74
1.15	500	150	4^0	15.89	37.03

4.1.1 Force (Load) – Time Curve:

After tested the all specimens of aluminum 5083 alloy by charpy test machine, drawing the relationship between load-time for all specimens. From load-time curves, observed the largest maximum load of all specimens was 4.52 KN in specimen that welded by rotational speed 800 rpm, welding speed 75 mm/min and tilt angle 1^0. Also in specimen that welded by rotational speed 800 rpm, welding speed 100 mm/min and tilt angle 2^0, it was 4.47 K N. Moreover, observed the lowest maximum load was 3.59 KN in specimen that welded by rotational speed 800 rpm, welding speed 125 mm/min and tilt angle 3^0. As shown in Table 4-2

General, the load is characteristic value of the onset of plastic deformation and it was determined as the load at the intersection of the linear rising portion of the load-time curve and the fitted curve through the oscillations of the load-time curve until reached the maximum load. At this point the value of maximum load that means the area under the curve until peak point is the toughness of alloys. Then the load at the initiation of unstable crack propagation, characterizes the start point of the unstable crack propagation and the load at the beginning of the rapid drop in load in the curve, the load at the end of unstable crack propagation, characterizes the point at crack arrest, that means the specimen fracture and machine of charpy test stopped tested. As shown in Figures 4-1 (a - o) load-time curves.

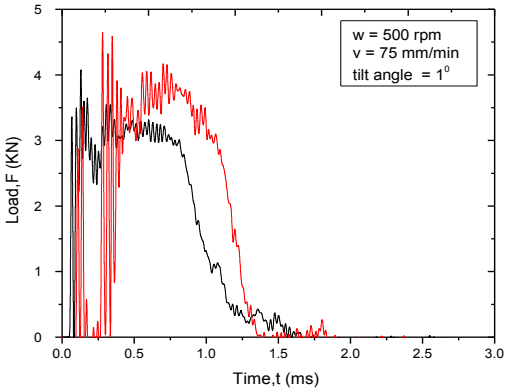

Fig.4-1a. load –time curve (500rpm,75mm/min)

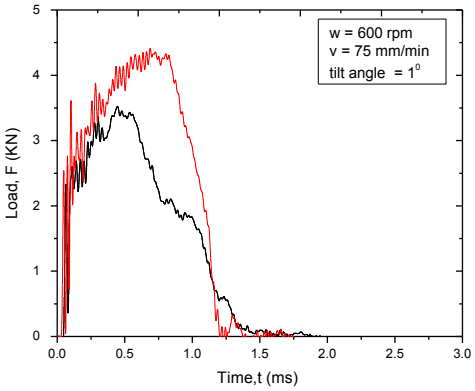

Fig. 4-1b. load –time curve (600rpm,75mm/min)

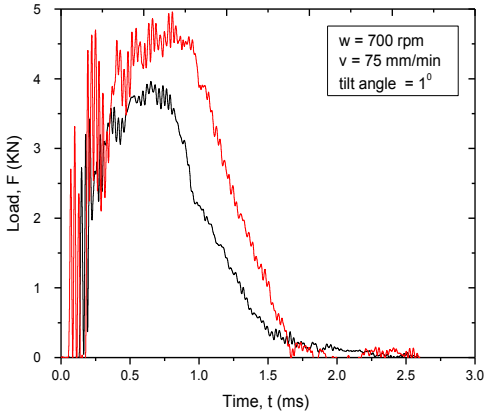

Fig.4-1c. load –time curve (700rpm,75mm/min)

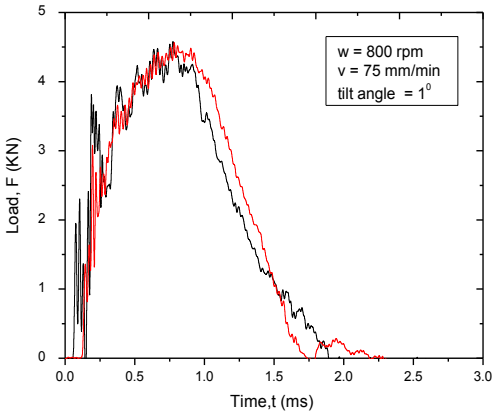

Fig.4-1d. load –time curve (800rpm,75mm/min)

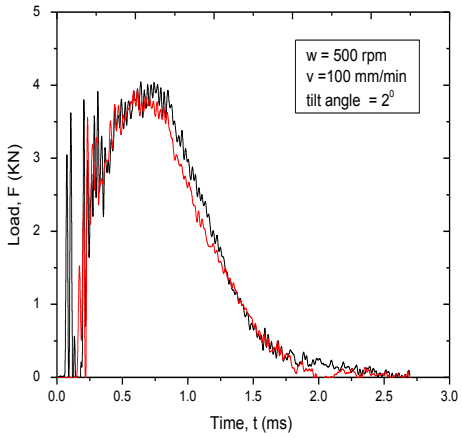

Fig.4-1e. load –time curve (500rpm,100mm/min)

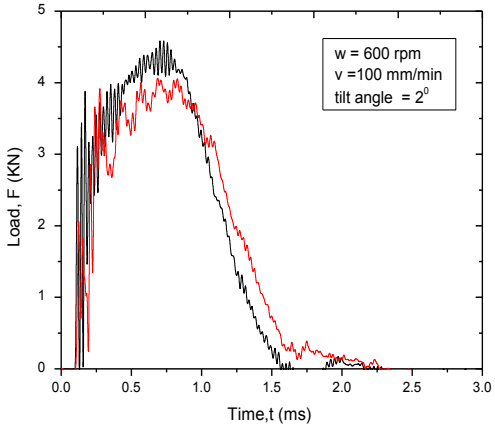

Fig.4-1f. load –time curve (600rpm,100mm/min)

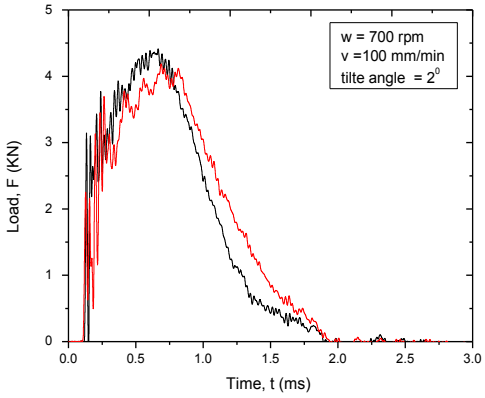

Fig.4-1g. load –time curve (700rpm,100mm/min)

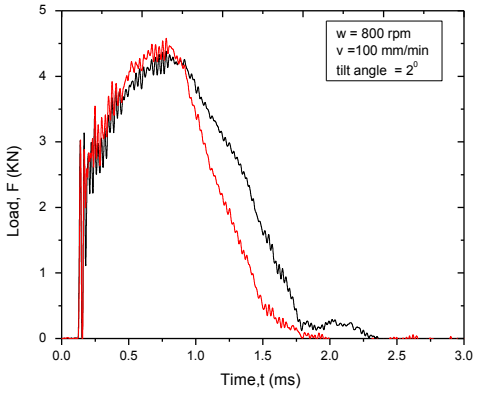

Fig.4-1h. load –time curve (800rpm,100mm/min)

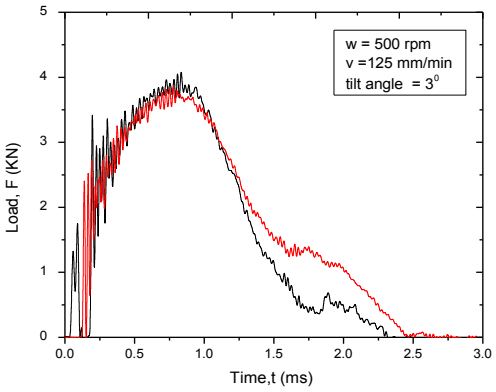

Fig.4-1i. load –time curve (500rpm,125mm/min)

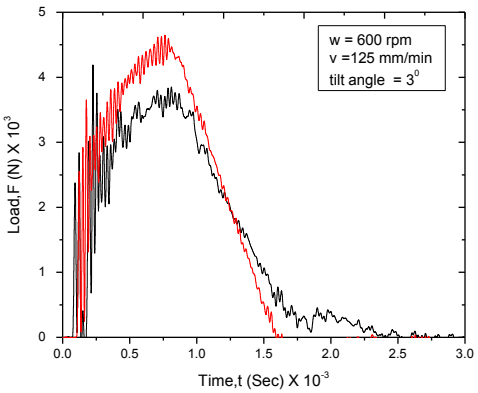

Fig.4-1j. load –time curve (600rpm,125mm/min)

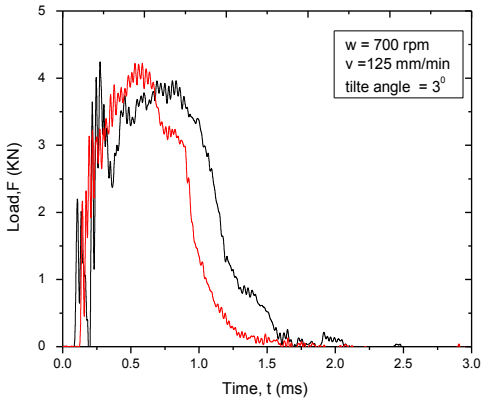

Fig.4-1k. load –time curve (700rpm,125mm/min)

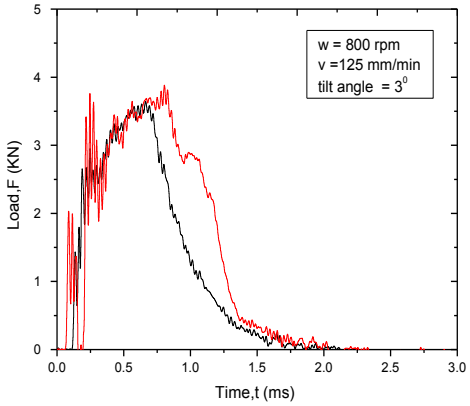

Fig.4-1l. load –time curve (800rpm,125mm/min)

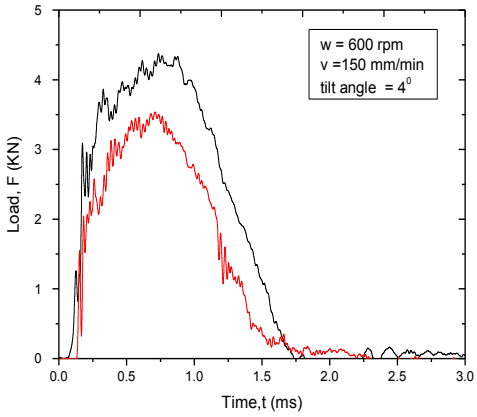

Fig.4-1m. load –time curve (600rpm,150mm/min)

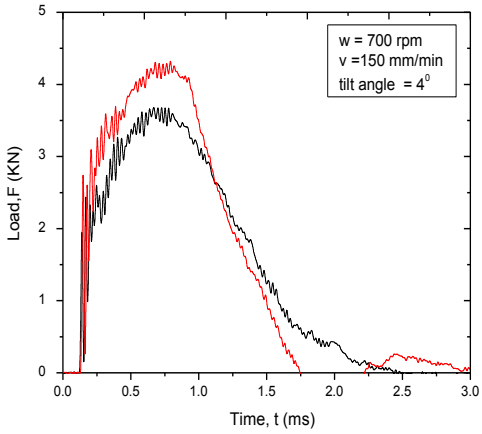

Fig.4-1n. load –time curve (700rpm,150mm/min)

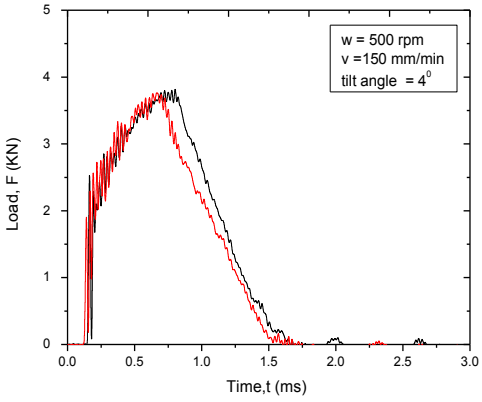

Fig.4-1o. load –time curve (500rpm,150mm/min)

Table 4-2. Calculation Area Under the Curve (Energy Initiation, E_1 and Energy Propagation, E_2)

No. Sample	Welding Parameters rpm, mm/min	Max. Load (KN)	Total Energy (J)	Energy Initiation E_1 (J)	Energy Propagation E_2 (J)
1.1	500, 75 , 1^0	4.12	15.8	7.4	8.4
1.2	600, 75 , 1^0	3.93	25.4	9.4	15.5
1.3	700, 75, 1^0	4.27	23.1	12.8	10.3
1.4	800, 75, 1^0	4.52	25.7	14.0	11.7
1.5	500, 100, 2^0	3.89	19.9	9.6	10.2
1.6	600, 100, 2^0	4.10	21.9	13.8	10.9
1.7	700, 100, 2^0	4.12	22.0	10.4	10.5
1.8	800, 100, 2^0	4.47	25.4	13.7	11.7
1.9	500, 125, 3^0	3.78	25.7	12.1	13.6
1.10	600, 125, 3^0	4.16	22.8	12.5	10.3
1.11	700, 125, 3^0	3.95	18.0	9.9	8.1
1.12	800, 125, 3^0	3.59	16.3	8.7	7.6
1.13	600, 150, 4^0	3.88	21.7	11.4	10.3
1.14	700, 150, 4^0	3.93	23.4	11.2	12.2
1.15	500, 150, 4^0	3.77	18.4	13.6	7.8

4.1.2 Force (Load) – Displacement Curve:

From relationship between load and displacement traces for all specimens under charpy impact are shown in load displacement curves. The load rises rapidly to maximum value and drops suddenly. This drop in load marks the boundary line of two distinct phases i.e., fracture initiation and fracture propagation phase of the total fracture event. The displacement seems to increase monotonically with time till the complete failure. Similar curves were obtained for all the specimens. The load and displacement data obtained with respect to time were reploted as load versus displacement.[40]

Shown from Figures 4-2 (a – o) load-displacement curves for all specimens these welded by different FSW parameters, reported the lowest area under the curve was 15.8 mm^2 in specimen that welded by rotational speed 500 rpm, welding speed 75 mm/min and tilt angle 1^0, then divided area to two portion, first of them from the start or zero to maximum load or peak point that area is called crack initiation E_1, it was 7.4 J. Second portion from maximum load to crack arrest is called crack propagation E_2. It was 8.4 J. On the other hand, specimens that welded by 800 rpm, 75 mm/min and 500 rpm, 125 mm/min respectively, observed the biggest area under the curve of all the specimens. It was 25.7 mm^2, and they have cracks initiation E_1 were 14.0 J, 12. 1 J respectively, also they have cracks propagation E_2 were 11.7 J, 13.6 J respectively. That means, the specimens had the biggest area, it had high toughness. Furthermore, the main approach is based on association of the cleavage portion of the fracture with the ratio of the drop in load value to the maximum load is considered the point at the beginning of crack extension. However, the ductile portion of the fracture can be formed also during flow of the material (plastic deformation), which begins at the point of yield. Shown in Figure 4-2(a – o) and Table 4-2.

General shows significant strain hardening and gradual load decrease at fracture the sharp drop in load indicates brittle fracture and fails by cleavage. Moreover, impact causes a region of plastic deformation to occur around the notch in the test specimen, followed by strain hardening. Then the stress and strain increase until the specimen ruptures. The energy required to fracture the specimen (the impact toughness) provides valuable information about how the material will behave under sudden impacts, although there are limitations on the applicability of the findings, like hardness tests, impact tests do not result in a number that definitively describes the material‘s toughness. Instead, impact test yield comparative data, which is interpreted in combination with an analysis broken surfaces of the specimens themselves. Post-fracture visual analysis can provide information on what percent of the area was ductile during impact as many of the factors are held constant as possible, the results of impact test reflect the toughness of the material, though even then the values found are useful only to compare to other results.

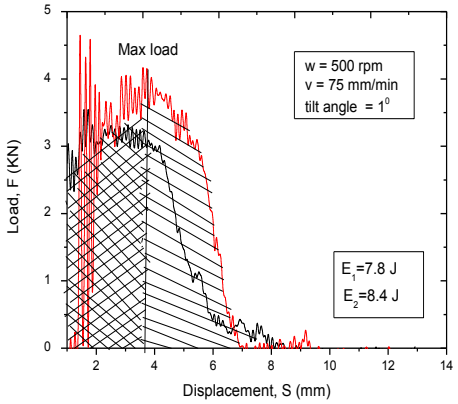

Fig.4-2a. load –displacement curve (500rpm,75mm/min)

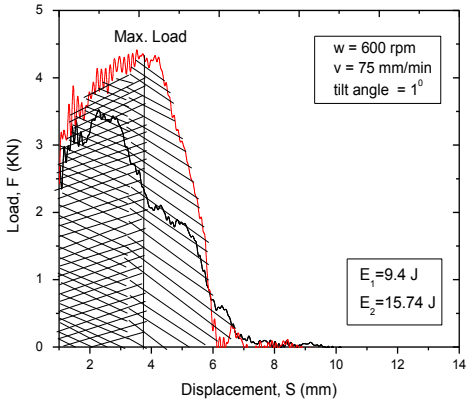

Fig.4-2b. load –displacement curve (600rpm,75mm/min)

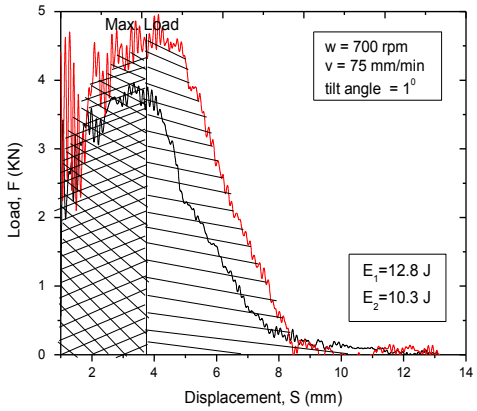

Fig.4-2c.load –displacement curve (700rpm,75mm/min)

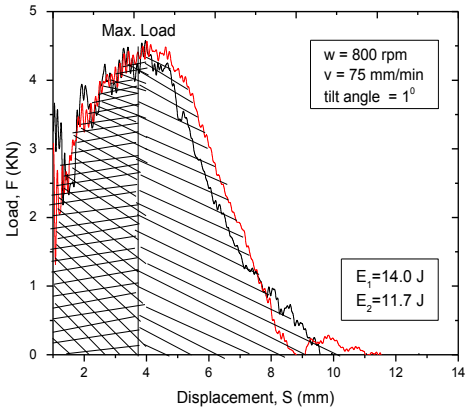

Fig.4-2d. load –displacement curve (800rpm,75mm/min)

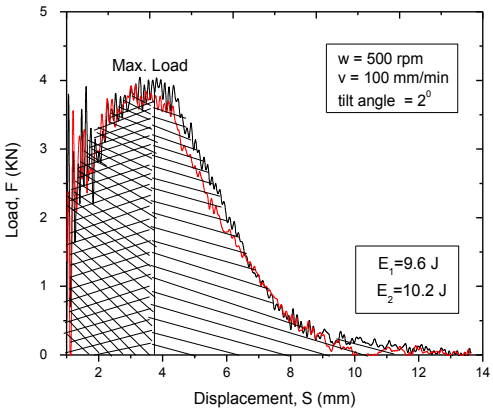

Fig.4-2e. load –displacement curve (500rpm,100mm/min)

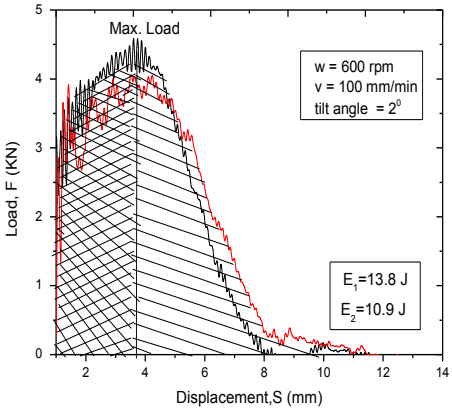

Fig.4-2f. load –displacement curve (600rpm,100mm/min)

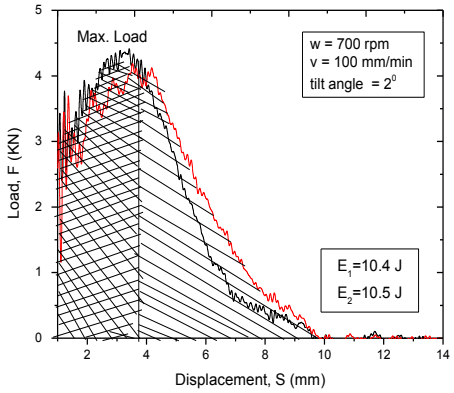

Fig.4-2g. load –displacement curve (700rpm,100mm/min)

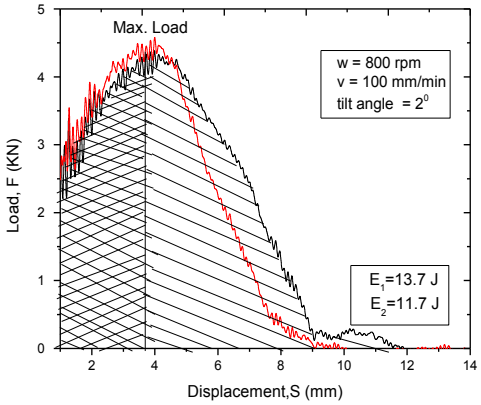

Fig.4-2h. load –displacement curve (800rpm,100mm/min)

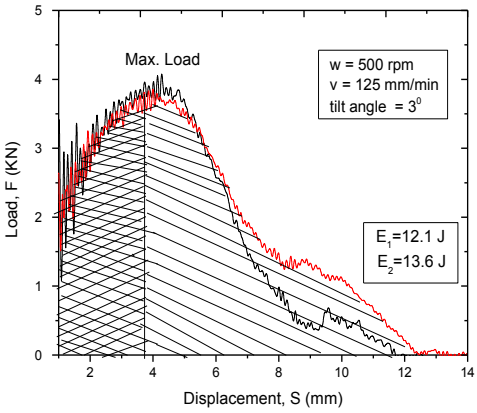

Fig.4-2i. load –displacement curve (500rpm,125mm/min)

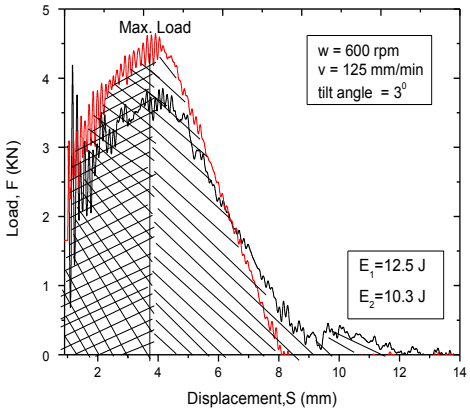

Fig.4-2j. load –displacement curve (600rpm,125mm/min)

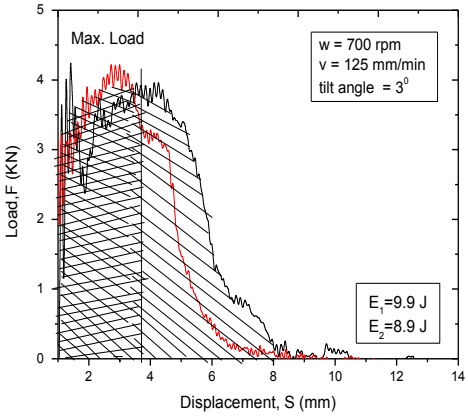

Fig.4-2k. load –displacement curve (700rpm,125mm/min)

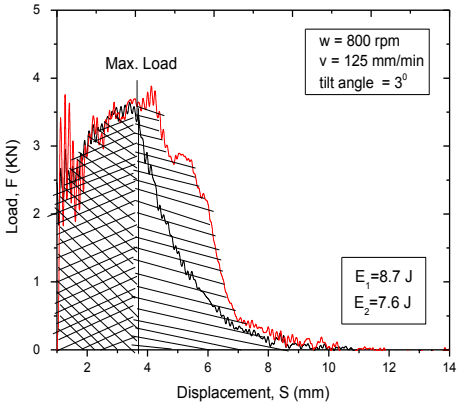

Fig.4-2l. load –displacement curve (800rpm,125mm/min)

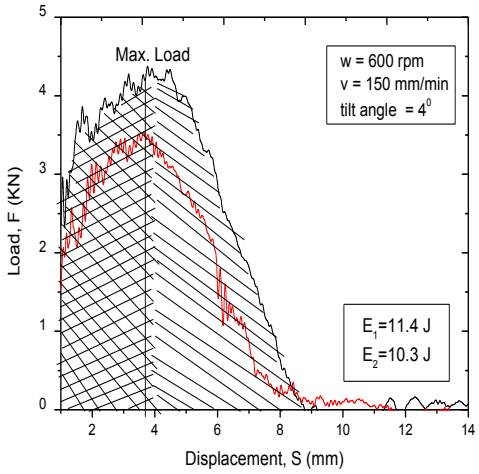

Fig.4-2n. load –displacement curve (600rpm,150mm/min)

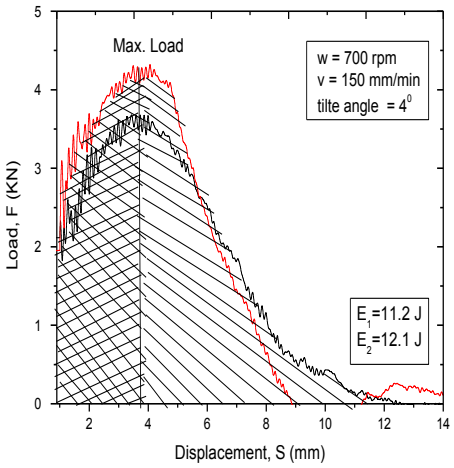

Fig.4-2m. load –displacement curve (700rpm,150mm/min)

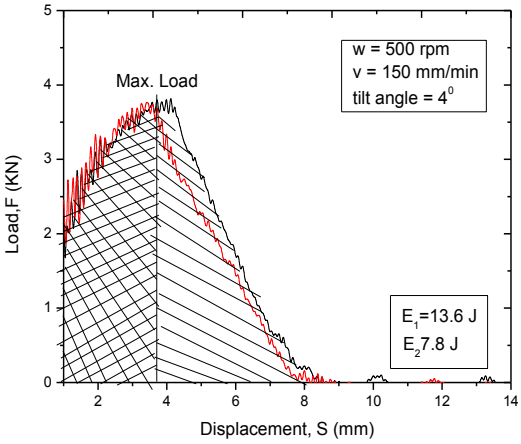

Fig.4-2o. load –displacement curve (500rpm,150mm/min)

Addition, from Figures 4-3, 4-4 shown the higher impact energy that means have high toughness at the specimens were welded by rotational speed 600 rpm and 700 rpm also the beast welding speed 100 mm/min and 125 mm/min. That means the big area under the curve; it has high absorbed energy and high toughness. On the other hand, less area under the curve, it has low absorbed energy and low toughness.

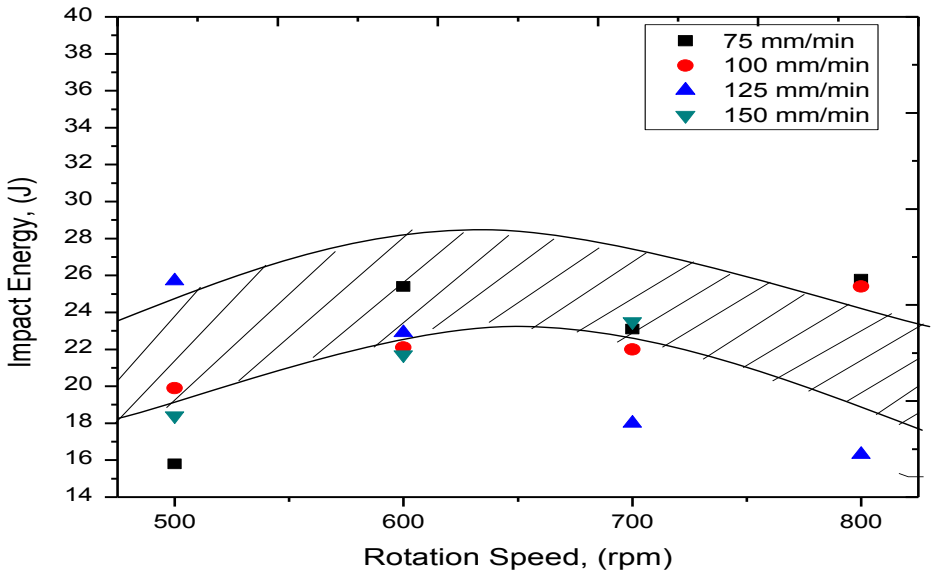

Figure 4-3. Relationship between impact energy and rotation speed

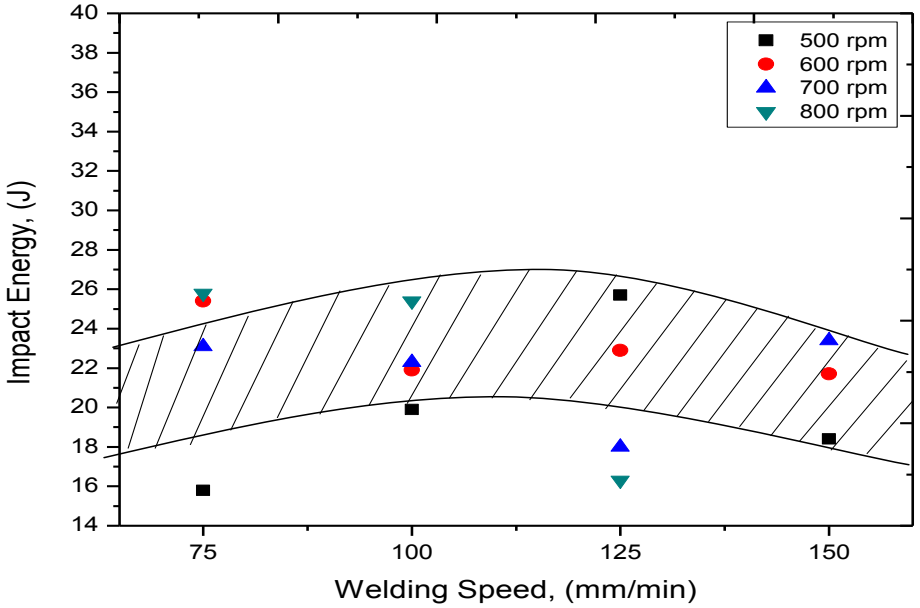

Figure 4-4. Relationship between impact energy and welding speed

4.1.3 Energy vs. Time Curve:

The charpy impact energy is affected by change in the fracture mechanism. The change in fracture mechanism therefore causes a gradual ductile to sharp brittle transition in the charpy impact energy. A brittle fracture is a low energy fracture and a ductile fracture is a high energy fracture. Microvoid coalescence is a ductile fracture mechanism and cleavage is a brittle fracture mechanism. However, it is possible for low energy or brittle fracture to occur by either ductile microviod coalescence or brittle cleavage, both fractures is toughness and fracture mechanism.

From Figure 4-5(a-o) shows the relationship between energy and time, it observed the transitional fracture refers to the change in fracture mechanism, typically from ductile to brittle as the time of the test increased, when the test is performed at relatively less time, the material undergoes cleavage (often referred to as brittle) fracture and the absorbed energy is very low, this region of the charpy curves is often referred to as lower shelf, and the slope region in the carve as crack extension is very rapid and cuts across the grains of the metal, also shows the increase in energy associated with fracture initiation and propagation phases. It can be seen that raise in fracture energy is mainly due to the propagation energy. Then the material undergoes to constant observed energy with change in time till end testing. This region as the brittle fracture is judged by the upper shelf energy. As shown in Figure 4-5(a – o).

Generally, the impact energy decreases with decreasing temperature as the yield strength increases and the ductility decreases. A sharp transition, where the energy changes by a large amount for a small temperature or time changes, if material has sharp ductile to brittle transition, the material has poor toughness.

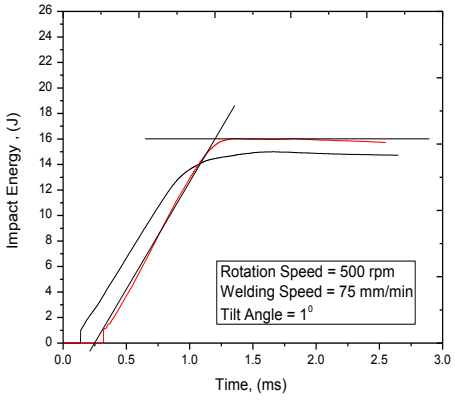

Fig.4-5a. Energy –Time curve (500rpm,75mm/min)

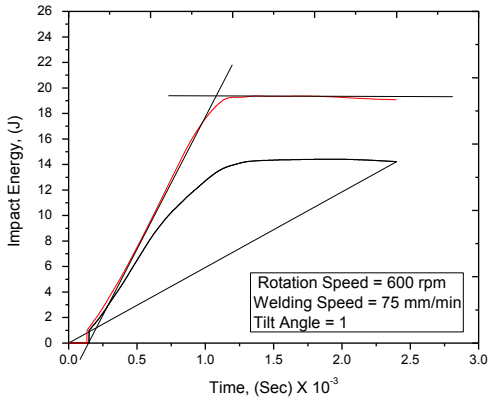

Fig.4-5b. Energy –Time curve (600rpm,75mm/min)

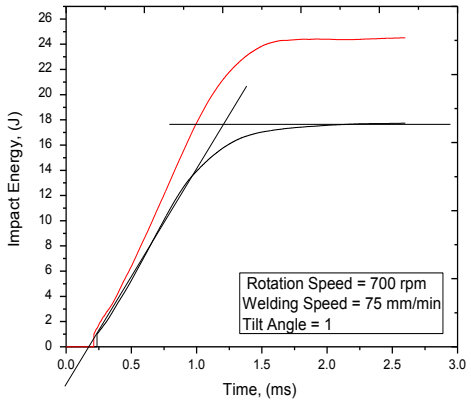

Fig.4-5c. Energy –Time curve (700rpm,75mm/min)

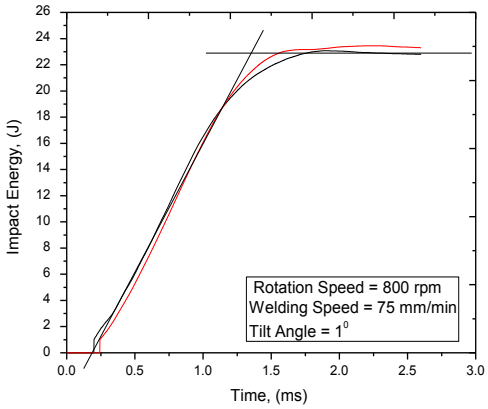

Fig.4-5d. Energy –Time curve (800rpm,75mm/min)

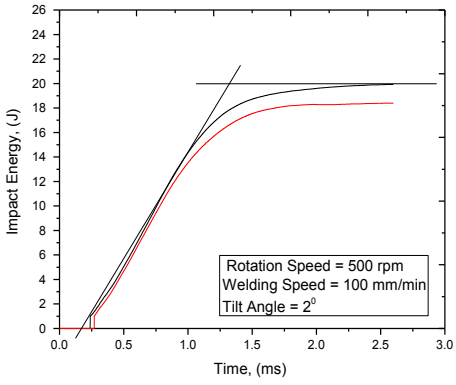

Fig.4-5e. Energy –Time curve (500rpm,100mm/min)

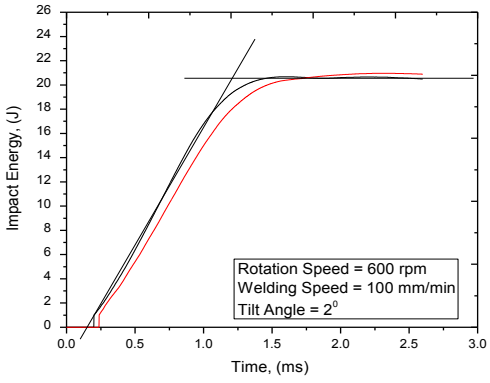

Fig.4-5f. Energy –Time curve (600rpm,100mm/min)

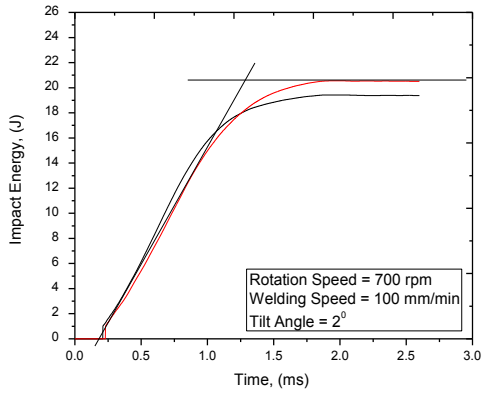

Fig.4-5g. Energy –Time curve (700rpm,100mm/min)

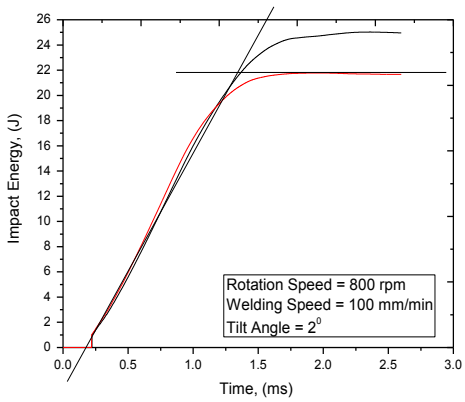

Fig.4-5h. Energy –Time curve (800rpm,100mm/min)

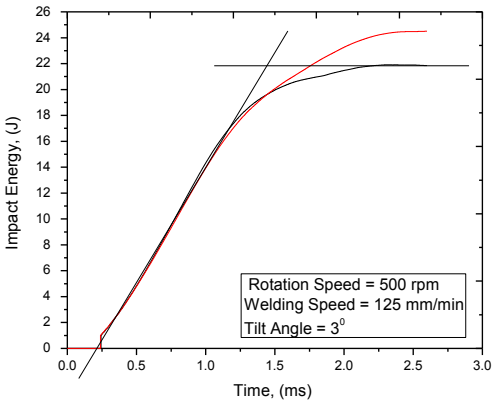

Fig.4-5i. Energy –Time curve (500rpm,125mm/min)

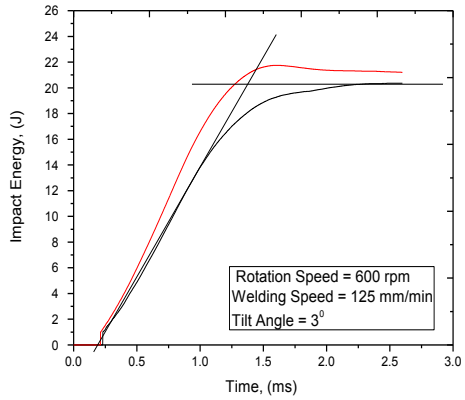

Fig.4-5j. Energy –Time curve (600rpm,125mm/min)

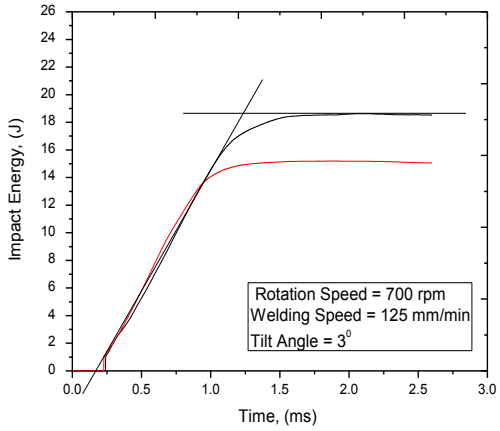

Fig.4-5k. Energy –Time curve (700rpm,125mm/min)

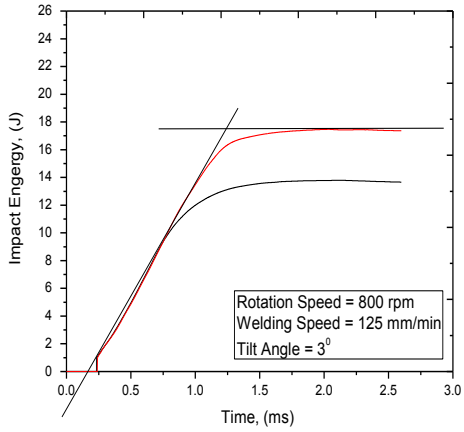

Fig.4-5l. Energy –Time curve (800rpm,125mm/min)

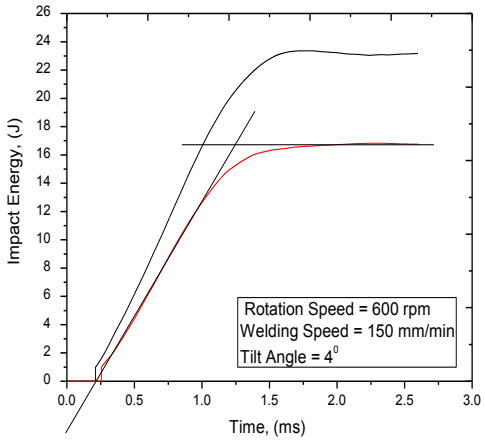

Fig.4-5n. Energy –Time curve (600rpm,150mm/min)

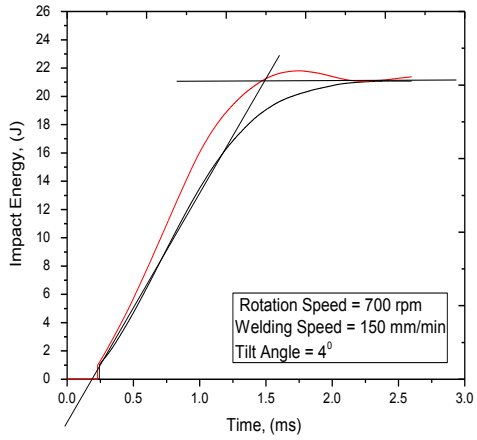

Fig.4-5m. Energy –Time curve (700rpm,150mm/min)

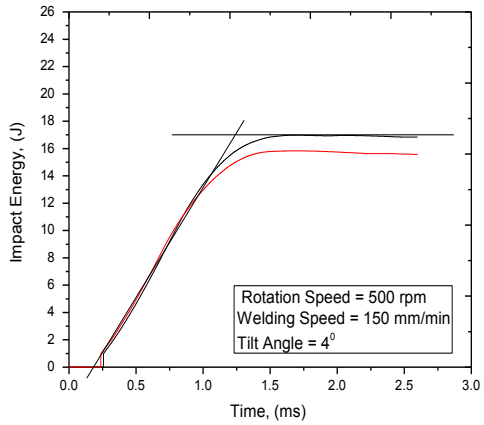

Fig.4-5o. Energy –Time curve (500rpm,150mm/min)

Additionally, from Figure 4-6 shows the change maximum impact energy with heat index and that observed the maximum impact energy was between 20 J and 22 J with heat index was between 4 rev/mm and 6 rev/mm. That means, the specimen has high impact energy, it has high absorbed energy and it has high toughness. As shown in Table 4-3.

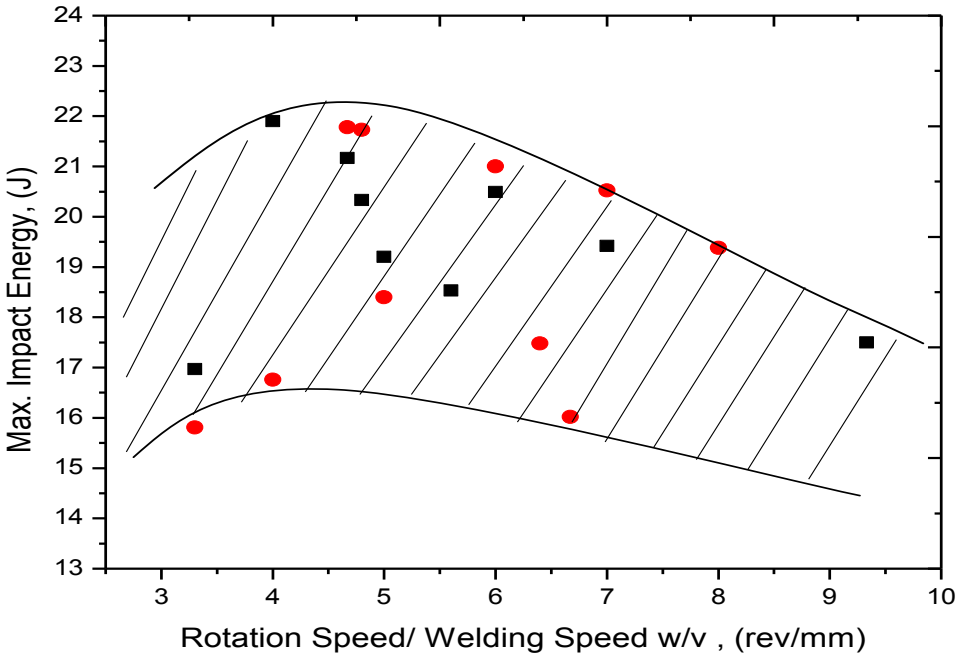

Figure 4-6. Relationship between maximum energy and heat index, w/v

Table 4-3. Shows Maximum Energy and Heat Index, w/v

Sample No.	Rotation Speed (rpm)	Welding Speed (mm/min)	Heat Index, ω/v (rev/mm)	Max. Impact Energy (J)
1.1	500	75	6.67	16.02
1.2	600	75	8	19.38
1.3	700	75	9.33	17.50
1.4	800	75	10.67	23.32
1.5	500	100	5	19.20
1.6	600	100	6	20.49
1.7	700	100	7	20.52
1.8	800	100	8	21.75
1.9	500	125	4	21.90
1.10	600	125	4.8	21.73
1.11	700	125	5.6	18.53
1.12	800	125	6.4	17.48
1.13	600	150	4	16.76
1.14	700	150	4.67	21.17
1.15	500	150	3.3	16.97

4.1.4 Rating of Computation Energy per Time dE/dt:

From Figure 4-7 shows the relationship between the impact energy per time dE/dt and heat index (rotational speed and welding speed (w/*v*)). Observed from this Figure, the optimized rate of computation impact energy (dE/dt) was between 18 KJ/sec to 20 KJ/sec and heat index (w/v) was between 5 rev/mm to 7 rev/mm, that means the beast absorbed energy for fracture specimen. Additionally, the optimized rate computation energy observed in specimens were welded by rotational speed 500 rpm to 700 rpm, welding speed 100 mm/min to 125 mm/min as shown in Table 4-4 and Figure 4-7 for changes of energy per time.

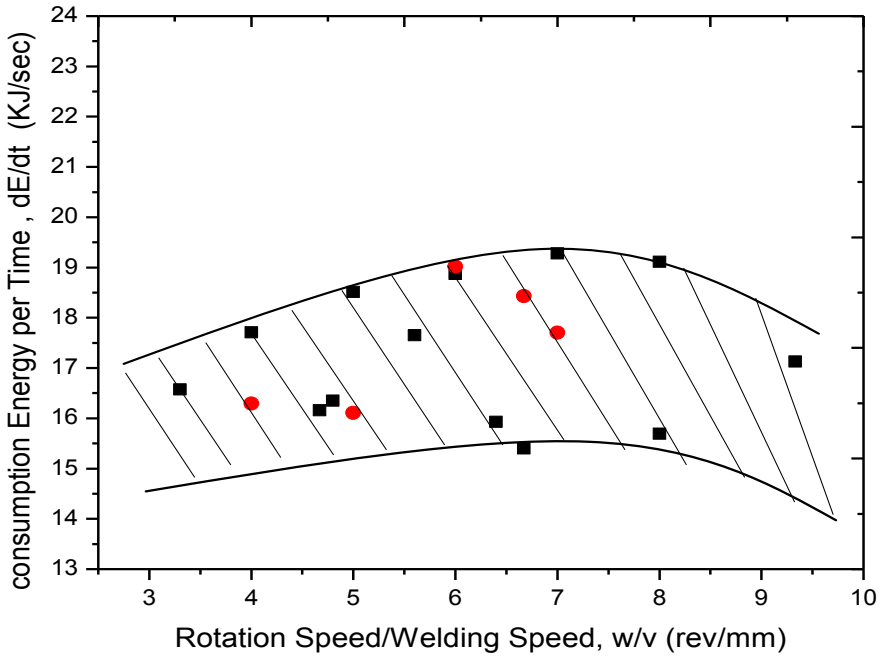

Figure 4-7. Relationship between consumption energy, dE/dt and heat index, w/v

Table 4-4. Shows Heat Index, w/v with Consumption Energy per Time dE/dt

Sample No.	Rotation Speed (rpm)	Welding Speed (mm/min)	Heat Index, ω/v (Rev/mm)	Consumption Energy per Time, dE/dt (kJ/sec)
1.1	500	75	6.67	18.43
1.2	600	75	8	15.69
1.3	700	75	9.33	17.13
1.4	800	75	10.67	20.29
1.5	500	100	5	18.51
1.6	600	100	6	18.87
1.7	700	100	7	19.28
1.8	800	100	8	19.11
1.9	500	125	4	17.71
1.10	600	125	4.8	16.35
1.11	700	125	5.6	17.65
1.12	800	125	6.4	15.93
1.13	600	150	4	16.29
1.14	700	150	4.67	16.16
1.15	500	150	3.3	16.57

4.1.5 Mechanical Behavior of Material:

The mechanical behavior of materials in Figure 4-8 observed the initiation fracture was starting from start charpy test to maximum load and from this point to rest charpy test is called the propagation fracture with absorbed energy until maximum absorbed then stabile energy to the end charpy test. Moreover, the point cross line of slop energy and line of maximum load is called transition point from ductile to brittle and cross point curve of load-time and curve energy-time is called the point of change absorbed energy as shown in (Figure 4-8). Often exhibits variations even for seemingly identical specimens and materials. The amount of shear in the surface failure of aluminum can be determined by looking at the fresh failure surface under low-power magnification.

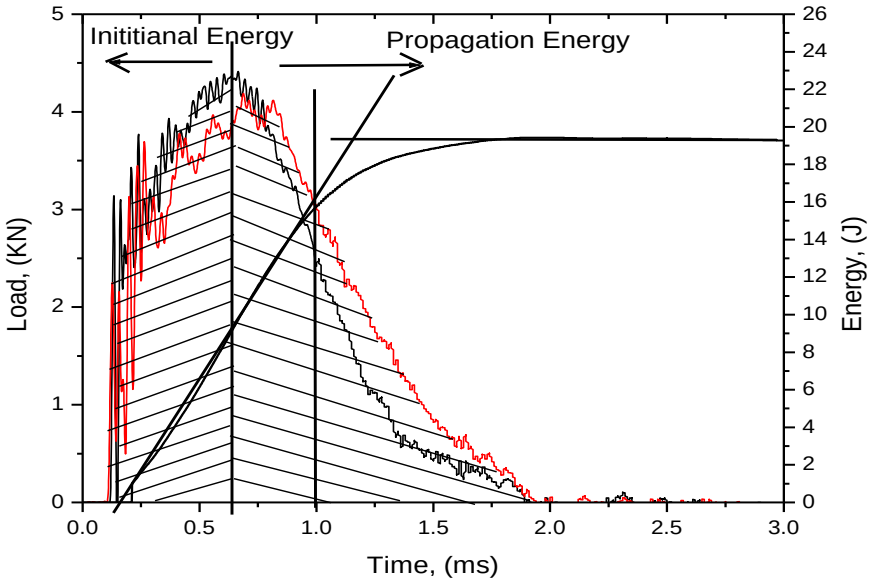

Figure 4-8. Impact Energy transition from ductile to brittle behavior.

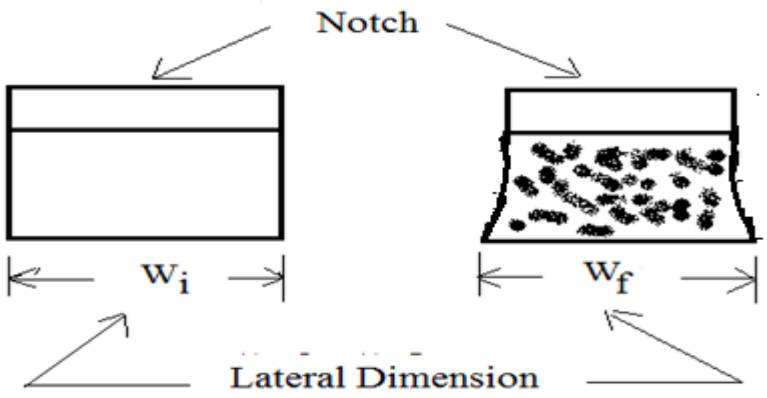

Figure 4-9. Lateral expansion of Charpy impact specimen.

A smooth surface is characteristic of shear. A fine grained fracture surface is characteristic of cleavage and brittleness (Figure 4-9).Often failures are mixed (part shear and part cleavage). If no plastic deformation accompanies fracture, it is generally a brittle fracture, i.e. cleavage. In the impact test the amount of plastic deformation is characterized by lateral expansion. Lateral expansion is a thickening of the specimen during fracturing. Looking at half the failed specimen that means the ductile fracture is accrued in specimen. The lateral expansion is measured as shown in Figure 4-9.

Where: lateral expansion = $\Delta W = W_f - W_i$

W_f = final lateral dimension

W_i = initial lateral dimension

4.1.6 Energy vs. Stress Curves:

Most of impact energy is absorbed by plastic deformation during the yielding of the specimen. Therefore, fractures are affecting the yield behavior and hence ductility of the material such as temperature, stress and strain rate will affect the impact energy. This type of behavior is more prominent in materials with a face centered cubic structure. Metals tend fail by one of two mechanisms, micro void coalescence or cleavage. That takes place along the crystal plane. Microvoid coalescence is the more common fracture mechanism where voids from as stress increases, and these voids eventually join together and failure occurs of the two fracture mechanisms cleavage involved for less plastic deformation hence absorbs far less fracture energy. The qualitative results of the impact test can be used to determine the ductility of a material. If the material breaks on a flat plane, the fracture was brittle, and if the material breaks with jagged edges or shear lips, then the fracture was ductile. Usually a material does not break in just one way or the other, and thus comparing the jagged to flat surface areas of the fracture will give an estimate of the percentage of ductile and brittle. For a given material the impact energy will be seen to decrease if the yield strength is increased, i.e. if the material undergoes some process that makes it more brittle and less able to undergo plastic deformation.

From Figure 4-10 (a – o) Energy - Stress curves, observed the specimen that welded by rotational speed 600 rpm, welding speed 75 and tilt angle 1^0, the feature of surface fracture were predominated ductile tearing with increasing stress unit yield point was maximum stress 30.1 N/mm^2. Then transitions from ductile to brittle tearing, also shown from Figures 4-10(e – o), the maximum stresses between 24.0 N/mm^2 to 27.6 N/mm^2 by impact energy between 10.0 J to 14.8 J. That means, when increased the stress, the absorbed energy is increased. Moreover, the feature of surface tearing depended on the various parameters of friction stir welding as rotational speed and welding speed. Moreover, from Figure 4- 11 and Table 4-5 observed the optimized maximum stress was between 26 N/mm^2 and 28 N/mm^2 with heat index was between 5 rev/mm and 7 rev/ mm.

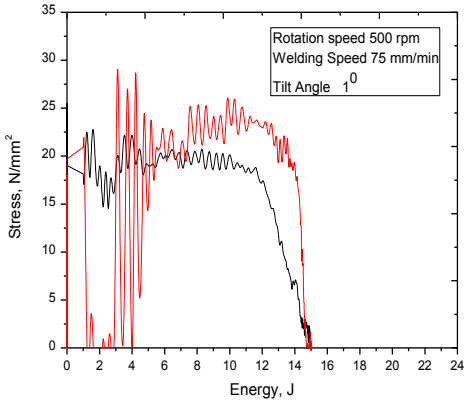

Fig.4-10a. Stress – Energy curve (500rpm,75mm/min)

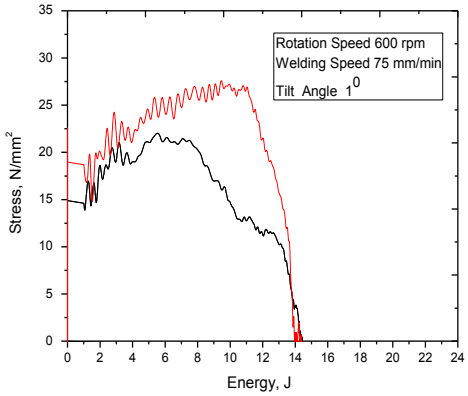

Fig.4-10b. Stress – Energy curve (600rpm,75mm/min)

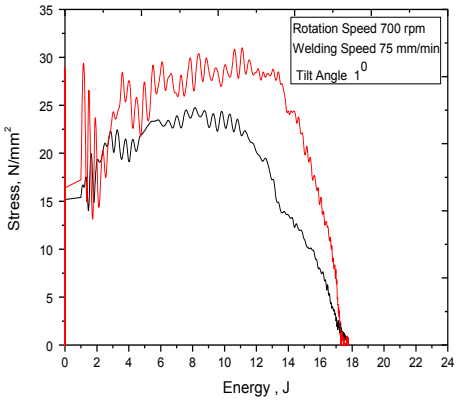

Fig.4-10c. Stress – Energy curve (700rpm,75mm/min)

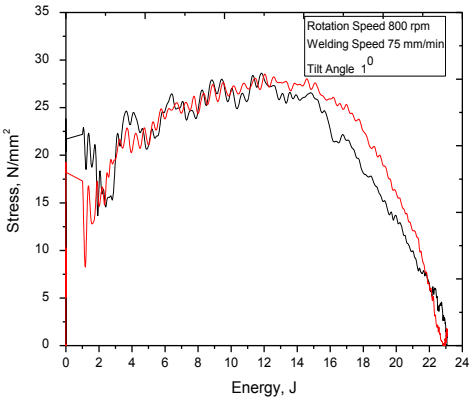

Fig.4-10d. Stress – Energy curve (800rpm,75mm/min)

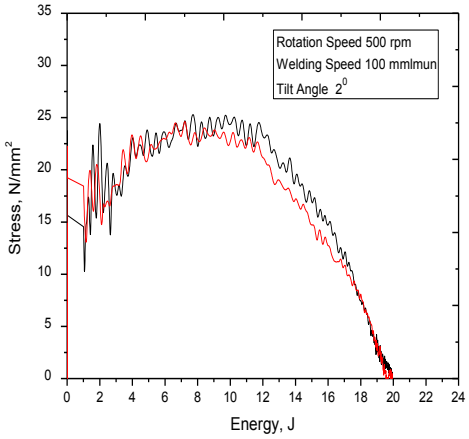

Fig.4-10e. Stress – Energy curve (500rpm,100mm/min)

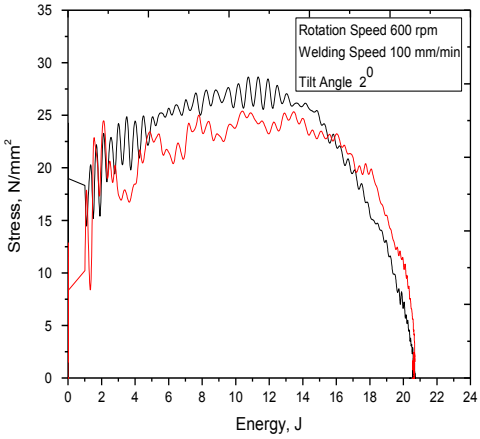

Fig.4-10f. Stress – Energy curve (600rpm,100mm/min)

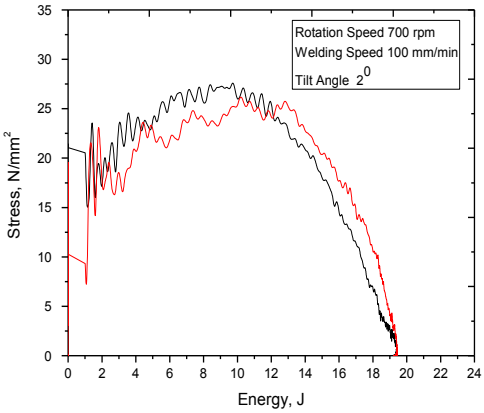

Fig.4-10g. Stress – Energy curve (700rpm,100mm/min)

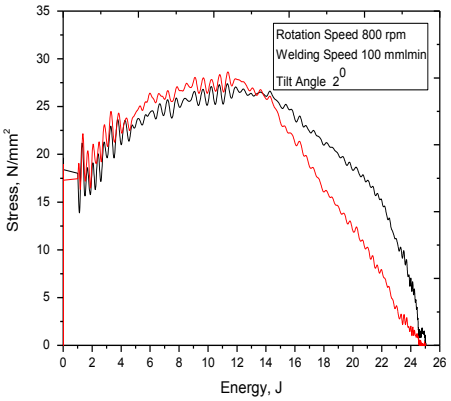

Fig.4-10h. Stress – Energy curve (800rpm,100mm/min)

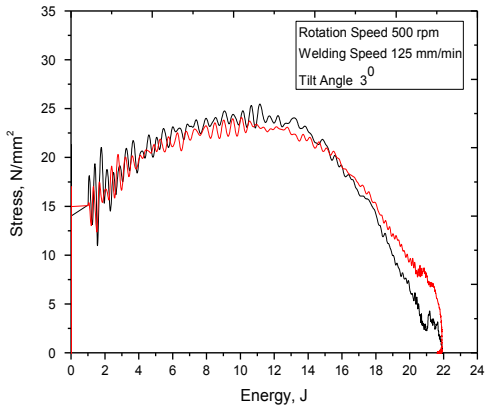

Fig.4-10i. Stress – Energy curve (500rpm,125mm/min)

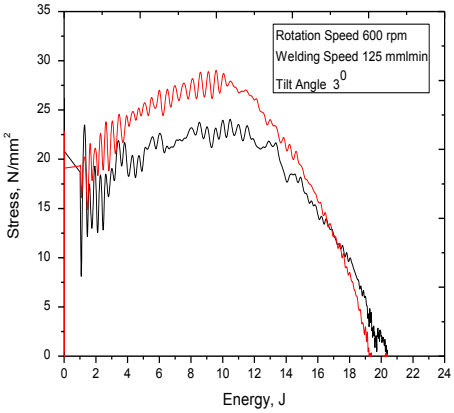

Fig.4-10j. Stress – Energy curve (600rpm,125mm/min)

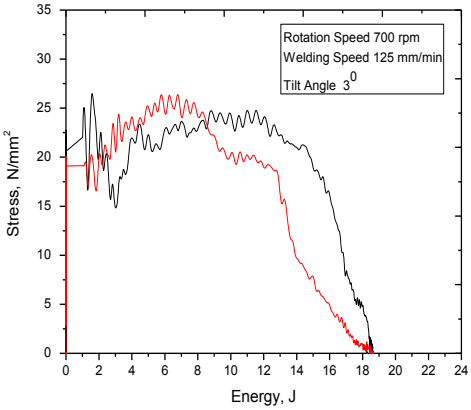

Fig.4-10k. Stress – Energy curve (700rpm,125mm/min)

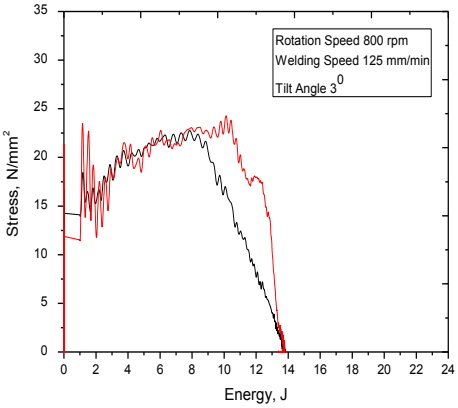

Fig.4-10l. Stress – Energy curve (800rpm,125mm/min)

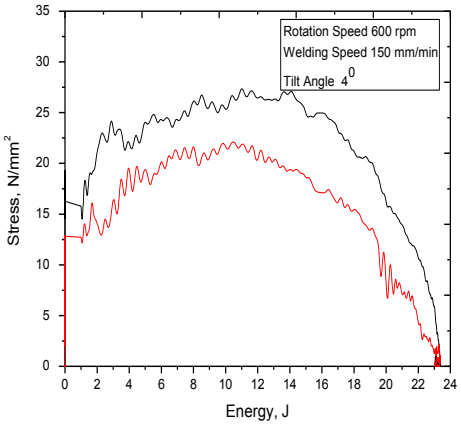

Fig.4-10n. Stress – Energy curve (600rpm,150mm/min)

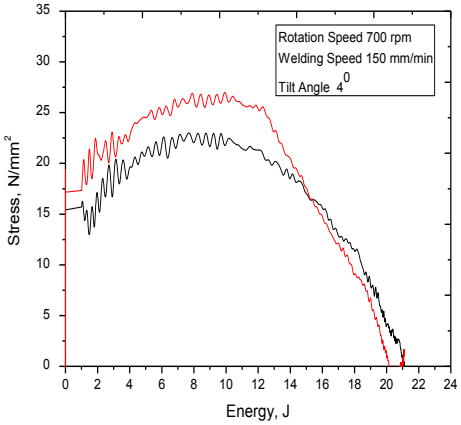

Fig.4-10m. Stress – Energy curve (700rpm,150mm/min)

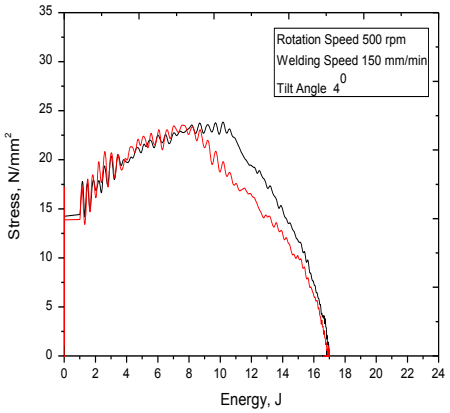

Fig.4-10o. Stress – Energy curve (500rpm,150mm/min)

Table 4-5. Shows the Heat Index, w/v and Stress

Sample No.	Rotation Speed (rpm)	Welding Speed (mm/min)	Tilt Angle (degree)	Heat Index, ω/v (Rev/mm)	Maximum Stress (N/mm^2)
1.1	500	75	1^0	6.67	23.2
1.2	600	75	1^0	8	26.8
1.3	700	75	1^0	9.33	23.3
1.4	800	75	1^0	10.67	27.6
1.5	500	100	2^0	5	24.9
1.6	600	100	2^0	6	27.6
1.7	700	100	2^0	7	27.5
1.8	800	100	2^0	8	27.7
1.9	500	125	3^0	4	25.1
1.10	600	125	3^0	4.8	27.7
1.11	700	125	3^0	5.6	25
1.12	800	125	3^0	6.4	24
1.13	600	150	4^0	4	27
1.14	700	150	4^0	4.67	27
1.15	500	150	4^0	3.3	24

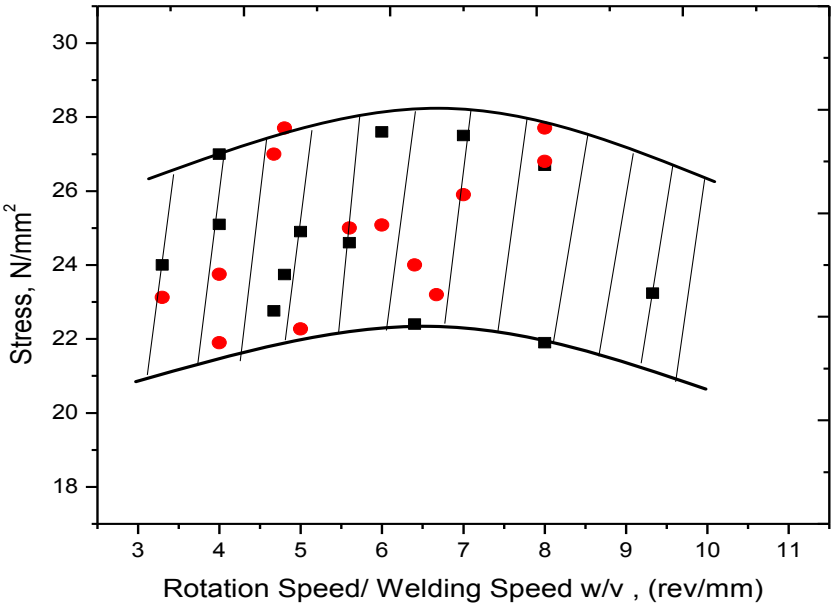

Figure 4-11. Relationship between Heat Index, w/v and stress.

4.1.7 Macro-Photographs of Charpy Test Specimens:

As result of charpy test, images of surface fracture of all specimens after testing by impact test by different rotational speed and welding speed ware shown from Figure 4-12a_1, the appearance of fracture is dominating dull (ductile fracture) and it has absorbed energy was 14.83 J . Shown in Figure 4.12a_2, views of fracture is shear or brittle fracture, it is about 20% and predominated ductile tearing. This specimen has absorbed energy was 16.02 J. Feature of fracture in Figure 4.12b_1, shown existed two type of fracture: one is brittle fracture about 15% and second is ductile about 85% with exist micro void. This sample, it has absorbed energy was 14.31 J. Furthermore, shown in Figure 4.12b_2, is predominated ductile tearing on surface fracture, also it has 19.38 J observed energy with existed semi cleavage, it coalescence with ductile fracture.

From Figures 4.12c to 4.12j they have same feature that have dull appearance (ductile fracture), plastic deformation. (See feature fracture in images below). Moreover, that fracture is coalescence with semi- cleavage facets and existed micro- void, also these have absorbed energy from range 17 J to 24 J (see Figures 4.5 (a – o)). From Figure 4.12k_1, shows the appearance ductile tearing; it is about 50% and 50% brittle fracture. This specimen has absorbed energy was 18.53 J. From views fracture of Figures 4.12k_2, 4.12l_2 that are predominated ductile fracture about 80% dull tearing and 20% brittle fracture, also these samples have absorbed energy, it was 15.20 J, 17.48 J respectively. Shown in Figure 4.12l_1, it has feature 60% predominated brittle cleavage and 40% dominating ductile tearing that has absorbed energy equals 13.75 J. Finally, from Figures 4.12n to 4.12o shows dominating dull, ductile tearing with semi cleavage coalescence with ductile tearing. These have absorbed energy were 16 J to 23 J. Furthermore, specimens were welded by rotation speed 700 rpm, 800 rpm, welding speed 75 mm/min, also specimens were welded by rotation speed between 500 to 800 rpm, welding speed 100 mm/min, and specimens were welded by rotational speed 500 rpm, 600 rpm, welding speed 125 mm/min. Additionally specimens were welded by rotation speed between 500 to 700 rpm and welding speed 150 mm/ min, they shown the same feature tearing were the dominating ductility fracture with edges lip were shearing or brittle.

Fig.4-12a$_1$. Macrophoto. fracture (500rpm,75mm/min)

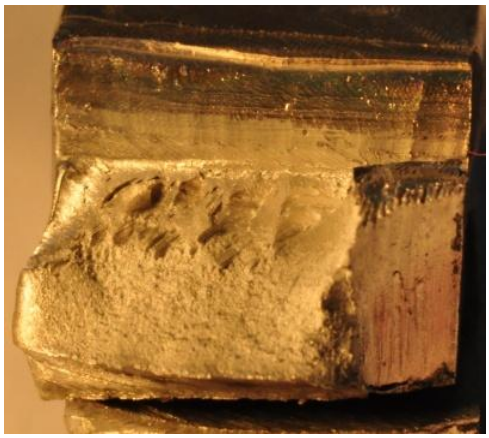

Fig.4-12a$_2$. Macrophoto. fracture (500rpm,75mm/min)

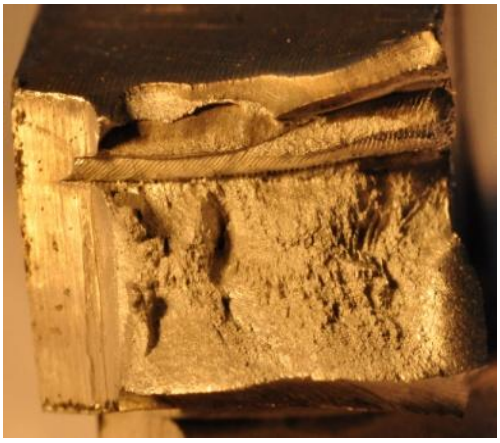

Fig.4-12b$_1$. Macrophoto. fracture (600rpm,75mm/min)

Fig.4-12b$_2$. Macrophoto. fracture (600rpm,75mm/min)

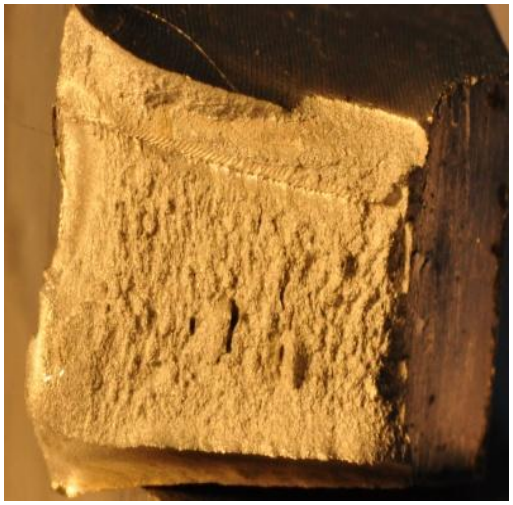

Fig.4-12c$_1$. Macrophoto. fracture (700rpm,75mm/min)

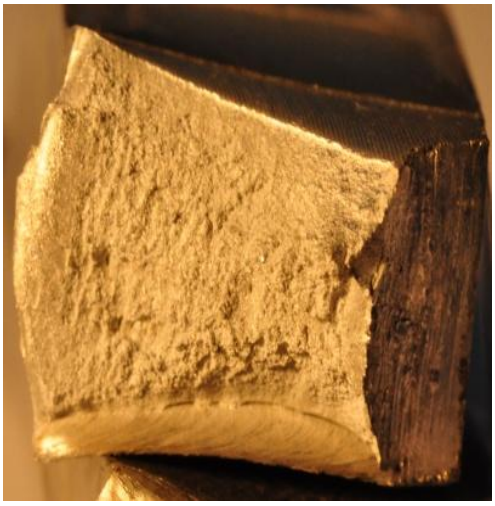

Fig.4-12c$_2$. Macrophoto. fracture (700rpm,75mm/min)

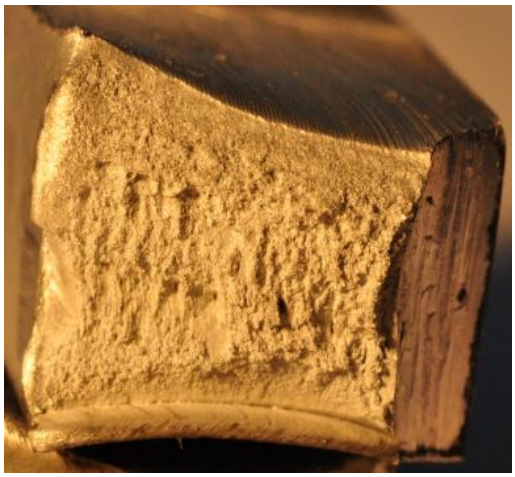

Fig.4-12d$_1$. Macrophoto. fracture (800rpm,75mm/min)

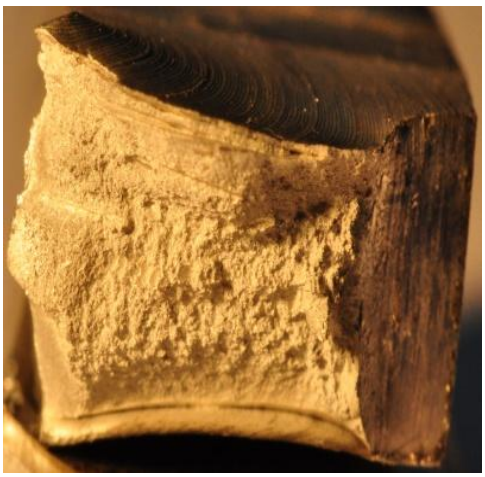

Fig.4-12d$_2$. Macrophoto. fracture (800rpm,75mm/min)

Fig.4-12e$_1$. Macrophoto. fracture (500rpm,100mm/min)

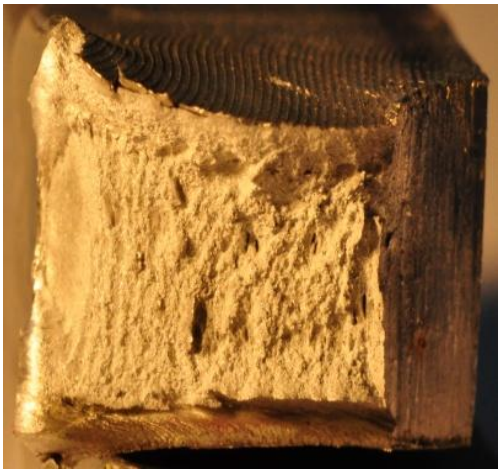

Fig.4-12e$_2$. Macrophoto. fracture (500rpm,100mm/min)

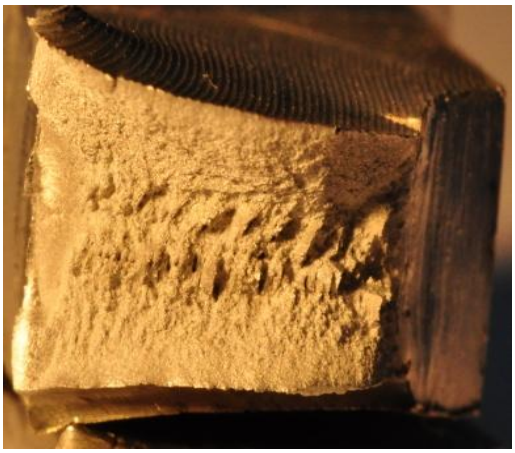

Fig.4-12f$_1$. Macrophoto. fracture (600rpm,100mm/min)

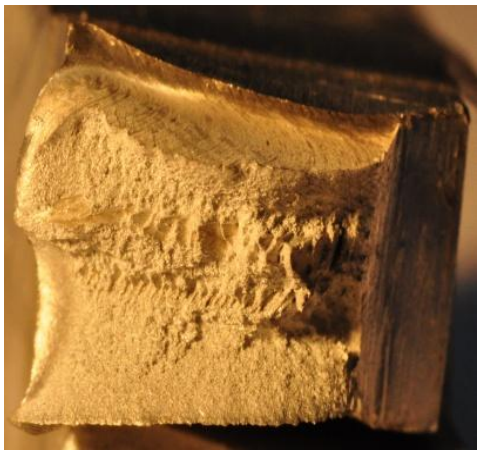

Fig.4-12f$_2$. Macrophoto. fracture (600rpm,100mm/min)

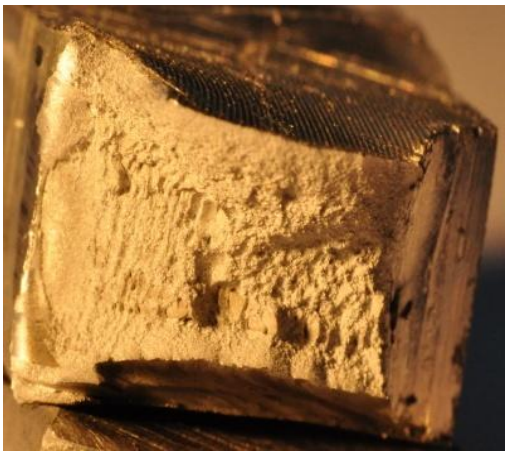

Fig.4-12g$_1$. Macrophoto. fracture (700rpm,100mm/min)

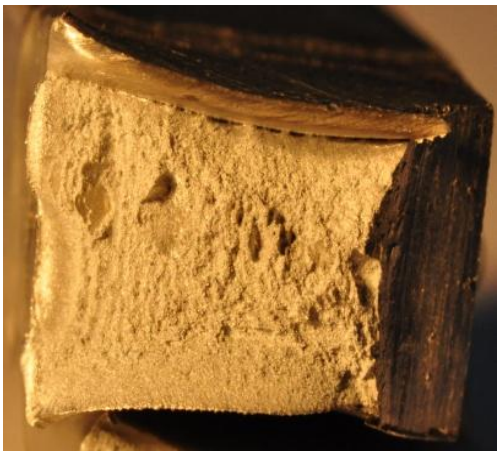

Fig.4-12g$_2$. Macrophoto. fracture (700rpm,100mm/min)

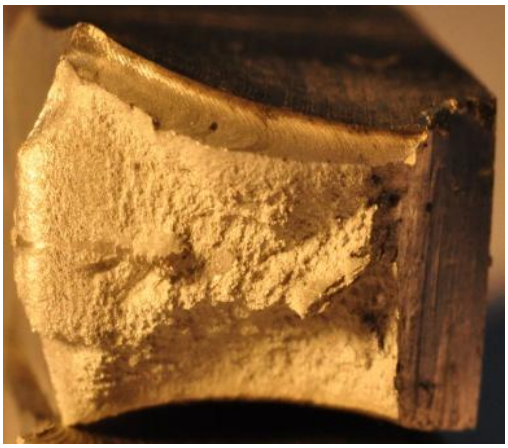

Fig.4-12h$_1$. Macrophoto. fracture (800rpm,100mm/min)

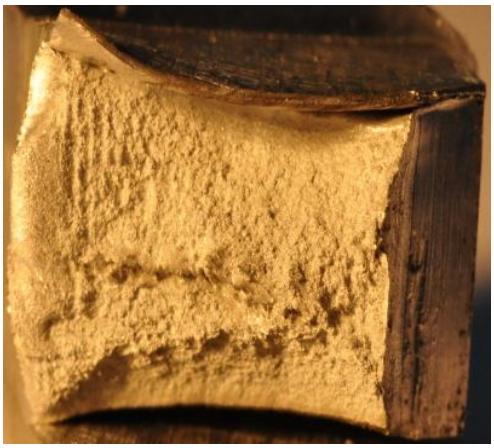

Fig.4-12h$_2$. Macrophoto. fracture (800rpm,100mm/min)

Fig.4-12i$_1$. Macrophoto. fracture (500rpm,125mm/min)

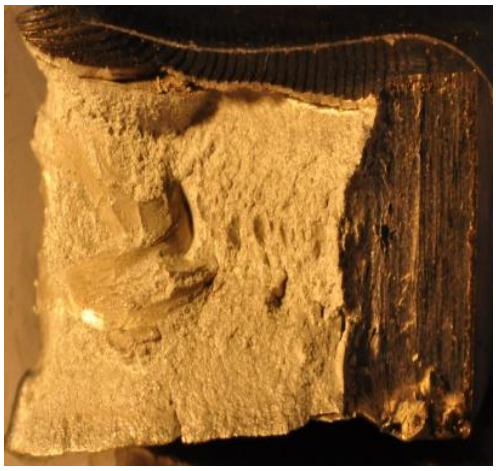

Fig.4-12i$_2$. Macrophoto. fracture (500rpm,125mm/min)

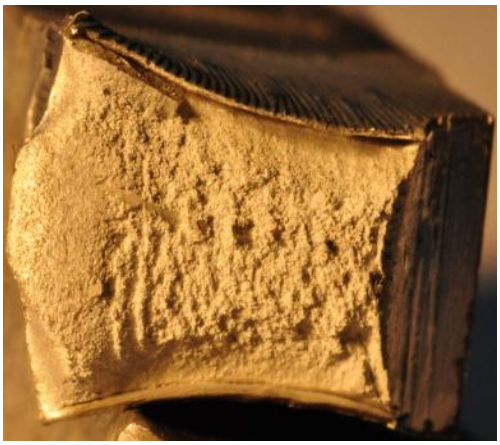

Fig.4-12j$_1$. Macrophoto. fracture (600rpm,125mm/min)

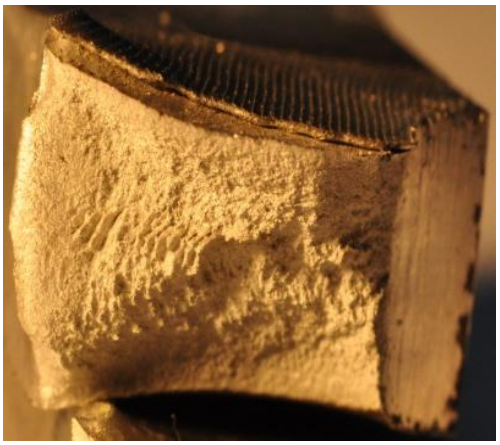

Fig.4-12j$_2$. Macrophoto. fracture (600rpm,125mm/min)

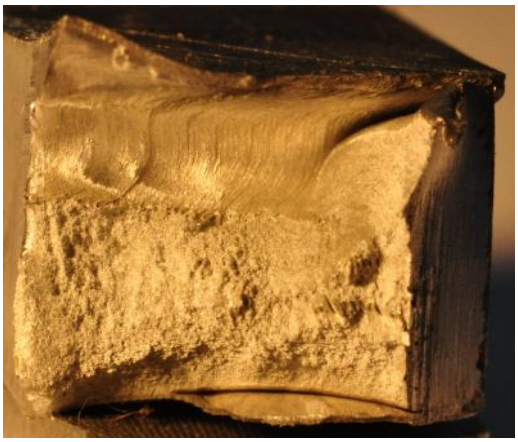

Fig.4-12k$_1$. Macrophoto. fracture (700rpm,125mm/min)

Fig.4-12k$_2$. Macrophoto. fracture (700rpm,125mm/min)

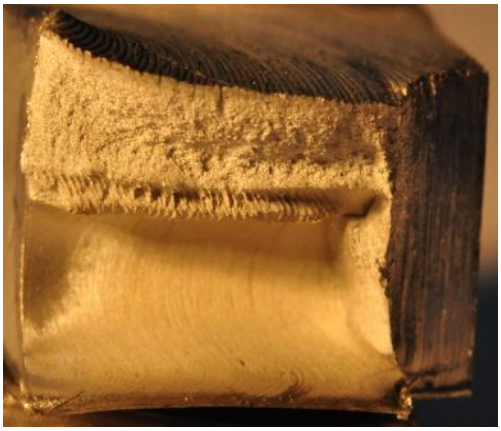

Fig.4-12l$_1$. Macrophoto. fracture (800rpm,125mm/min)

Fig.4-12l$_2$. Macrophoto. fracture (800rpm,125mm/min)

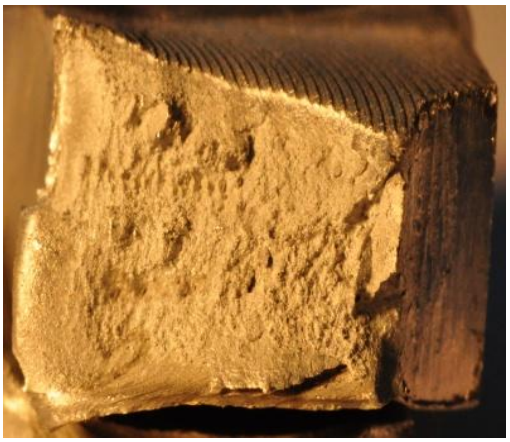

Fig.4-12n$_1$. Macrophoto. fracture (600rpm,150mm/min)

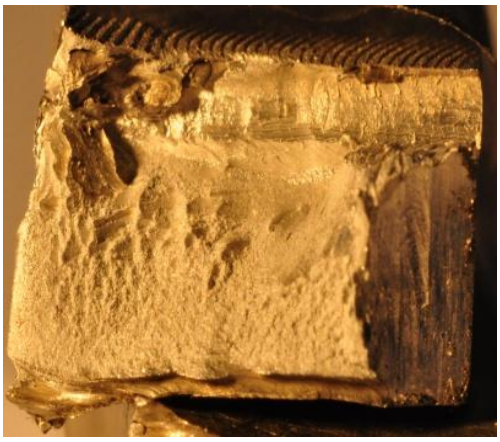

Fig.4-12n$_2$. Macrophoto. fracture (600rpm,150mm/min)

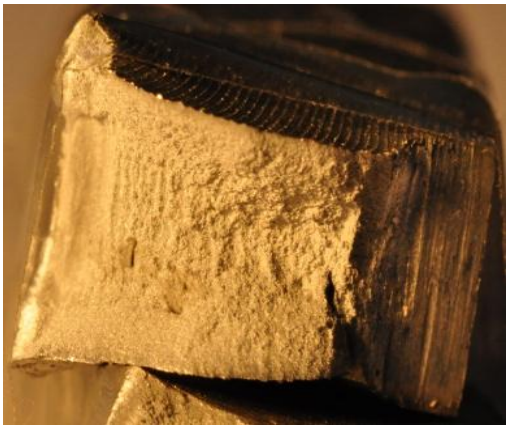

Fig.4-12m$_1$. Macrophoto. fracture (700rpm,150mm/min)

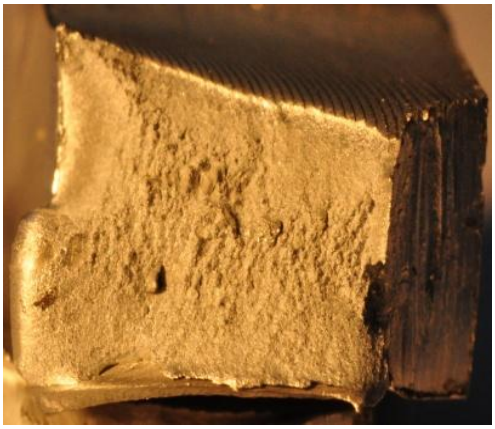

Fig.4-12m$_2$. Macrophoto. fracture (700rpm,150mm/min)

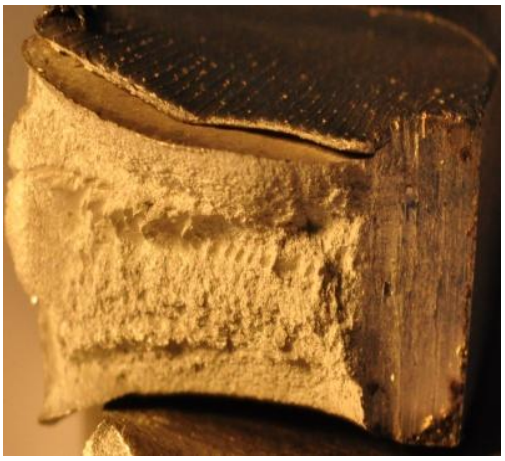

Fig.4-12o$_1$. Macrophoto. fracture (500rpm,150mm/min)

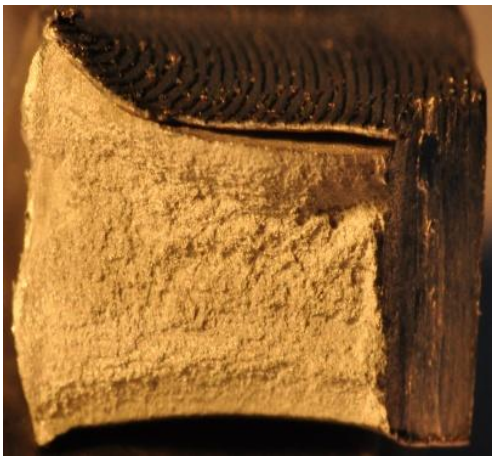

Fig.4-12o$_2$. Macrophoto. fracture (500rpm,150mm/min)

4.1.8 Investigations of Photographs Scanning Electron Microscope (SEM):

In term of using SEM for investigations for understood fracture mechanism after done charpy test, from Figure 4-13 shown the surface tearing of specimens ware welded by rotational speed 500 rpm, welding speed 75 mm/min and tilt angle 1^0, it was ductile fracture with existed the microvoid near the notch also upper side the specimen was more heating than lower side due to contact with shoulder and pin. Moreover, from Figure 4-14 observed the predominated ductile fracture with existed the fracture and microvoid in the nugget zone and shown the shear or cleavage in the lower surface of specimen that was welded by 600 rpm, 75 mm/min and tilt 1^0. Also from Figure 4-15, 4-16 shown the type of tearing close to notch were brittle then propagation fracture in nugget zone by ductile tearing due to exist semi cleavage and microvoid also the side of specimens tearing as edge lip of shear fracture these specimens were welded by 700 rpm, 800 rpm, 75 mm/min and tilt angle 1^0. That means, if absorbed energy is high, the specimens have high toughness.

Furthermore, observation from Figures 4-17 to 4-19 that specimens were welded by rational speed between 500rpm to 700 rpm and constant welding speed was 100 mm/min and tilt angle 2^0, the dominating ductile fracture in nugget zone with existed cleavage and void, also the upper surface of specimens were affected by more heating due to shoulder and probe.

Addition, from Figure 4-20 shown the type of tearing as brittle fracture due to less absorbed energy with existed fracture that specimen was welded by 800 rpm, 100 mm/min and tilt angle 2^0. From Figures 4-21 to 4-24, shown the same surface fracture were dominated ductile coalescence by edge lip of brittle fracture with exist microvoid in the nugget zone and seen in the stirred zone onion ring that specimens were welded by 500 rpm, 600 rpm, welding speed 125 mm/min, tilt 3^0 and specimens were welded by 600 rpm, 500 rpm, welding speed 150 mm/min and tilt angle 4^0 respectively. That means if specimens have low absorbed energy, the specimens have low toughness.

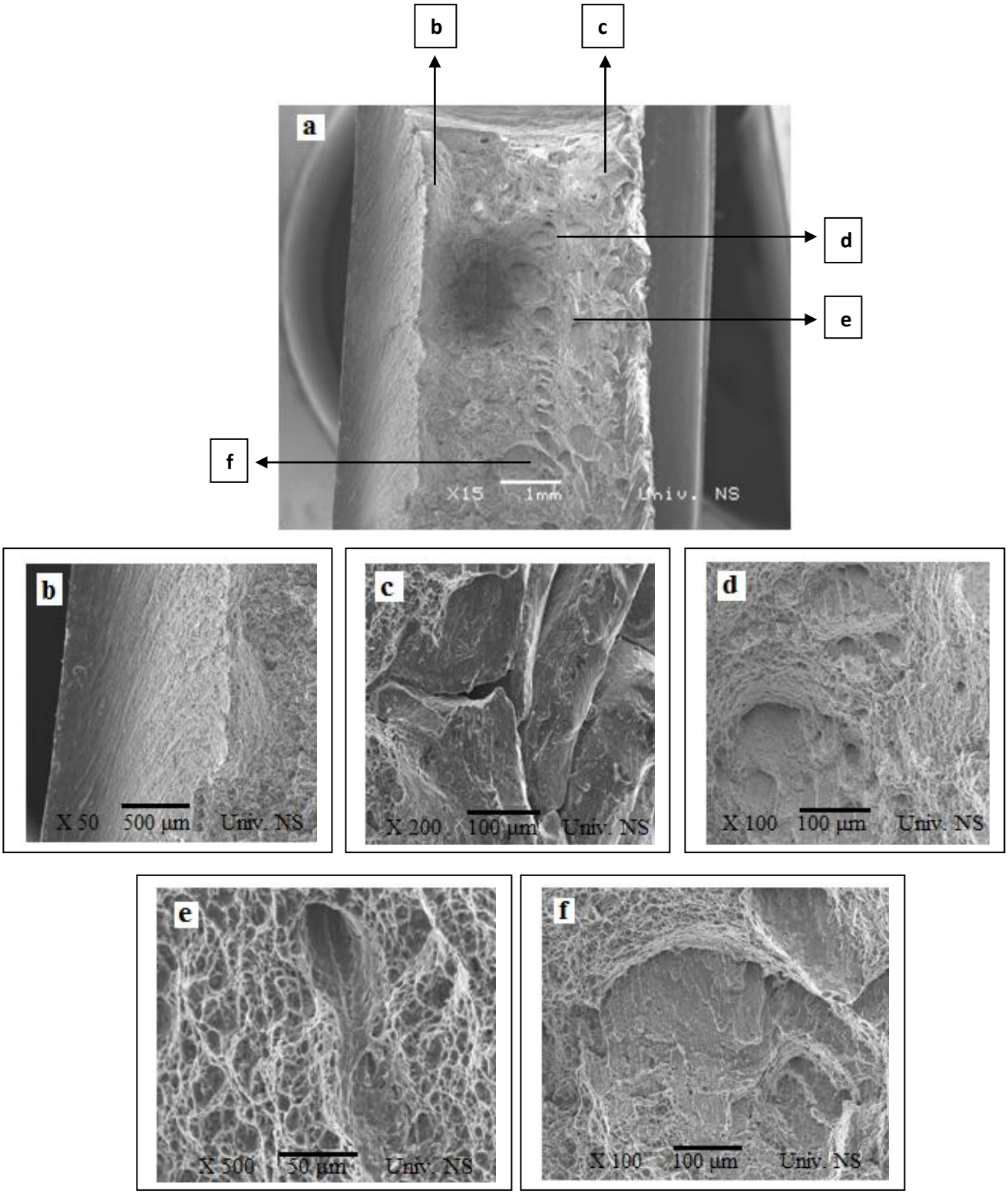

Figure 4-13(a – f). SEM Surface Fracture by Parameters (500 rpm, 75 mm/min and Tilt 1^0).

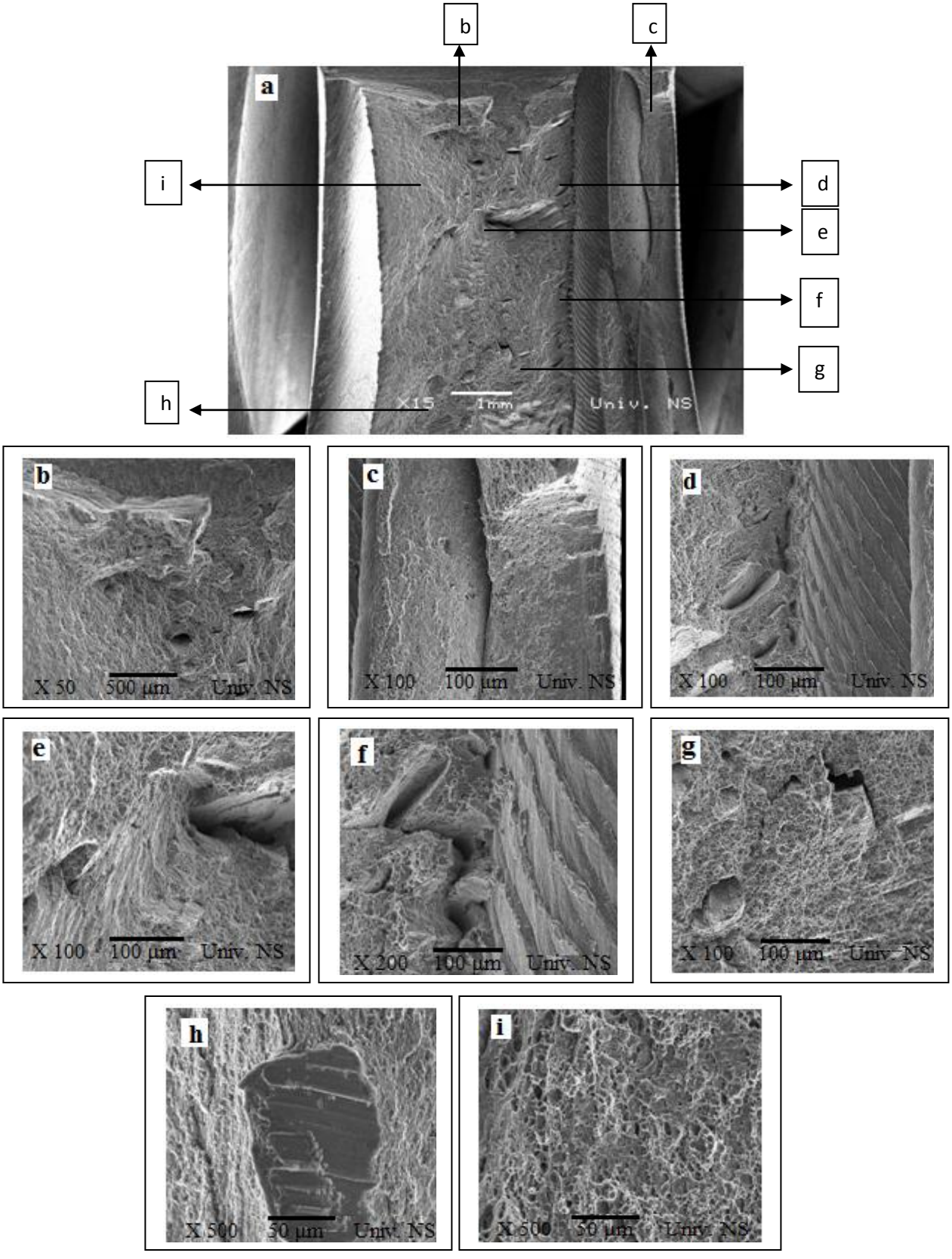

Figure 4-14(a – i). SEM Surface Fracture by Parameters (600 rpm, 75 mm/min and Tilt 1^0).

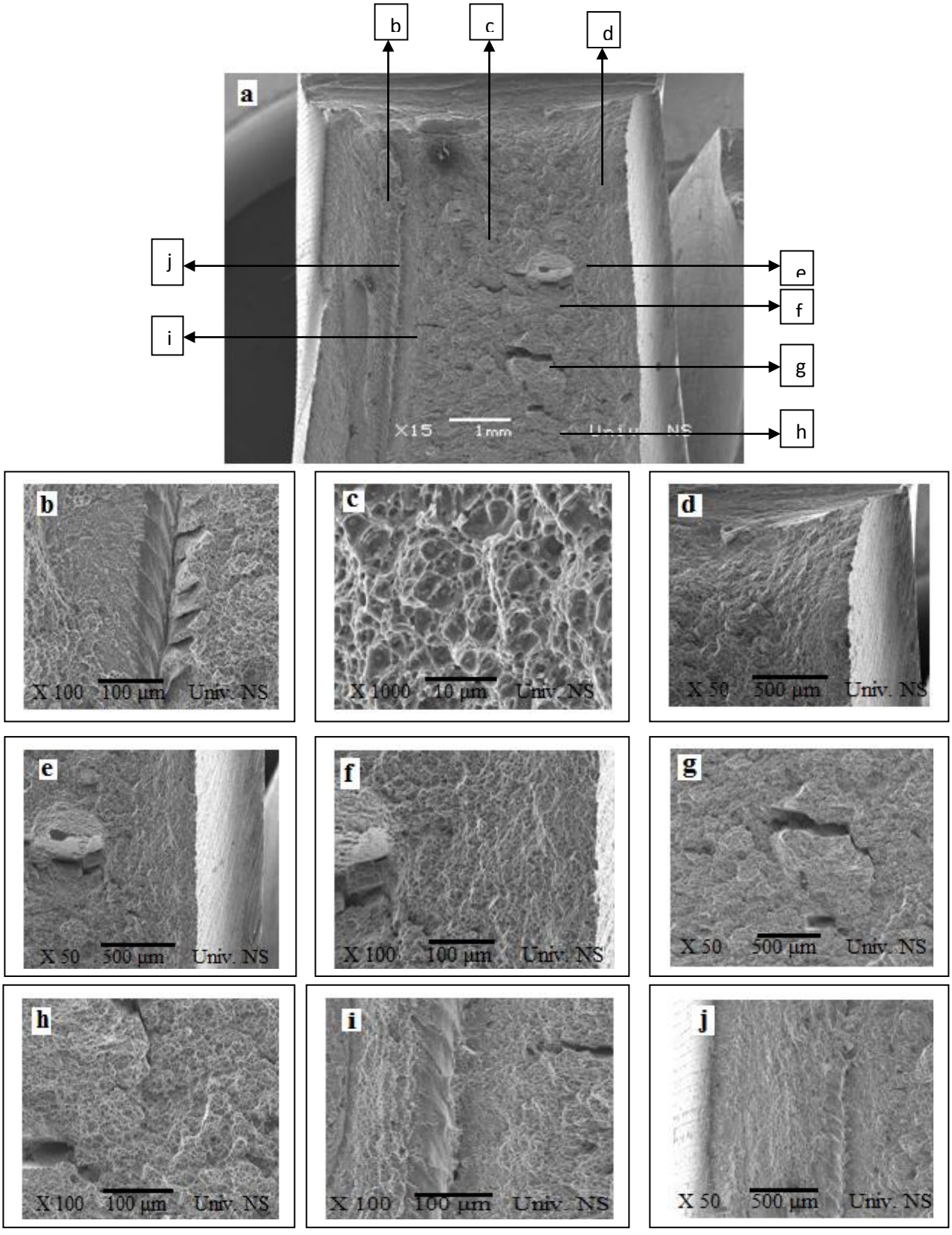

Figure 4-15(a- j). SEM Surface Fracture by Parameters (700 rpm, 75 mm/min and Tilt 1^0).

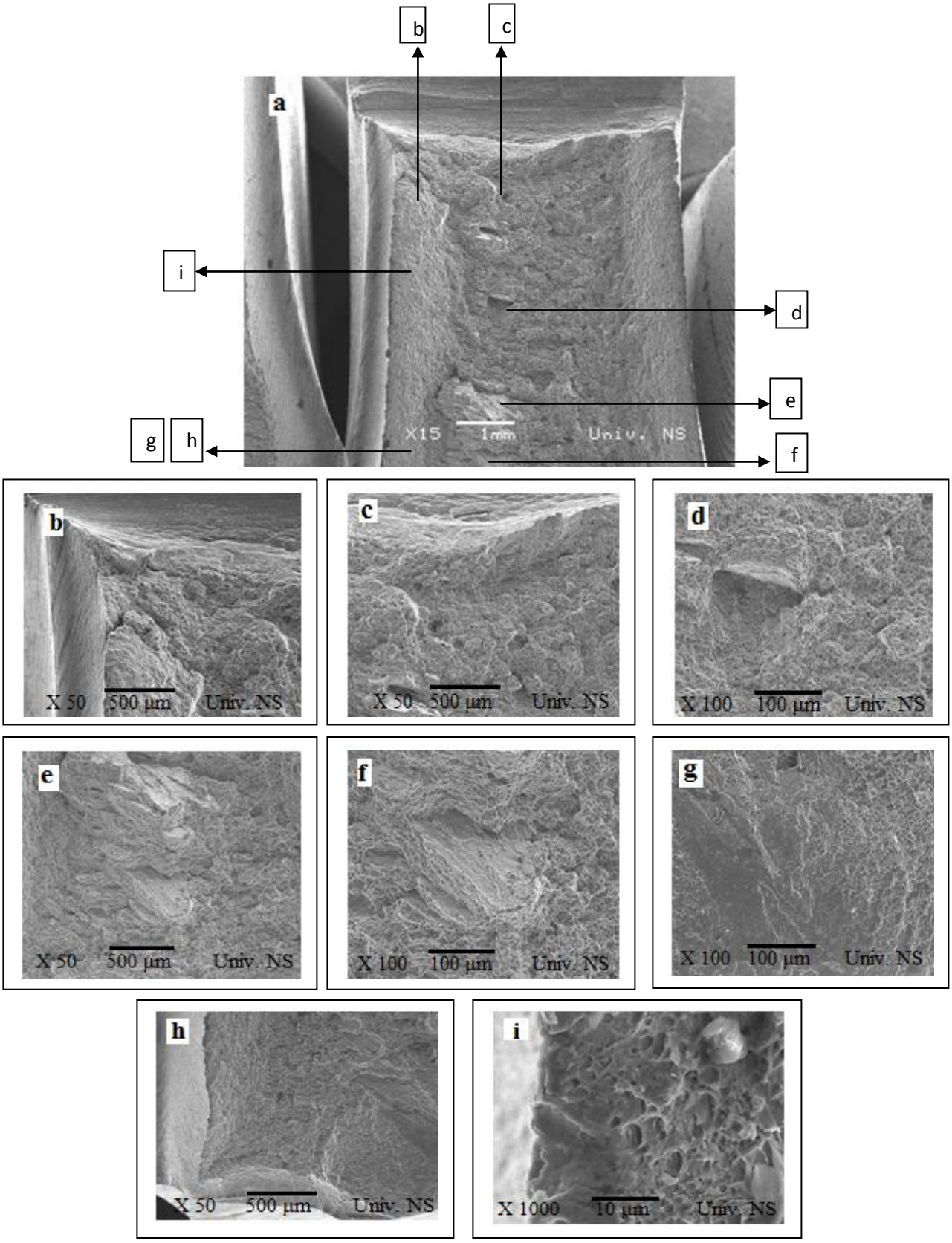

Figure 4-16(a – i). SEM Surface Fracture by Parameters (800 rpm, 75 mm/min and Tilt 1^0).

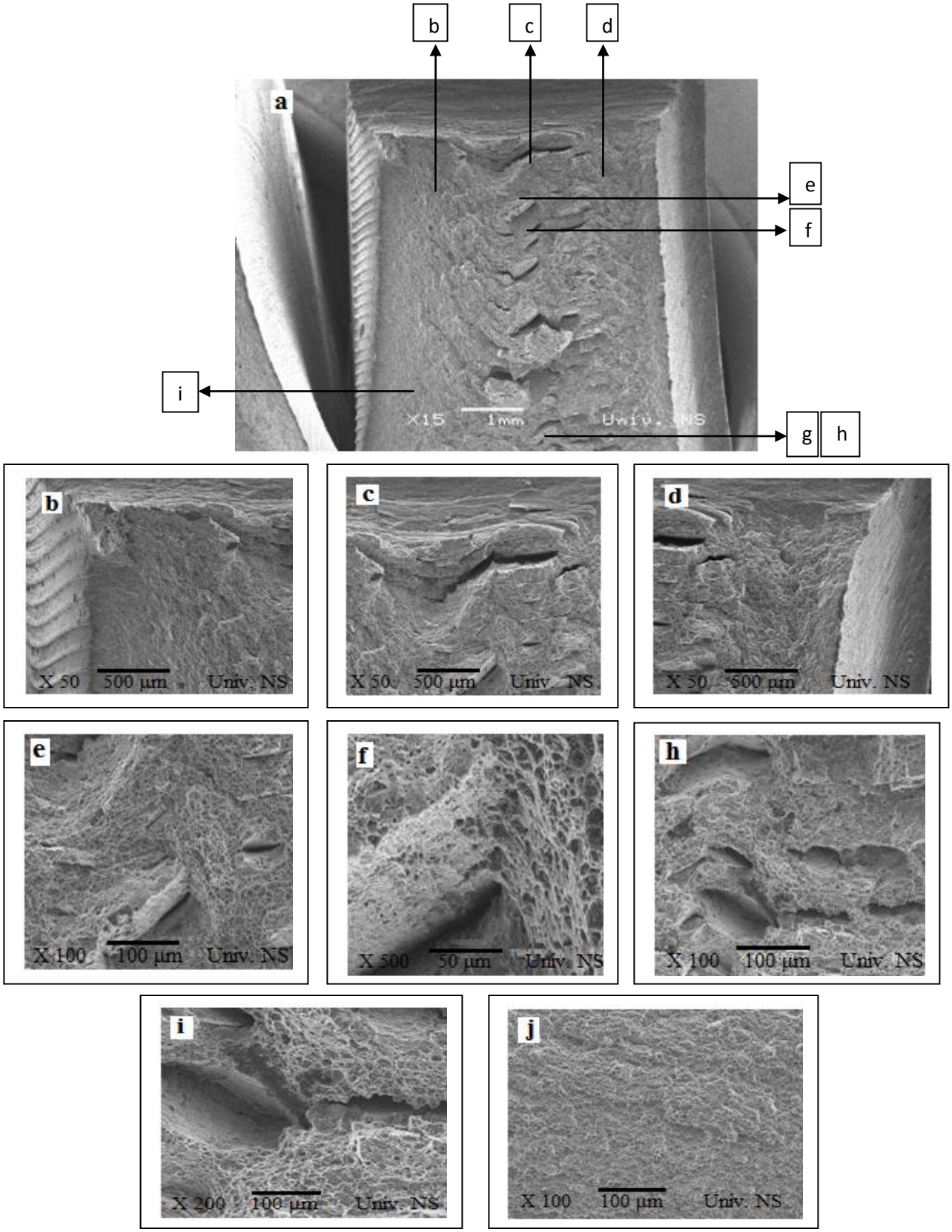

Figure 4-17(a – j). SEM Surface Fracture by Parameters (500 rpm, 100 mm/min and Tilt 2^0).

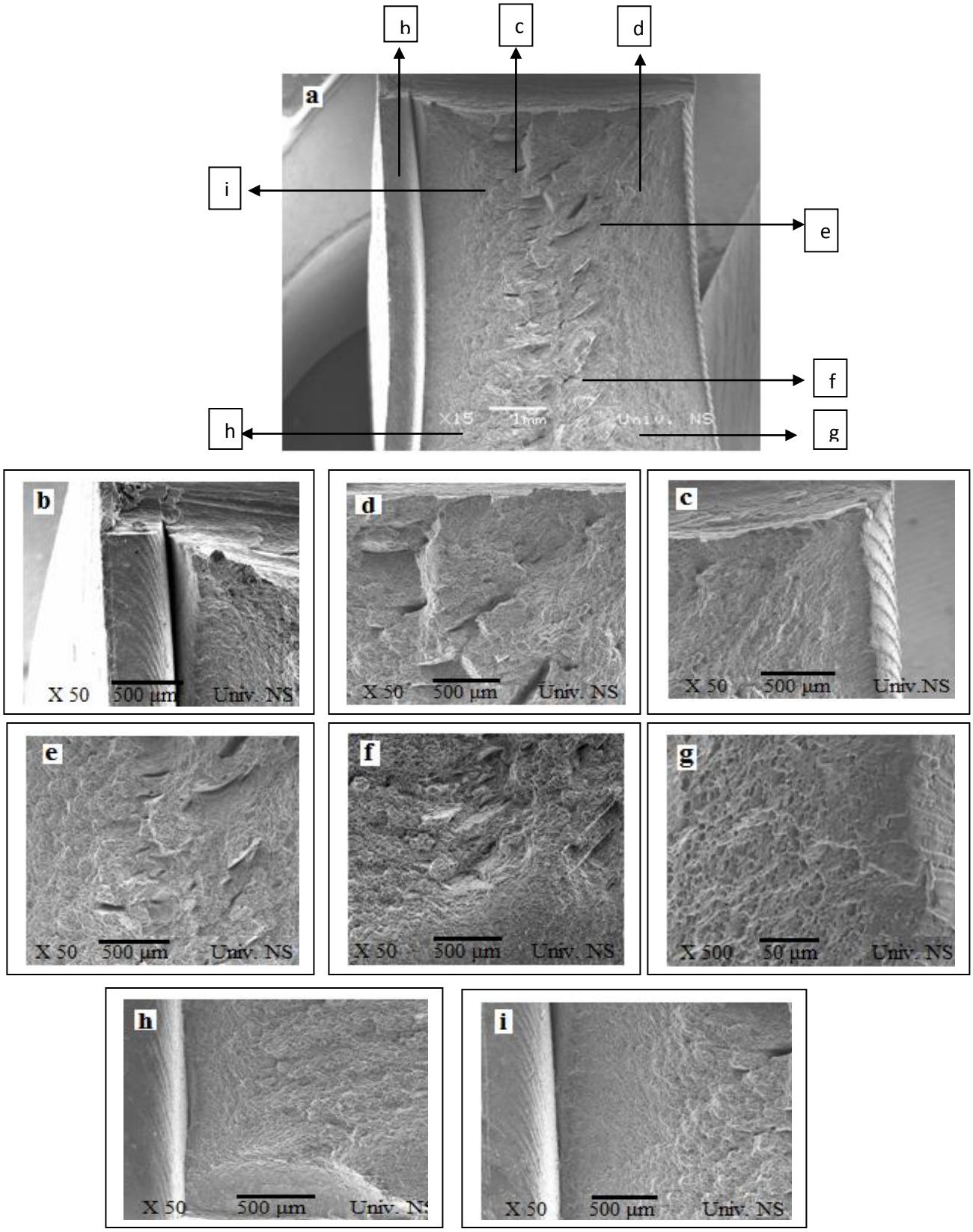

Figure 4-18(a – i). SEM Surface Fracture by Parameters (600 rpm, 100 mm/min and Tilt 2^0).

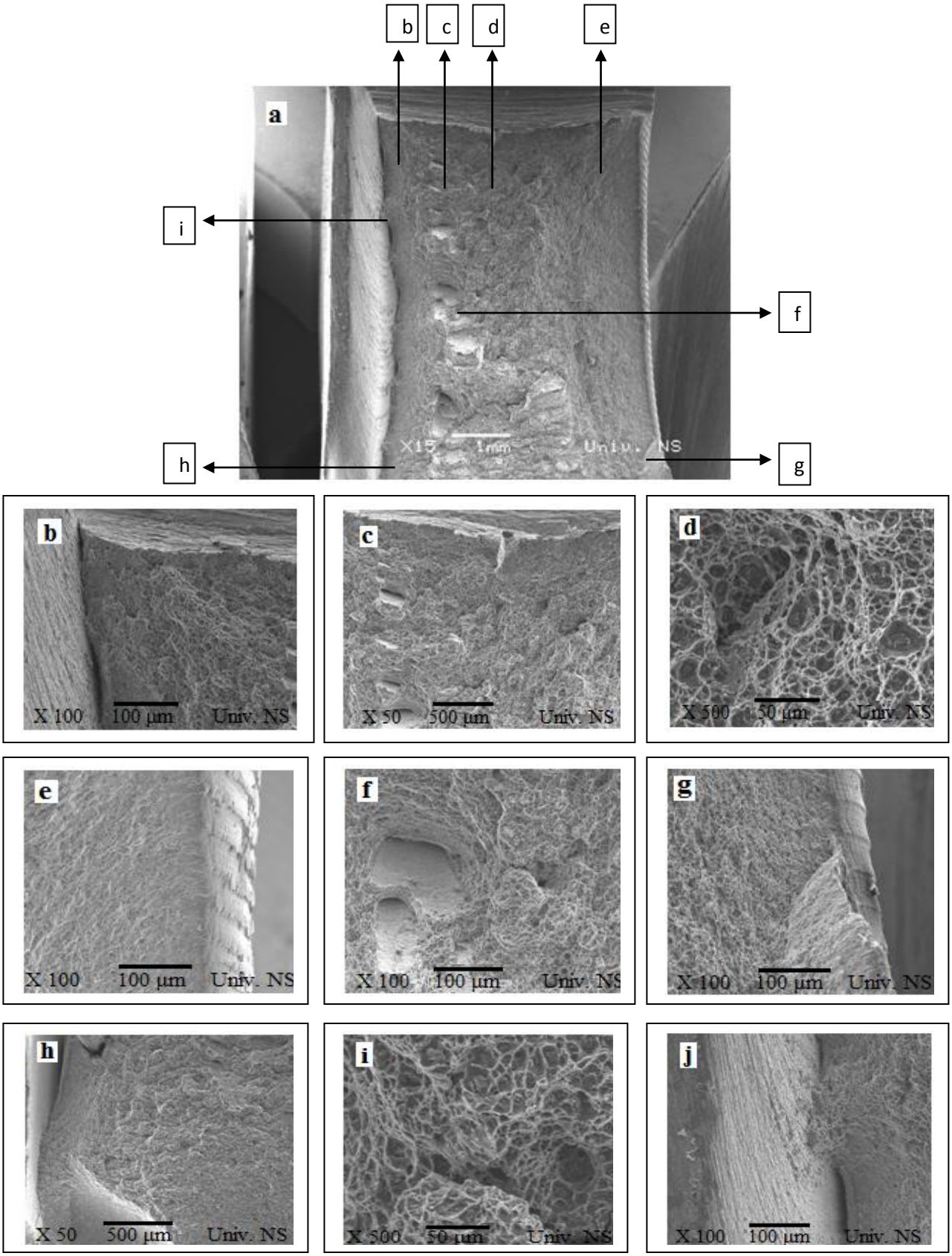

Figure 4-19(a – j). SEM Surface Fracture by Parameters (700 rpm, 100 mm/min and Tilt 2^0).

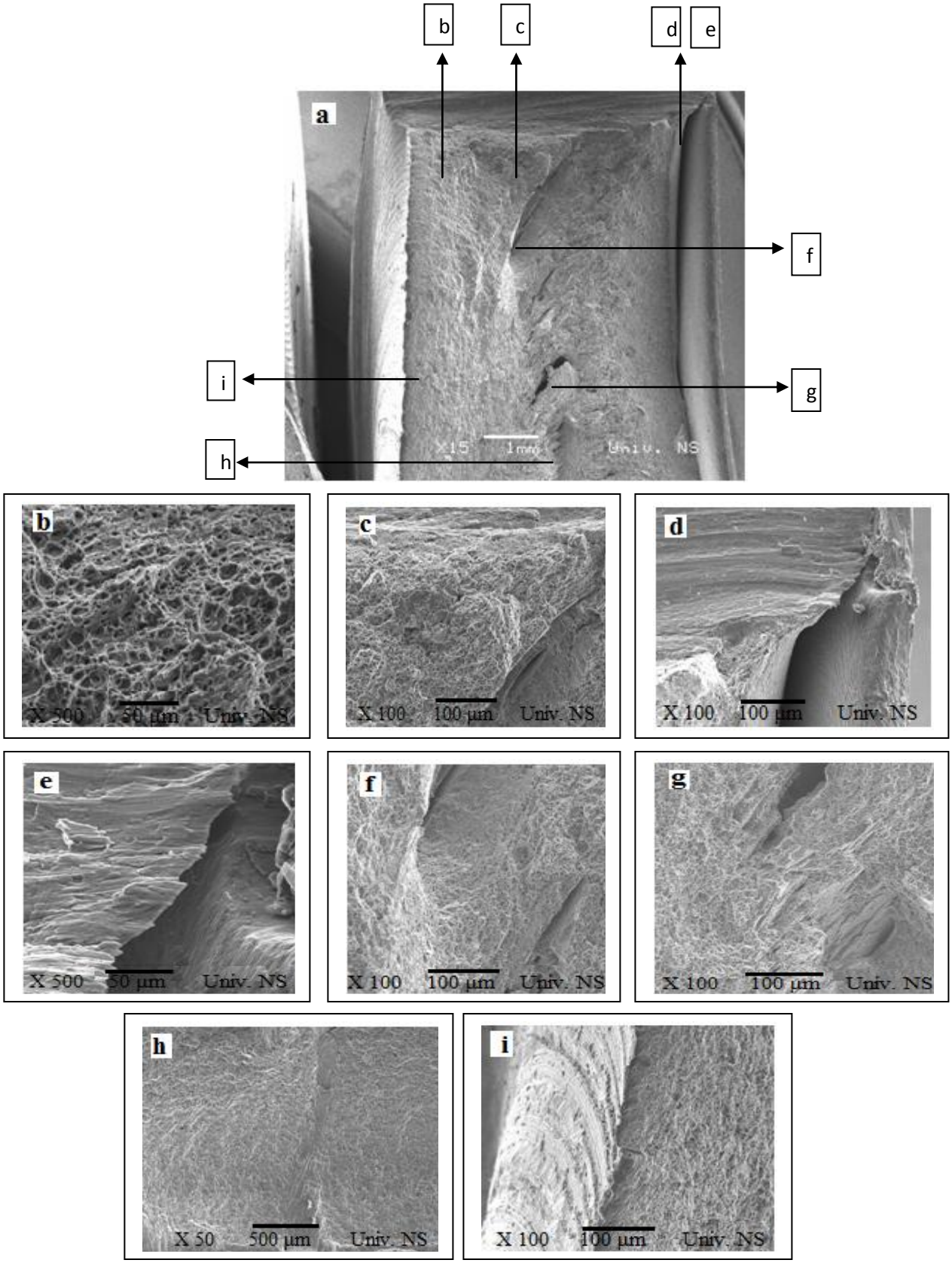

Figure 4-20(a – i). SEM Surface Fracture by Parameters (800 rpm, 100 mm/min and Tilt 2^0).

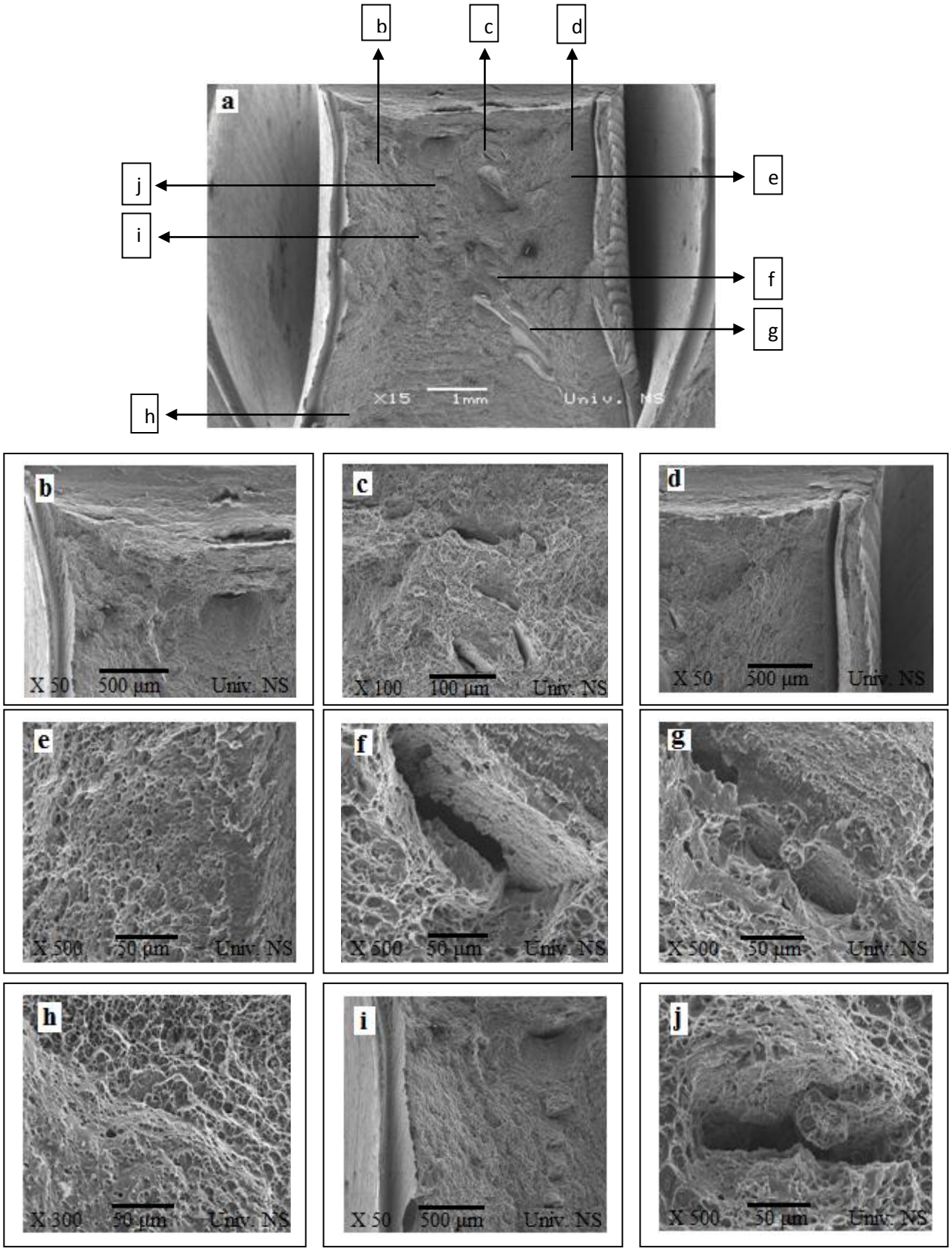

Figure 4-21(a – j). SEM Surface Fracture by Parameters (500 rpm, 125 mm/min and Tilt 3^0).

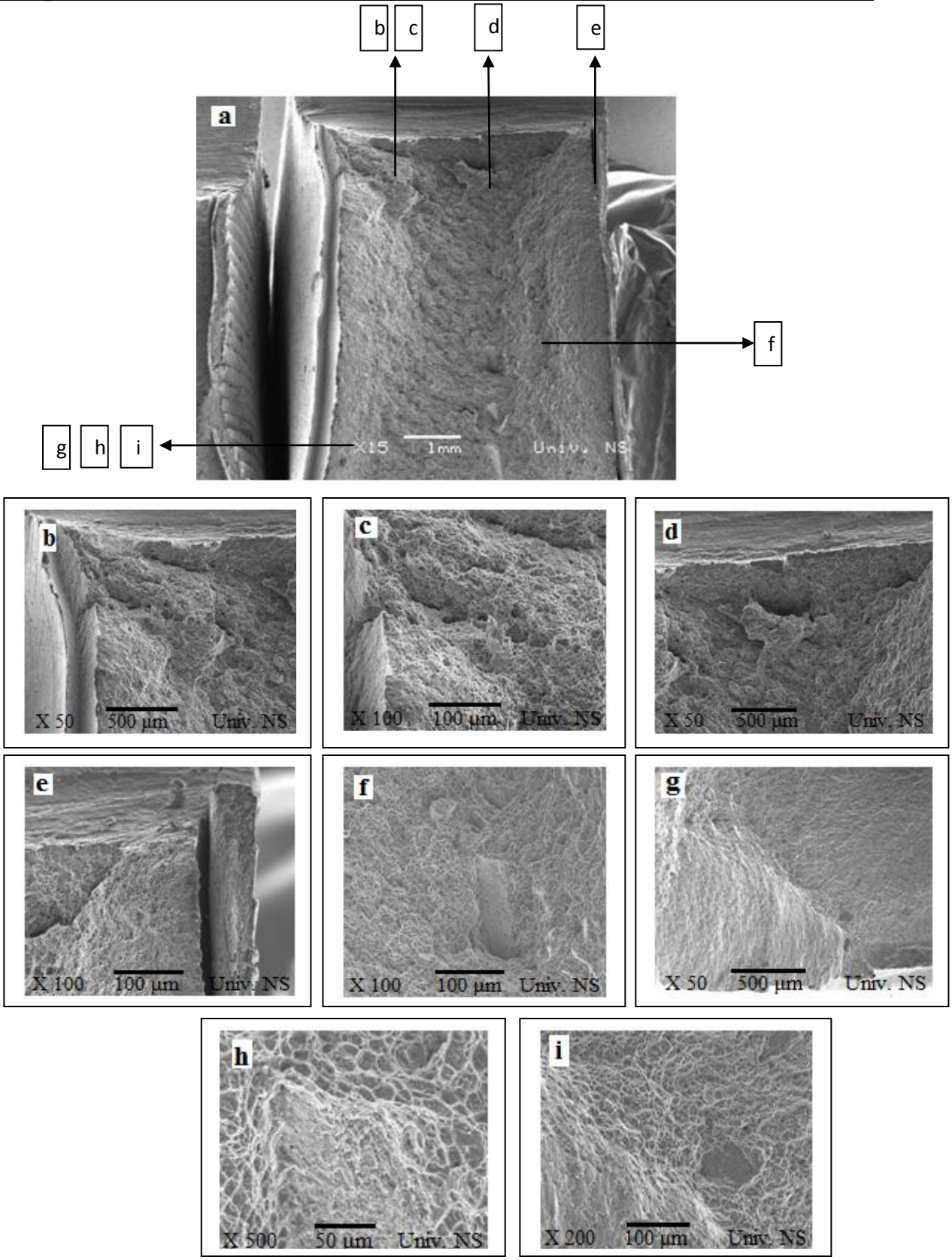

Figure 4-22(a – i). SEM Surface Fracture by Parameters (600 rpm, 125mm/min and Tilt 3^0).

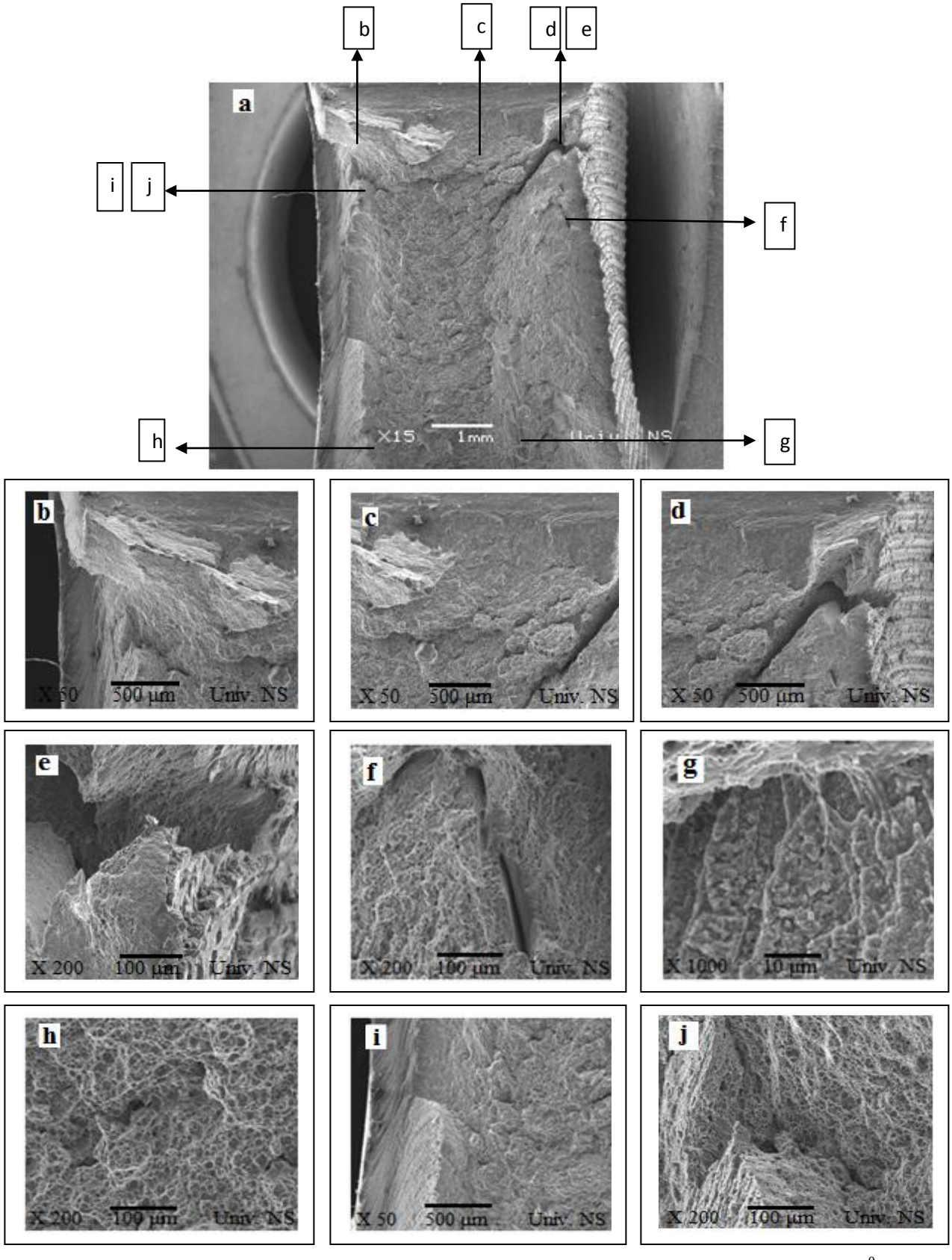

Figure 4-23(a – j). SEM Surface Fracture by Parameters (600 rpm, 150mm/min and Tilt 4^0)

.

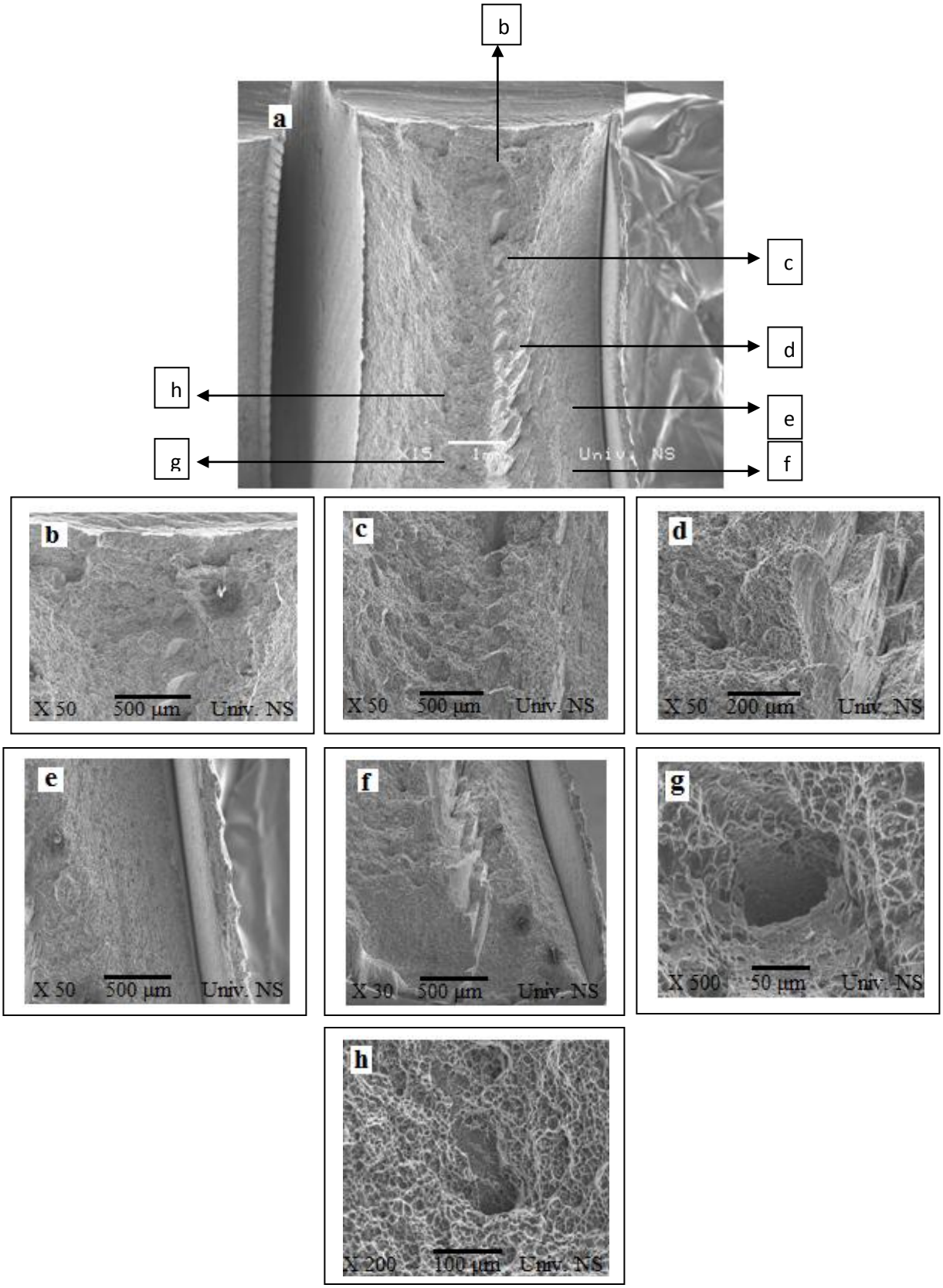

Figure 4-24(a – h). SEM Surface Fracture by Parameters (500 rpm, 150 mm/min and Tilt 4^0).

4.1.9 Energy Dispersive X-ray Spectroscopy (EDX) Analysis:

Energy dispersive X-ray spectroscopy is a relatively simple yet powerful technique used to identify the elemental composition of as little as a cubic micron of material. The equipment is attached to the SEM to allow for elemental information to be gathered about the specimen under investigation. The technique is non-destructive used for the elemental analysis or chemical characterization of specimen. Shown in Figure 4-25 (a –e), the SEM microphotographs and EDX analysis results of the surface fracture after done charpy test of aluminum 5083 alloy.

The EDX pattern, shown in Figure 4-25(e), in spectrum 1; reveals only existed aluminum (Al), manganese (Mn) and iron (Fe). The presence of these elements indicates that the specimen consist of elements present in aluminum 5083 alloy (e.g. Al, Mg). Observed in the spectrum 1, higher aluminum (Al) by weight percentage was 67.97% and small number of manganese (Mn) was 11.18%, also observed the existed iron (Fe) was 20.85%. Moreover, from spectrum 2, observed the magnesium (Mg) and aluminum (Al) are not big different by weight% were 36.11%, 36.54 respectively, also it has silica (Si) about 27.44%, due to increased temperature during friction stir welding and phase of precipitation. As the same figure in spectrum 3, SEM and EDX analysis have shown that they are rich in aluminum (Al) was 80.02% and less amount of magnesium (Mg) and manganese (Mn) was 2.03%, 7.57% respectively, also it existed iron was 10.38%. Furthermore, shown in spectrum 4; it has rich of iron (Fe) was 56.63% that caused existed fracture in specimen and observed less amount of aluminum (Al) and manganese (Mn) was 20.11% and 23.27% respectively. Shown EDX analysis in Table 4-6 .

Shown in Figure 4-25(f), observed in spectrum 5 rich in aluminum (Al) element was 94.92% and small amount of magnesium (Mg) was 5.08% as well as observed in spectrum 6, it has aluminum (Al) 82% and small amount of magnesium (Mg) was 6.60%. Shown Table 4-7 for EDX analysis by weight% .

Furthermore, shown in Figure 4-24(g), spectrum 7; observed the rich aluminum (Al) element was 74.26% and small amount manganese (Mn) was 10% also iron about 15.74%. Moreover, shown in spectrum 8, it was existed rich of aluminum (Al) and iron (Fe) were 38.84%, 34.11% respectively. That means exist the fracture in specimen due to increase

heating and depended on the phase precipitation, also observed in spectrum 8 existed manganese (Mn) element was 27.05%.

From Figure 4.25 (h), observed in spectrum 9 existed element of oxygen (O) was 4.56%, magnesium (Mg) was 4.04%, silicon (Si) was 4.048% and small number of potassium (K) was 0.78 and manganese (Mn) was 0.87% also shows it has rich of aluminum (Al) was 85.28%. Shown EDX analysis Table 4-7 and shows EDX analysis chart in Figure 4-25 (i) .

General, The rapid quenching rate contributed to non-equilibrium conditions in the aluminum base. This led to the formation of new alloy elements and hence changed the microstructure of the solidified surface layer as well as the chemical composition of the alloyed surface. The formation of the new alloyed elements was further validated via SEM examination and EDX analysis. The spectrum of the chemical composition of the coating material on the Al matrix is shown in Figure 4-25(a – i) and detailed weight percentages for each element analyzed with EDX spectroscopy are listed in Tables 4-6 to 4-7, the EDX analysis shows that the chemical composition of the modified surface had changed, which confirms that a convection process took place during the alloying process.[115]

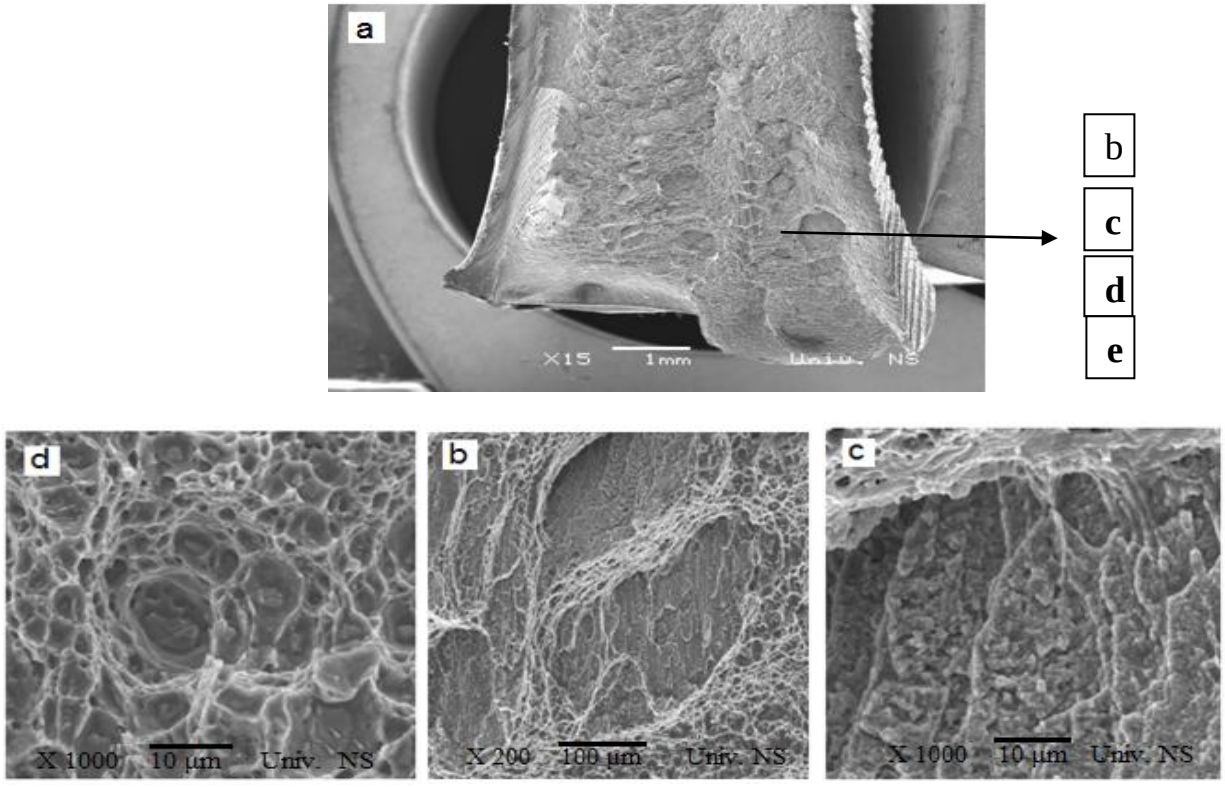

Figure 4-25(a – d). SEM Images of Fracture Surface at Parameters (600 rpm, 150mm/min and Tilt 4^0)

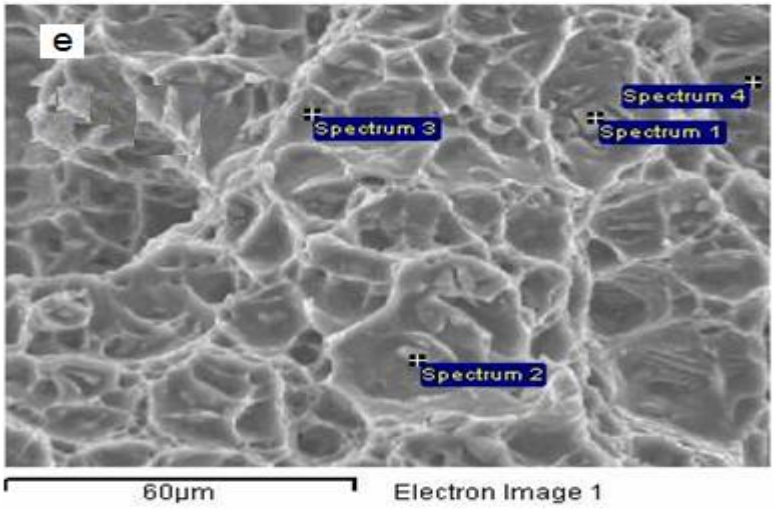

Figure 4-25(e). SEM Image and EDX Spectrums 1, 2, 3 and 4

Table 4-6. EDX Analysis of Spectrums 1, 2, 3 and 4 by Weight%

Spectrum	Mg %	Al %	Si %	Mn %	Fe %	Total
Spectrum1		67.97		11.18	20.85	100.00
Spectrum2	36.11	36.54	27.44			100.00
Spectrum3	2.03	80.02		7.57	10.38	100.00
Spectrum4		20.11		23.27	56.63	100.00

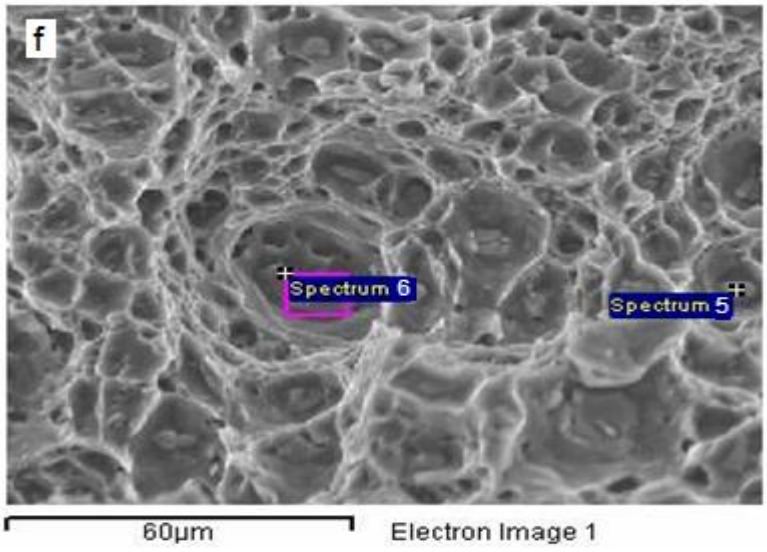

Figure 4-25f. SEM Image and EDX spectrums 5 and 6.

Table 4-7. EDX Analysis of Spectrums 5 to 9 by Weight%

Spectrum	O %	Mg %	Si %	Al %	Mn %	Fe %	K %	Total
Spectrum 5		5.08		94.92				100.00
Spectrum 6		6.60		82.00	11.40			100.00
Spectrum7				74.26	10.00	15.74		100.00
Spectrum8				38.84	27.05	34.11		100.00
Spectrum 9	4.56	4.04	4.48	85.28	0.87		0.78	100.00

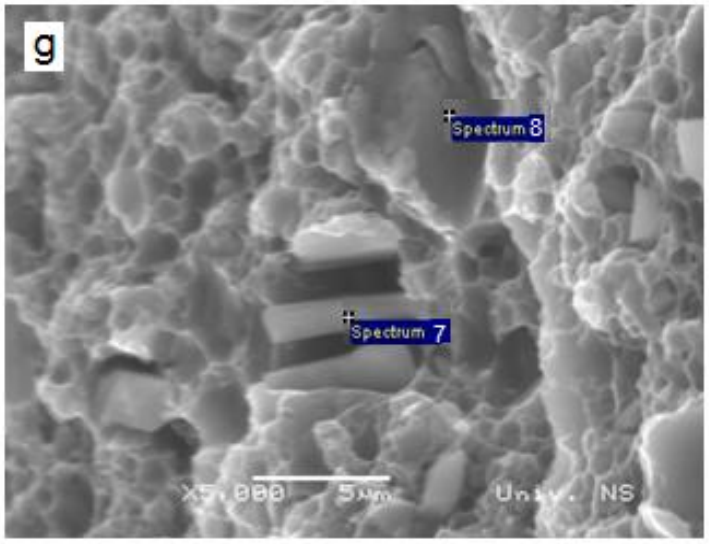

Figure 4-25g. SEM Image and EDX spectrums 7 and 8.

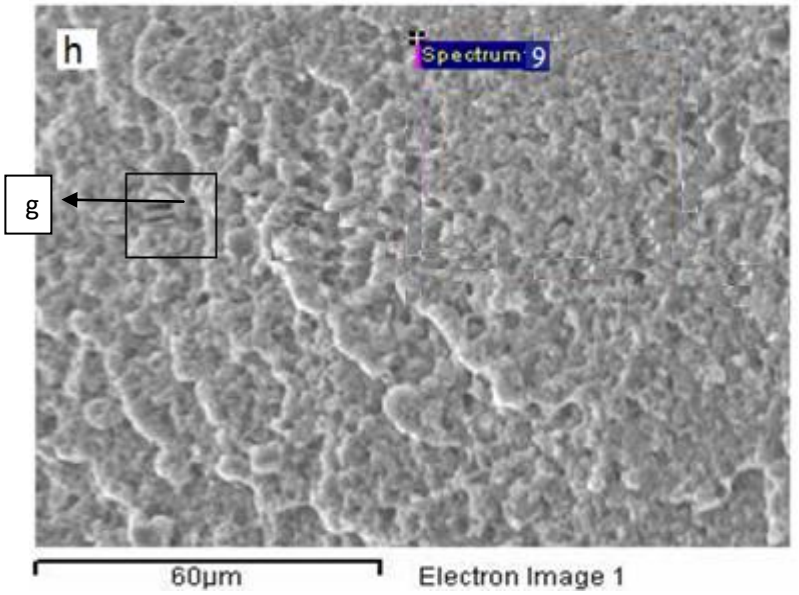

Figure 4-25h. SEM Image and EDX Spectrum 9.

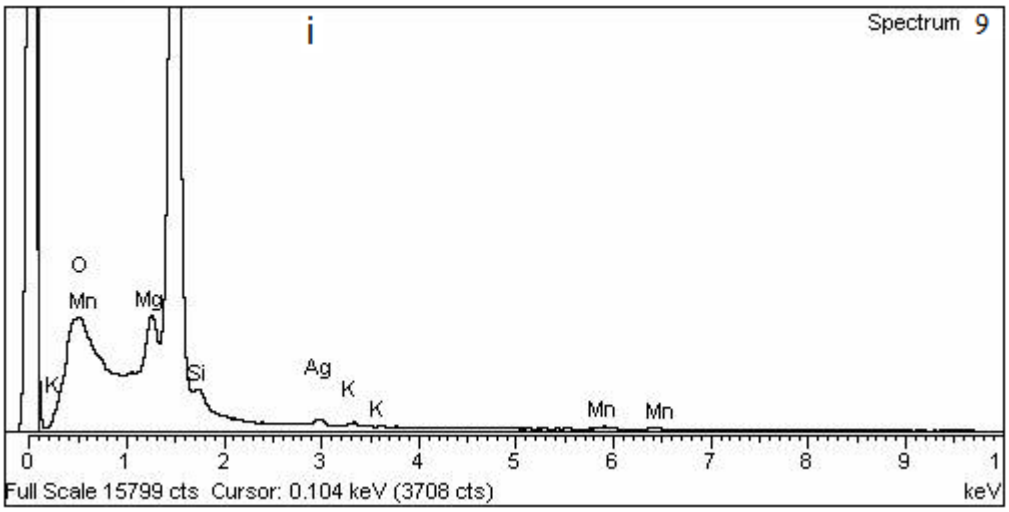

Figure 4-25i. SEM chart of EDX analysis of spectrum 9.

CHAPTER 5: DISCUSSION

5.1 Friction Stir Welding Investigation:

In FSW process, a rotating tool having a shoulder moves along the welding line. Rotational motion of the shoulder generates frictional heat leading to a softened region around the pin while the shoulder prevents deforming material from being expelled. In fact, a weld joint is produced by the extrusion of material from the leading side to the trailing side of the tool.

During the penetration phase, the rotating tool pin penetrates into the work piece until the tool shoulder come to contact with the work piece. The plastization of material under the tool increase with increase rotational speed and with decrease tool traverse speed result the reduction of vertical force. Also the increase of welding speed of tool will significantly decrease the temperature of the welded plate; especially in the welding zone of work piece increase because the heat generation input increased. Heat generation during friction stir welding arises from two main sources: deformation of material around the tool pin and the friction at the surface of the tool shoulder. Furthermore, the temperature in advance side is higher than retreating side because material flow and plastic deformation around tool is moving from advance side to retreating side.

Regarding to the literature review, it was found [17] the defined (w^2/v) as a pseudo heat index, using experimental view, and discussed effect of that input heat following Equation (2-1) indicates the relation between maximum temperature during FSW and main friction stir welding parameters of aluminum alloys. Found the specimen was welded by rotational speed 800 rpm and welding speed 75 mm/min were the higher maximum temperature during FSW, it was 410 C^0 that means when increasing the rotational speed at the same or constant welding speed led to increasing heat generation during FSW as shown in Table 2-1. However, observed at specimen by welded by parameters 500 rpm, 150 mm/min that means gain lower temperature during FSW, it was 378 C^0. Also it was found when increase in speed rate results more heat input [17]. In this cause tool rotation speed is more

effective than feed rate. As well results in this research, when decrease rotational speed and increase traverse speed, the heat generation decreased as shown in Figure 2-4.

Furthermore, axial load that measured from experimental work decreases with increase in rotational speed because that decrease in strength due to temperature increases in penetration position [117].

According to [80], it was indicated to the zirconica ceramic tool shoulder inset generated generally 30 – 70% more heat (0.5 – 2 mm wider visual HAZ width) than the reference hot work tool steel. Also referred to change in frictional behavior has been evidenced for different welding parameter sets predicting the same theoretical heat input. Especially, the hard metal tool shoulder demonstrated the same heat generation despite significant reductions of load or rotation.

In this study by Equation 3-17 as indicate to heat generation during FSW with different tool's pin and shoulder that found the shoulder has diameter 26 mm and pin has diameter 5.9 mm, they have higher heat generation during FSW was 1183.2 W at rotational speed 800 rpm with constant welding speed. Otherwise, the shoulder has diameter 13 mm and pin has diameter 5mm, its lower heat generation that means, the shoulder diameter has big effect on the generated of heat during FSW than pin diameter as shown in Figure 2-8 and Table 2-2.

Regarding to analytical model for estimation of the amount of heat generated during FSW, it was reported [14], that used complex and multi run procedures to find how mach mechanical energy transferred into heat during FSW, it is necessary to find what parameters influence heat generation and how much they influence the process. Moreover, it was indicated [107] to experimentally obtained temperature increase more slowly in comparison with the numerical results. The reason for this increase is that the left-hand thread of the tool pin caused the appearance of the "drill effect". However, from the moment contact between the tool shoulder and the plates is established. That means, the heat generated by friction between the work piece and the tool can account for the largest percentage of the generated heat, also reported when increasing the plunge speed decreases

the amount of heat generated by friction and increases the heat generated by plastic strains. In fact, increasing the tool rotation speed increases the amount of heat generated by friction and decreases the heat generated by plastic strains. Also it was presented [16] that analytical heat generation estimate correlate with the experimental heat generation, by assuming either a sliding or sticking condition. For the sliding condition, a friction coefficient that lies in the reasonable range of known metal to metal contact values is used in order to estimate the experimental heat generation. In this research , by using correlated Equations 2-20 to 2-23 and Figures 3- 9 to 3-13, found the maximum heat when used ratio between diameter of shoulder and pin for each rotational speed 500, 600, 700 and 800 rpm to find total power generation how percentage heat generation produced by shoulder as shows in Figures 2-15 and Table 2-3.

Generally, regarding to heat input measurements, there are three approaches that are followed in indicating the heat input during FSW. The first approach [14] utilizes computational techniques to predict the heat and temperature distribution during FSW. Such models are getting more accurate provided that the material thermal behavior is uniformly defined. The second approach [16] carries out thermal measurements using thermocouples or other devices like heat camera. The third approach [14] uses the power and torque measurements to predict the heat input during FSW. One major factor that contributes to the complexity of the heat input phenomenon is the multiplicity of variables and factors that are included in FSW. These factors include in addition to the rpm and feed rate, the z-axis force, the tool geometry, machine efficiency, cooling system, and material properties. A major difficulty is determining suitable value for the friction coefficient. The conditions under the tool are both extreme and very difficult to measure. Other experimental data and numerical models showed that there is a definite increase in temperature with the increase in the rotational speed.

According to [10], it was presented; a dynamometer has been used to determine the effects of the FSW parameters and tool geometry on the forces and torques generated during processing. Also reported, the down force Fz experienced by the FSW tool increased with the plunge depth selected for the welding operation and the horizontal

forces Fx increased significantly with the traverse speed, but much less with the rotation speed of the FSW tool. Moreover, the torque T developed during welding increased significantly with the rotation speed of the FSW tool, and was almost independent on traverse speed. Also as expected the use a larger FSW tool shoulder diameter caused higher torques to be developed during welding, the effect being significantly greater than that from increasing the tool center pin diameter.

Referred to [102], it was indicated that metallurgical observation reveals that tilt angle of stir tool affects the metal patterns which include two direction flows. One is the bottom flow and second is surface flow, therefore, Vertical tool angle has affected the location of assemble point of both flows. Increment of push angle made the points upwards or outside of plate surface. This flow might be effective vanishing defects.

In this study, used four tilt angles, 1^0, 2^0, 3^0 and 4^0 with different FSW parameters, and observation when change the tilt angles to large angles, the penetration of tool to be more less depth in work piece at the same force, also the force in the retreating side is quite large, it produced the more heat generated in this side if neglected the rotational speed and traveling speed.

5.2 Microstructure Characterization:

It was indicated [109], the first trial to classify the FSW weld microstructure for aluminum alloys were divided the FSW microstructure into four distinct regions, which are: HAZ, TMAZ, WN, and base metal. However, various studies indicated that this classification is not typical for all aluminum alloys, for different metals, or even for the same material. Various features were observed, such as the existence of the concentric rings (onion rings) within the WN, appendages extending from the top of the WN, as well as "banded structures" extending from the base of the WN. In fact, the term weld nugget was recently replaced by the Stir Zone (StZ) in most literature referring to the zone in the weld that was previously occupied by the tool pin. The geometry of these zones is totally dependent on the process parameters.

It was reported [113], that the nugget zone is characterized by a relatively homogeneous microstructure, with small; equiaxed grains (mean size 5 – 10 μm). This zone is almost totally re-crystallized, with little or no inter-granular deformation. In the case of the conical shape pin no onion type rings are present, while in the case of the screw type pin this type of structure is clearly evident. Furthermore, the microstructure of the advancing side is generally characterized by a sharp boundary between the nugget and the TMAZ (Figure 2-16). Close to the nugget the microstructure of the advancing side consists of small, relatively equiaxed grains (mean grain size 5 – 10 μm), whereas the TMAZ, close to the weld nugget, has larger, elongated grains (mean grain size 14 – 20 μm), while the retreating side of the FSW joint has a more complex microstructure, with generally no clear boundary between the nugget and the TMAZ (Figure 2-16). Although towards the nugget side a smaller grain size than the TMAZ can be found, a number of large grains are also included. Close to the weld surface and inside the TMAZ a large number of grains with low angle boundaries are evident.

Regarding to ref. [36] , that explained the shape of the friction stir zone transformed from basin shape to elliptical as the traverse speeds increased owing to increased deformation. The size of the friction stir zone gradually decreased with the increase in the traverse speed on both the FSW alloys due to the increase in the rate of deformation, leading to widening of the friction stir zone.

In the current study, aluminum 5083 alloy, 6.2 mm thick sheets were FS welded. The classification of the weld zone macrostructure divides it into four distinct regions (Fig. 2-16), which are: the heat affected zone (HAZ), thermo-mechanically affected zone (TMAZ), and stir zone (SwZ). By investigating the macrostructures of all the weld conditions, the thickness (*t*) of the SwZ increased with the increasing in the welding speed, and decreasing the rotational speed (rpm) discretely too. That means, microstructural analysis indicated no expansion in the size of the heat affected zone with reduced travelling speed.

5.3 Fracture Surface Analysis:

It was reported [37], that metals tend to fail by one of two mechanisms, micro void coalescence or cleavage and micro void coalescence is the more common fracture mechanism where voids form as strain increases, of the two fracture mechanism cleavage involved for less plastic deformation ad hence absorbs for less fracture energy. Also the notch serves as stress concentration zone and same materials are more sensitive towards notches than other the notch depth and tip radius are therefore very important.

According to ref. [118], it was presented in case of the round V- notch charpy test; the initiation of the crack propagation was strongly influenced by the shape of the notch tip. When the notch tip had a smooth circular geometry, the initiation of crack was significantly delayed.

In current research, features of the surface tearing give us inform action about the mechanism of crack growth and also about the nature of the crack or defect from which the fracture nucleated. For deep understood fracture mechanism used macro photographs and scanning electron microscope images to explain behavior of failure. As the results, macro photographs and SEM analysis on the surface fracture shown the type and mechanism fracture for specimens that welded by various FSW parameters and found the relationship between fracture mechanism and absorbed energy.

From Figures 4-1 (a – o) for relationship between load- time curve that observed the largest maximum load of all specimens was 4.52 KN in specimen was welded by rotational speed 800 rpm, welding speed 75 mm/min and tilt angle 1^0. Also from Figures 4-3 and 4-4, observed the optimized FSW parameters for welded Al5083 were 600 rpm, 700 rpm and 100 mm/min, 125 mm/min. In the fact, the largest area under the curve, it has high impact energy and toughness also less area under the curve, it has low toughness.

From Figure 4-5(a – o) for energy- time curve, it observed the test specimen continues to absorb energy and work hardens at the plastic zone at the notch. If the specimen cannot absorbed more energy, fracture occurs. Moreover, the specimen less absorbed energy

undergoes cleavage (often referred to as brittle) fracture, otherwise, if the specimen high absorbed energy undergoes ductile fracture and it has high toughness. Also brittle fracture is low energy fracture and ductile fracture is a high energy fracture. Moreover, the impact energy decreases with decreasing temperature as the yield strength increases and the ductility decrease. If material has sharp ductile to brittle transition, the material has poor toughness.

From Figure 4-5d and 4-5h, the maximum absorbed energy was between 17 J and 24 J in specimen was welded by FSW parameters 700 rpm, 800 rpm and welding speed 75 mm/min, 100 mm/min also specimen that welded by rotational speed 500 rpm and traverse speed 125mm/min and from figure 4-6 observed the optimized maximum impact energy was between 21 J and 22 J with heat index between 4 rev/mm and 7 rev/mm.

According to consumption energy per time dE/dt and heat index (w/*v*) observed the impact energy per time changed by change the rotational speed and traverse speed (w/*v*). from Figure 4-7 observed the optimized consumption energy per time was between 17 KJ/sec and 19 KJ/sec with heat index 6 rev/mm to 8 rev/mm. as shown in Table 4-4.

From Figures 4-10 (a – o), energy - stress curve observed the specimens have maximum absorbed energy, that have maximum stress. Furthermore, the optimized maximum stress was between 26 N/mm^2 and 28 N/mm^2 with heat index, w/v was 5 rev/mm and 7 rev/mm. That means, if the stress increased, the absorbed energy increased which high absorbed energy that has high toughness.

In the fact, the presence of notch on the surface of the fast area of the specimen creates a concentration of stress or localization of strain during charpy impact test. The effect of the localized strain at the base of the notch causes the specimen to fail through the plane at relatively low values of energy.

5.3.1 Micro photograph Investigation:

Since the focus of the rest is on digital imaging [119], it was seemed fitting that we should define exactly what is meant by digital imaging technology. Digital imaging systems can use image analysis technologies for easy, accurate, and precise measurement

of percent shear fracture area. These systems generally consist of a camera, lens, lighting, data acquisition software, and image analysis software. Percent shear measurement via this method involves capturing the image of the fracture surface, outlining the brittle area, and outlining the outside region of the fracture surface. The software automatically integrates the areas to determine surface fracture analysis (SFA). Furthermore, to demonstrate the precision of the digital imaging system in a typical shear area application (without using precision-made tooling such as the reticule), the digital imaging system was used to measure the percent shear drawing of a Charpy bar with areas drawn which give 20%, 40%, 60%, and 80% shear. Also used digital imaging systems to determine the simulated percent shear areas. The brittle areas were denoted by the inner square or circle center, while the ductile areas were defined by the remaining outer area. Both square and circles were used to simulate the various contours outlined on a typical Charpy bar

As the finding in this research, observed in micro photograph, the specimens were fracture by one of two fracture mechanism, micro void coalescence or cleavage. Micro void coalescence is common fracture mechanisms where voids form. And second fracture mechanism is cleavage involved far less fracture energy. If the material was break on a flat plane tearing, the fracture was brittle, and if material was break with jagged edges or shear lips, the fracture was ductile. As comparing the fracture mechanism, type of fracture surface was dull to flat tearing areas that gave an estimated the percentage of ductile to brittle ratio.

From Figure 4-12 (a – j), observed the appearance of fracture was dominated dull (ductile fracture) and it has maximum adsorbed energy. From Figure 4-12b_1, shown two type of fracture, one was brittle fracture about 15% and second was ductile fracture about 85% also absorbed energy in this specimen was 14.22 J. From Figure 4-12k_1 observed the appearance ductile tearing, it was 50% ductile and 50% brittle fracture. In this specimen has absorbed energy been 18.24 J. Furthermore, from Figures 4-12k_2, 4-12l_2 observed the predominated ductile fracture about 80% dull tearing and 20% brittle fracture, this specimens have absorbed energy 14 J to 17 J. Addition, from Figure 4-12l_1, observed the 60% brittle fracture and 40% ductile tearing that has 13.39 J of absorbed energy.

5.3.2 SEM and EDX analysis:

As the results, for deep understood behavior fracture mechanism used the SEM. From Figure 4-13 shown the surface tearing of specimen was welded by FSW parameters 500 rpm, 75 mm/min, it observed the ductile fracture with micro void near the notch also upper side the specimen was effect by extra heating than lower side. Also from Figure 4-14 observed the predominated ductile fracture with existed fracture and micro void in the stirred zone also existed shear in lower surface. That specimen welded by FSW parameters 600 rpm and 75 mm/min.

From Figures 4-15, 4-16 observed the brittle tearing closed to notch then propagation fracture in stirred zone by ductile tearing due to existed semi cleavage and micro void. Inside specimen existed tearing as edge lip of shear fracture. This specimen was welded by 700 rpm, 800 rpm and welding speed 75mm/min. moreover, from Figures 4-17, 4-18 observed the dominated ductile fracture in the upper surface affect by high temperature due to contact of shoulder.

From Figure 4- 20 observed the tearing surface by brittle fracture due to less absorbed energy with existed fracture in the specimen that welded by parameters 500 rpm and 100 mm/min. Furthermore, from Figures 4-21 to 4-24 observed specimens have same surface fracture were dominated ductile coalescence by edge lip of brittle fracture with existed micro void in the nugget zone also shown the onion ring that specimen welded by rotational speed 500 rpm, 600 rpm and welding speed 125 mm/min and 125 mm/min.

According to energy dispersive x-ray spectroscopy (EDX) analysis is a relatively simple technique used to identify the element composition of a little as cubic micron of material. From Figure 4-25e, spectrum 1 observed the existed aluminum (Al) was 67.97% by weight% and small number of manganese (Mn) was 11.18% and iron (Fe) was 20.85%. From spectrum 2 observed existed elements magnesium (Mg) was 36.11%, aluminum (Al) was 36.54%, silicon (Si) was 27.44% that existed due to increased temperature during FSW and phase precipitation. Also shown in spectrum 3 rich aluminum (Al) was 80.02%, and less amount of magnesium (Mg) , iron (Fe).and manganese (Mn) were 10.385, 2.03%

and 7.57% respectively. Moreover, from spectrum 4 observed existed rich iron (Fe) was 56.63%, and aluminum (Al) was 20.11%, manganese (Mn) was 23.27% as shown EDX analysis in Table 4-6.From Figure 4-25f observed rich aluminum (Al) was 94.92% and small amount of magnesium (Mg) was 5.08% as shown in Table 4-6.

From Figure 4.25h observed in spectrum 9 the existed element of oxygen was 4.56%, magnesium was 4.04%, silicon was 4.04% and small amount of potassium was 0.78%, manganese was 0.87% with observed rich of aluminum was 85.28% as shown in EDX analysis Table 4-7 and shown in Figure 4-25i for EDX analysis chart.

In fact, the aluminum 5083 alloys are homogenous that means the all component elements distribution as the same in the all specimens but due to increase heating during FSW and phase precipitation causes the change of microstructures and chemical properties.

CONCLUSION

This research, an attempt has been made to understand the influences parameters of friction stir welding (FSW) as rotational, travel speed and tilt angles on the fracture resistance in aluminum 5083 alloy by tested specimens by charpy impact test. Fifteen different sets of parameters were used to fabricate the joints, while one type of geometry concerning the welding shoulder and pin were used. The main conclusion obtained in this research can be summarized as follows:

- Regarding to heat generation during FSW, that divided into two parts; frictional heat generated by the tool and heat generated by material deformation near the pin and tool shoulder region. Furthermore, it is a complex process of transformation of specific type of energy into heat and it is difficult to estimate the temperature inside the weld affected zone during the welding, but it can be estimated probably maximum temperature during FSW on surface work piece by analytical procedure, this process is very complex because it includes a significant number of variables and parameters or estimate heating during FSW by modeling process or experimental work as thermocouples or infrared camera. Heat generated from shoulder surface and pin tool have a relevant influence both on the metal flow and on the heat generation due to friction forces. Therefore, the shoulder contributes of the major friction to generated heat during FSW and heat generated from probe tip is negligible compared with the total heat generation.

- As finding, by used analytical procedure, the material alloy specimen was welded by parameters rotational speed 800 rpm, travel speed 75 mm/min and tilt angle 1^0, it has maximum temperature during FSW was 410 C^0 and low temperature in specimen that welded by rotational speed 500 rpm and welding speed 150 mm/min was 378 C^0.

- As shown in relationship between the rotational speed and maximum temperature, when increase the rotational speed, the temperature will be increased. Also when the traversing speed is increased, the maximum temperature will be decreased.

- Estimation welding force during FSW is difficult when the axis of the welding tool is horizontal due to the geometry of the FSW process. When the axis of the welding tool is vertical the estimation of the welding force is less complex then it is horizontal. However, the estimation force and friction coefficient by torque. Furthermore, it can be estimated temperature during FSW by an infrared camera or by thermocouples embedded at specific spots in work pieces the infrared camera catches thermal images of surface captured by the camera frame, but the temperature in the depth of work pieces and welding tool cannot be estimated.

- From the previous researches are reported in the literature review, it is clear that microstructure plays a vital role in the improvement of the mechanical properties of aluminium alloy. Friction stir welding process generates three distinct microstructural zones that result from the welding process as following: nugget zone also known as the dynamically recrystallized zone (DRZ) where the tool piece pin passes into this zone and by experience, it has high deformation and high heat, generally consists of fine equated grains due to recrystallisation, the thermo mechanically affected zone (TMAZ) and the heat affected zone (HAZ), all zones together are called welding zone. The shape of the friction stir zone transformed from basin shape to elliptical, due to the increased deformation at increased traversing speeds. The size of the friction stir zone gradually decreased with the increase in the traverse speed in the FSW alloy due to the increase in the rate of deformation, leading to widening of the friction stir zone.

- In terms of mechanical and failure properties, selected charpy impact test to measure the absorbed energy caused the failure specimens. Also used as an economical quality control method to determine the notch sensitivity and impact toughness of engineering material. Fracture is caused by the growth of on existing crack (V-notch). As finding,

less energy absorbed during the fracture surface is brittle, if the absorbed energy is higher, the tearing is ductile fracture and material alloy has high toughness.

- A fracture surface produced by ductile fracture is extremely rough which indicates that a great deal of plastic flow has taken place; also ductile crack growth involves excessive plastic deformation which consumes a lot of the energy associated with the applied stresses. On the other hand, brittle crack growth proceeds with little plastic deformation where cracks grow rapidly. Brittle fracture is flat and do not show evidence of plastic deformation.

- As results, the higher average absorbed energy was 23.25 J from specimens that welded by parameters 800 rpm, 75 mm/min, 100 mm/min and tilt angle 1^0, 2^0. That means the material alloy absorbed high energy; it has high toughness and dominated ductile failure.

- The optimized consumption energy per time dE/dt in material specimens were welded parameters of heat index between 6 rev/min and 8 rev/min, also when stress increase, the absorbed energy increase.

- According to relationship between load- displacements, the material specimen has biggest area under the curve, it has high toughness. These alloys were welded by 600 rpm, 700 rpm, welding speeds 100 mm/min, 125 mm/min, tilt angles 2^0 and 3^0. Otherwise, less area under the curve that means the material specimen has low toughness.

- SEM – EDX, used for detected fracture and micro void to deep understood of fracture mechanism that found the existed of almost specimens microvoid and dominated of ductile tearing on surface fracture with coalescence inside edge shear lips and EDX analysis to indentify the element composition as little as a cubic micron of material surface fracture that found the rich aluminum about 80% by weight and sufficient of

elements distribution in alloy as Mg, Mn, Si and Fe, that means, the material alloy is homogenous.

- As the results, the optimized parameters of friction stir welding for welded aluminum 5083 alloy is heat index, w/v 5rev/mm and 7 rev/mm. and tilt angles 2^0 and 3^0. That means, the welding zone of alloy was welded by this FSW parameters, it has high resistance fracture.

- Finally, In future work repeated tested the same material alloys (Al 5083) by heat index between 5 rev/mm and 7 rev/mm and by another mechanical properties testing, like tensile test and microhardness for precisely restricted the optimized FSW parameters for welded aluminum 5083 alloy to gain high toughness in welded joints.

REFERENCE

1- J. D. Cost, J. A. M. Ferrira and L.P. Borrego; International Journal of Fatigue, Volume No. 37, April 2012, PP 8 – 16

2- H. Larsson, L. Karlsson, L-E. Svensson, ESAB AB, Gotehorg and V. T. Utreckling; "Friction Stir Welding of AA5083 and AA6082 Aluminium", Svestsaren No 2, 2000.

3- V. Ocenasek, M. Slamovac, J. F. Santons, P. Vilaca; METAL, Hradec nad Moravic, 2005.

4- http://www.esab.de/de/de/support/upload/FSW-Technical-Handbook.pdf

5- T. J. Minton; "Firction Stir Weld of Commercially Available Superplastic Aluminium", http://bura.brunel.ac.uk/handle/2438/4247

6- H. Bisadi, A. Tavakoli, M. T. Sangsaraki, K. T. Saragaraki; Materials and Design, Vol. 43, 2013, PP. 80–88.

7- M. Kutz; "Handbook of Materials Selections", John Wiley & Sons, Inc., New York, 2002.

8- M. Kutz; "Handbook of Mechanical Engineering, John Wiley & Sons, Inc John Wiley & Sons, Inc., Second Edition, Washington, D.C, 1998.

9- L. Griffing; "Welding Handbook (Metals and Their Weldebility)", Sixth Edition, AWS, Florida, 1972.

10- R. Johnson; "Force in Friction Stir Welding of Aluminium Alloys", TWI Members Report, Vol. 716, 2000, PP. 1-18.

11- www.Sapagroup.com/us/profiles.

12- B. Richards; "Microstructure Property Correlation in Friction Stir Welded Al 6061-T6 Alloys", http://www.wpi.edu/Pubs/E-project/Available/E-project - 051310-235516/unrestricted/FSW_Al6061_MQP_BTR.pdf

13- T.Lorentzen;http://www.bayards.nl/Meriad-CMS-New/store/files/1265221220_ Bayards Friction Stir Welding presentation.pdf

14- M. M. Mijajlovic, N. T. Pavlovic, S. V. Jovanovic, D. S. Jovanovic, and M. D. Milic; Thermal Science, Vol. 16, Suppl. 2, 2012, PP. S351 – S362.

15- M. M. Attallah; "Microstructure- Property Development in Friction Stir Welds of Aluminum Based Alloys", University of Birmingham Research Archive, Unit Kingdom, September, 2007.

16- H. Schmidit, Hattel and J. Wert; Modelling and Simulation in Materials Science and Engineering Vol. 12, 2004, PP 143–157.

17- S. Satlari, H. Bisadi, M. Sajed; International Journal of Mechanics and Applications, Vol. 2, No.1, 2012, PP. 1 – 6.

18- R. Nandan, T. DebRoy and H. Bhadeshia; Progress in Materials Science, Vol. 53, August, 2008, PP. 980 – 1023.
19- V. K. Singla; "Experimental Study and Parametric Design of Impact Testing Methodology", Thapar University, June 2009.
20- T. Udomphol; "Laboratory 6: Impact testing, Mechanical Metallurgy Laboratory 431303, http://eng.sut.ac.th/metal/images/stories/pdf/Lab_6Impact_Eng.pdf.
21- Y. S. Sato, H. Kokawa, M. Enomoto and S. Jogan; Metallurgical and materials Transaction A, Volume 30 A, September, 1999, PP. 2429.
22- I. Boromei, L. Ceschini and A. Morri; Metallurgical Science and Technology, PP.12 – 21
23- D. Klobcar, L. Kosec, A. Pietros and A. Smoley;, Materials and Technology Vol. 46, No. 5, 2012 , PP. 483–488.
24- C. Chuenarrom, P. Benjakul, P. Daosodsai; Materials Research, Vol. 12, October, 2009, PP. 473 – 476.
25- T. Udomphol; "Laboratory 2: Hardness testing Mechanical Metallurgy Laboratory 431303, http://sut.ac.th/Engineering/Metal/pdf/MechmetLab/En/02_Hardness_en.pdf.
26- H. K. Mohanty, M. M. Mahapatra, P. Kumar, P. Biswas and N. R. Mandal; Journal Marine Science and Application, Vol. 11, 2012, PP. 200 – 207.
27- G. G. Roy, R. Nandan and T. DebRoy; Science and Technology of Welding and Joining, Vol. 11, No. 5, 2006, PP. 606 -608.
28- M. Merlin, G. Timelli, F. Bonollo and G. L. Garagnani; Journal of Materials Processing Technology, 2009, PP. 1060 – 1073.
29- M. Merlin, L. Pivetti and G. L. Garagnani; Metallurgical Science and Technology,Vol. 26, No. 1, 2008, PP. 22 -29, Italy,.
30- S. A. Khodir, T. Shibayanagi and M. Naka; Materials Transactions, Vol. 47, No. 1, 2006, PP. 185 to 193.
31- P. Threadgill, A. Leonard, H. Shercliff and P. Withers; International Materials Reviews, vol.54. no.2, March 2009, PP. 49-93.
32- G. Biallos, R. Braun, C.D. Donne, G. Staniek and W. A. Kagsser; "Mechanical Properties and Corrosion Behaviour of Friction Stir Welded 2024- T3", First International Symposium on Friction Stir Welding, Thousand Oaks, California, USA, 1999.
33- R. S. Mishra, Z.Y. Ma; Materials Science and Engineering, Report 50, 2005, PP. 1–78.
34- K. Colligan; "Dynamic Material Deformation During Friction Stir Welding of Aluminum", First International Symposium on Friction Stir Welding, Thousand Oaks, California, USA, 1999.
35- R. S. Mishra, M. W. Mahoney; ASM International, First Edition, 2007, PP. 51 -70.

36- S. G. Pawar; "Influence of Microstructure on the Corrosion Behaviour of Magnesium Alloys", University of Manchester, School of Materials, Manchester, England, 2011.
37- N. Singh; "Experimental Study and Parametric Design of Impact Testing Methodology", University of Thapar, Patiala, June, 2009.
38- R. K. Nanstad and M. A. Sokolov; "Charpy Impact Test Results on Fine Materials and Nist verification Specimens Using Instrumented 2-mm and 8-mm Strikes", Metals Ceramics Division, ODK Ridge National Laboratory, Philadelphia, USA, 1995.
39- O. K. Chopra and A. Sather; "Initial Assessment of the Mechanisms and Significance of Low Temperature Embrittlement of Cast Stainless Steels in LWR System", U.S. Nuclear Requlatory Commission, Office of Nuclear Regulatory Research, Washington DC, USA, August, 1990.
40- S. Ravi, M. Todo, K. Arakawa and K. Takahashi; "Effect of Annealing on the Fracture Behaviour of Polyethylene", Research Institute for Applied Mechanics, Kyushu University, Japan.
41- M. P. Manahan; ASTM Standardization News, October, 1996. PP 23 – 29.
42- J. J. Muhsin and H. M. Muhammed; Journal of Engineering & Applied Sciences, Vol. 7 No. 4, 2012, PP.436.
43- N. T. Kumbhar and K. Bhanumurtthy*;* Asian J. Exp. Sci., Vol. 22, No. 2, 2008, PP. 63-74
44- N. Thurldy; "Advances in High Rotational Speed- Friction Stir Welding for Novel Applications", Wichita State University, May 2009.
45- C. E. D. Rowe, W. Thomas; "Advance in Tooling Materials for Friction Stir Welding", TWI and Cedar Metals Ltd.
46- J. Adamowski, C. Gambaro, E. Lertora, M. Ponte and M. Szkodo; International Scientific Journal, Volume 28, No. 8, 2007, PP. 453 – 460.
47- M. N. Ilman; "Comparative Study on Fatigue Crack Growth Rate Behaviours of Friction Stir Welded Aluminium Alloys 2024-T3 and 6061-T6", Seminar Nasional Tahunan Teknik Mesin (SNTTM), Palembang, 2010, PP. 69 – 74.
48- Z. Carzhi, Y. Xin-qi and L. Guo-hong; Trans. Nonferrous Met, Soc.,Vol. 15, No. 4, 2005, PP. 789 – 794.
49- F. M. Mazzolani; EAA - European Aluminium Association, 2007.
50- Z. Zhang, J. Bie, Y. Liu and H. Zhang; Journal Material Science and Technology, Vol.24, No.6, 2008, PP. 907 – 914.
51- N. M. Al-Araji, K. M. Kadum and A. A. Al-Dayni; International Journal of Scientific and Engineering Research, Volume 2, Issue 12, 2011.
52- S. A. Alidakht, A. Abdallah-zadeh, S. Sdeymani, T. Saeid and H. Assadi; Materials Characterization, Vol.63, 2012, PP. 90 – 97.

53- M. K. Kulekci, E. Kaluc, A. Sik and O. Basfark; The Arabian Journal for Science and Engineering, Vol.35, No.1B, 2010, PP. 321 – 330.
54- H. S. Patil and S. N. Soman; International Journal of Engineering, Science and Technology, Vol.2, No.5, 2010, PP. 268 – 275.
55- G. R. Babu, K. G. Murti and G. R. Janardhana; ARPN Journal of Engineering and Applied Sciences, Volume 3, No. 5, 2008, PP. 68 – 74.
56- P. M. Moreira, A. M. De-Jesus, A. S. Ribeiro and P. M. De-Castro; "Fatigue Crack Growth in Friction Stir Welding of 6082-T6 and 6061-T6 Aluminium Alloys: a Comparison", University of Porto, Porto. Portugal, 2009.
57- G. M. Cantin, S. A. David, W. M. Thomas, E. Lara-Curzio and S. S. Babu; Science and Technology of Welding and Joining, Vol. 10, No. 3, 2005, PP. 268 – 280.
58- H. Horn; "Friction Stir Welding of Aluminium Foam Materials", Institut Fiir Werkstoffkunde und SchuieBtechnik, Hamburg, 1999.
59- T. Khaled; Metallurgy Federal Aviation Administration, ANM-112N, July 2005.
60- K. J. Colligan; "Friction Stir Welding for Ship Construction", Concurent Technologies Corporation, Web.www.nmc.ctc.com, 2004.
61- E. Olsen; "Friction Stir Welding of High Strength Automotive Steel", Brigham Young University, August 2007.
62- L. E. Murr, R. D. Floves, O. V. Flores, J. C. Mc-Clure, G. Liu and D. Brown;, Mat Res Innovat, Vol.1, 1998, PP. 211 – 223.
63- Y. J. Chao, X. Qi and W. Tang; Journal of Manufacturing Science and Engineering, Vol. 125, 2003, PP. 138 – 145.
64- B. Parida, S. Pal, P. Biswas, M. M. Mohapatra and S. Tikader; International Journal of Applied Research in Mechanical Engineering, Volume 1, No. 2, 2011.
65- N. Banwasi; "Mechanical Testing and Evaluation of High-Speed and Low Speed Friction Stir Welds", Bangalore University, Bangalore, India, 2005.
66- L. Radovic and M. Nikacevic; Scientific Technical Review, Vol. L VIII, No. 2, 2008, PP. 14 – 20.
67- T. Radetic, M. Popovic, E. Romhanji, B. Milovic and R. Dodok; Metalurgija-MJoM, Volume 17, No.1, 2011, PP. 41 – 47.
68- W. B. Lee, Y. Yeon and S. Jung; Scripta Materialia, Vol. 49, 2003, PP. 423 – 428.
69- J. Przydatek; "A Ship Classification View on Friction Stir Welding", First International Symposium on Friction Stir Welding, Thousand Oaks, California, USA, 1999.
70- D. Veljic, M. Perovic, A. Sedmak, M. Rakin and N. Bajic; Materials and technology, Vol.46, No.3, 2012, PP. 215–221.
71- M. V. Trifunovic, N. S. Bajic and D. M. Bajic; "Thermal Science, Vol. 16, No. 2, 2012, PP. 527 – 534.

72- D. Veljic, M. Perovic, M. Rakin, A. Sedmak and D. Bajic;, Journal of Mechanical Engineering, Volume 2011.
73- O. T. Midling, J. S. Kvale and O. Dahl; "Industrialisation of the FSW Technology in Panels Production for the Maritime Sector", First International Symposium on Friction Stir Welding, Thousand Oaks, California, USA, 1999.
74- M. Kumagai and S. Tanaka; "Proparties of Aluminum Wide Panels by Friction Stir Welding", First International Symposium on Friction Stir Welding, Thousand Oaks, California, USA, 1999.
75- K. Colligan; "Dynamic Material Deformation During Friction Stir Welding of Aluminum", First International Symposium on Friction Stir Welding, Thousand Oaks, California, USA, 1999.
76- L. E. Srensson and L. Karlsson; "Microstructure, Hardness and Fracture in Friction Welded AA6082", First International Symposium on Friction Stir Welding, Thousand Oaks, California, USA, 1999.
77- H. Hori, S. Makita and H. Hino; Friction Stir Welding of Rolling Stock for Subway", First International Symposium on Friction Stir Welding, Thousand Oaks, California, USA, 1999.
78- R. Pedwell, H. Duvies and A. Jefferson; "The Application of Friction Stir Welding to Aircraft Wing Structures", First International Symposium on Friction Stir Welding, Thousand Oaks, California, USA, 1999.
79- C. J. Dawes and W. M. Thomas; "Development of Improved Tool Designs for Friction Stir Welding of Aluminum", First International Symposium on Friction Stir Welding, Thousand Oaks, California, USA, 1999.
80- O. T. Midling and G. Rorvik; "Effect of Tool Shoulder Material on Heat Input During Friction Stir Welding", First International Symposium on Friction Stir Welding, Thousand Oaks, California, USA, 1999.
81- L. Magnusson, Saab AB and L. Kallman; "Mechanical Properties of Friction Stir Welds in Thin Sheet of Aluminium 2024, 6013 and 7475", Second International Symposium on Friction Stir Welding, Gothenburg, Sweden, 2000.
82- G. J. Bendzsak, T. H. North and C. B. Smith; "An Experimentally Validated 3D Model for Friction Stir Welding Second International Symposium on Friction Stir Welding, Gothenburg, Sweden, 2000.
83- T. W. Nelson, B. Hunsaker and D. P. Field; "Local Texture Characterization of Friction Stir Welds in 1100 Aluminum, Friction Stir Welding", First International Symposium on Friction Stir Welding, Thousand Oaks, California, USA, 1999.
84- T. Dickerson, H. R. Shercliff and H. Schmiclt; "A Weld Marker Technique for Flow Visualization Friction Stir Welding", 4th International Symposium on Friction Stir Welding, Utah, USA, May 2003.
85- Y. S. Sato, H. Kokawa, M. Enomoto, S. Jogan and T. Hashimoto; "Distributions of Hardness and Microstructure in Friction Stir Weld of Al Alloy 6063", 3rd

International Symposium on Friction Stir Welding, Port Island, Kobe, Japan, 2001.

86- M. G. Dawes, S. A. Karger and T. L. Dickerson; "Strength and Fracture Toughness of Friction Stir Welds in Aluminum Alloys", 2nd International Symposium on Friction Stir Welding, Gothenburg, Sweden, 2000.

87- M. Strangwood, J. E. Berry, D. P. Cleugh, A. J. Leonard and P. L. Threadgill; "Characterization of Thermo-Mechanical Effects on Microstructureal Development in Friction Stir Welded Age Hardening Aluminum-Based Alloys", First International Symposium on Friction Stir Welding, Thousand Oaks, California, USA, 1999.

88- M. C. Juhas, G. B. Viswanathan and H. L. Fraser; "Microstructural Evolution in Ti Alloy Friction Stir Welds", 2nd International Symposium on Friction Stir Welding, Gothenburg, Sweden, 2000.

89- M. J. Russell and H. R. Shercliff; "Analytical Modelling of Microstructure Development in Friction Stir Welding", First International Symposium on Friction Stir Welding, Thousand Oaks, California, USA, 1999.

90- A. J. Leonord; "Microstructure and Ageing Behaviour of FSWs in Aluminum Alloys 2014A-T651 and 7075-T651", 2nd International Symposium on Friction Stir Welding, Gothenburg, Sweden, 2000.

91- Kh. A. A. Hassan, A. F. Norman and P. B. Prangnell; "The Effect of Welding Conditions on the Microstructure and Mechanical Properties of the Nugget Zone in AA7010 Alloy Friction Stir Welds", 3rd International Symposium on Friction Stir Welding, Port Island, Kobe, Japan, 2001.

92- Ɵ. Frigaard, Ɵ. Grong, J. Hjelen, S. G. Sen-Dahi and O. T. Midling; "Characteristion of the Subgrain Structure in Friction Stir Welded Aluminum Alloys Using the SEM-EBSD Technique", First International Symposium on Friction Stir Welding, Thousand Oaks, California, USA, 1999.

93- G. H. Payganeh, N. B. Mostafa, Y. Dadgar, F. A. Ghasemi and M. S. Boroujeni; International Journal of the Physical Science, Vol.6, No.19, 2011, PP. 4595 – 4601.

94- D. G. Kinchen, Z. Li and G. P. Adams; "Mechanical Properties of Friction Stir Welds in Al-Li 2195-T8", First International Symposium on Friction Stir Welding, Thousand Oaks, California, USA, 1999.

95- T. Dickerson, Q. Shi, H. R. Shercliff; "Heat Flow into Friction Stir Welding Tools", 4th International Symposium on Friction Stir Welding, Utah, May 2003.

96- K. Colligan, I. Ucok, K. Mc-Ternan, P. J. Konkol and J. R. Pickens; "Friction Stir Welding of Thick Section 5083-H131 and 2195-T8P4 Aluminum Plates", 3rd International Symposium on Friction Stir Welding, Port Island, Kobe, Japan, 2001.

97- T. Nishihara and Y. Nagasaki; "Measurement of Tool Temperature During Friction Stir Welding", 4th International Symposium on Friction Stir Welding, Utah, May 2003.
98- A. Von-Strombeck, J. F. Dos-Santos, F. Torster, P. Laureano and M. Kocak; "Friction Toughness Behaviour of Friction Stir Welding Joints on Aluminum Alloys", First International Symposium on Friction Stir Welding, Thousand Oaks, California, USA, 1999.
99- M. Ericsson, R. Sandstrom and J. Hagstrom; "Fatigue of Friction Stir Welded Al Mg Si- Alloy 6082", 2nd International Symposium on Friction Stir Welding, Gothenburg, Sweden, 2000.
100- W. M. Thomas; "Friction Stir Welding of Ferrous Materials; A Feasibility Study", 1st International Symposium on Friction Stir Welding, Thousand Oaks, California, USA, 1999.
101- T. J. Lienert and R. J. Grylls; "Microstructural Evolution in Friction Stir Welds on 6061-T651", 1st International Symposium on Friction Stir Welding, Thousand Oaks, California, USA, 1999.
102- T. Shinoda; "Effect of Tool Angle on Metal Flow Phenomenon in Friction Stir Welds", 3rd International Symposium on Friction Stir Welding, Port Island, Kobe, Japan, 2001.
103- K. Aota, H. Okamura, E. Masakuni and H. Takai; "Heat Inputs and Mechanical Properties Stir Welding", 3rd International Symposium on Friction Stir Welding, Port Island, Kobe, Japan, 2001.
104- M. Hayashi and K. Oyama; "Mechanical Properties of Friction Stir Welded 5083 Alumimum Alloy at Cryogenic Temperatures", Metal Research Centre, Japan.
105- G. E. Dietor; "Mechanical Metallurgy" McGraw-Hill Book Company (UK) Limited, SI Metric Edition, Singapore, 1988.
106- Y.C. Jang, J.K. Hong, J.H. Park, D.W. Kim and Y. Lee; Journal of Materials Processing Technology, Vol. 2 0 1, 2 0 0 8, PP 419–424.
107- D. M. Vgljic, M. P. Rakin, M. M. Perovic and B. L. Medo; "Heat Generation During Plunge Stage in Friction Stir Welding", Faculty of Mechanical Engineering, University of Belgrade, Belgrade, Serbia.
108- V. J. Farron; "Effect of Microstructure and Strain Ageing on Toughness of Nuclear PWR Reactor Weld Metals", School of Metallurgy and Material, University of Birmingham, Birmingham, UK, 2009.
109- M. M. Attallah; "Influence of Friction Stir Welding on the Microstructure Evolution; Mechanical Properties and Supperplastic Behavior of Al-Cu-Li Alloy (AA2095). School of Science & Engineering, American University in Cairo, Cairo, Egypt, June 2003.
110- C. H. Wang; "Introduction to Fracture Mechanics", Defense Science and Technology Organization (DSTO), Melbourne, 1996.

111-W. Mirihanage and N. Munasinghe; "Modification of AA5083 Weld Joint Characteristics", International Symposium of Research Students on Materials Science and Engineering, Chennai, India, 2004.

112-S. S. Yilmaz, B. S. Unlu and I. Aydin; "Environmental Welding: The Friction Stir Welding", 3rd International Symposium on Sustainable Development, Sarajevo, Bosnia, May 2012, PP. 6.

113-S. K. Chionopoulos, CH. I. Sarafoglou, D. I. Pantelis and V. J. Papazoglou; "Effect of Tool Pin and Welding Parameters on Friction Stir Welded (FSW) Marine Aluminium Alloys", 3rd International Conference on Manufacturing Engineering (ICMEN), Chalkidiki, Greece, 2008.

114-A. Mohamed and R. Britton; "Enhancing a Junior Level Materials Lab with SEM Images", University of Manitoba, Canada.

115-N. Bidin, M. Abdullah, M. S. Shaharia, Y. A. Alwafi, D. G. Riban and M. Yasin; Journal Math. Fund. Sci., Vol. 45, No. 1, 2013, PP 53-60.

116-D. Deepak, R. S. Sidhu and V. K. Gupta; "Preparation of 5083 Al-SiC Surface Composite by Friction Stir Processing and Its Mechanical Characterization", International Journal of Mechanical Engineering, Vol.3, Issue 1, January 2013.

117- A. Morri, L. Orazi, F.Tarterini; "Experimental system to determine the start of fracture propagation during impact test", http://www.ysesm.ing.unibo.it/ YSESM2004/Abstracts /Tarterini.pdf

118-H. Serizawa, Z. Wu and H. Murakawa; Joining and Welding Research Institute (JWRI), Osaka, University, Ibaraki, Osaka, Japan, Vol. 30, No.2, 2001, PP. 97.

119- M. P. Manahan, Jr., C. N. McCowan, and M.P. Manahan, Sr.; Journal of ASTM International, 2008.

120-I. Galvao, R.M. Leal, D.M. Rodrigues, A. Loureiro; Journal of Materials Processing Technology, used the SEM 2012, PP. 1 - 23.

Biography of the Author

Abdasalam M. Eramah was born on 1st July 1966 in Zentan - Libya, Libyan nationality. He finished his secondary school from Al-Naser high school in Zentan, Libya in 1984. In 1990, he received his B.Sc. degree from Tripoli University, Faculty of Engineering- department of Mining Engineering. In 2002, Abdasalam received M.Sc. degree in Geomechanics and Tunnelling Engineering from Tripoli University, department Mining Engineering. Also in 2005, he received M.Sc. degree in Drilling and Geoengineering from Faculty of Drilling Oil and Gas, AGH University of Science and Technology, Krakow-Poland. Since October 2009, He has been Ph.D. candidate at the University of Belgrade, Faculty of Mechanical Engineering.

In the period 1991-1994, he worked as laboratory engineering at Nasser University, Tripoli, Libya. From 1994-2002, he worked as an assistant researcher at Tripoli University, department of Mining Engineering. From 2002-2008, he worked as lecturer at Tripoli University, department of Mining Engineering. He taught some subjects such as: mineral processing, Rock Mechanics and mine machinery. He engaged in his Ph.D. research and worked under supervision of Professor Aleksandar Sedmak in the field of material sciences, the influence friction stir welding parameters on fracture of metals.

So far, Abdasalam has published 6 papers in domestic and international scientific journals with impact factor and participated in 3 conferences.

Прилог 1.

Изјава о ауторству

Потписани-а Абдасалам М Ерамах

број уписа Д 44/09

Изјављујем

да је докторска дисертација под насловом

УТИЦАЈ ПАРАМЕТАРА ФРИКЦИОНОГ ЗАВАРИВАЊА НА МЕШАЊЕМ ОТПОРНОСТ НА ЛОМ ЗАВАРЕНОГ СПОЈА ЛЕГУРЕ Al 5083

- да предложена дисертација у целини ни у деловима није била предложена за добијање било које дипломе према студијским програмима других високошколских установа,
- да су резултати коректно наведени и
- да нисам кршио/ла ауторска права и користио интелектуалну својину других лица.

Потпис докторанда

У Београду, 19. 11.2013.

_____

Прилог 2.

Изјава о истоветности штампане и електронске верзије докторског рада

Име и презиме аутора Абдасалам М Ерамах

Број уписа Д 44/09

Студијски програм _____

Наслов рада УТИЦАЈ ПАРАМЕТАРА ФРИКЦИОНОГ ЗАВАРИВАЊА МЕШАЊЕМ НА ОТПОРНОСТ НА ЛОМ ЗАВАРЕНОГ СПОЈА ЛЕГУРЕ Al 5083

Ментор Проф. др Александар Седмак

Потписани Абдасалам М Ерамах

изјављујем да је штампана верзија мог докторског рада истоветна електронској верзији коју сам предао/ла за објављивање на порталу **Дигиталног репозиторијума Универзитета у Београду.**

Дозвољавам да се објаве моји лични подаци везани за добијање академског звања доктора наука, као што су име и презиме, година и место рођења и датум одбране рада.

Ови лични подаци могу се објавити на мрежним страницама дигиталне библиотеке, у електронском каталогу и у публикацијама Универзитета у Београду.

Потпис докторанда

У Београду, 19.11.2013.

_____

Прилог 3.

Изјава о коришћењу

Овлашћујем Универзитетску библиотеку „Светозар Марковић“ да у Дигитални репозиторијум Универзитета у Београду унесе моју докторску дисертацију под насловом:

УТИЦАЈ ПАРАМЕТАРА ФРИКЦИОНОГ ЗАВАРИВАЊА МЕШАЊЕМ НА ОТПОРНОСТ НА ЛОМ ЗАВАРЕНОГ СПОЈА ЛЕГУРЕ Al 5083

која је моје ауторско дело.

Дисертацију са свим прилозима предао/ла сам у електронском формату погодном за трајно архивирање.

Моју докторску дисертацију похрањену у Дигитални репозиторијум Универзитета у Београду могу да користе сви који поштују одредбе садржане у одабраном типу лиценце Креативне заједнице (Creative Commons) за коју сам се одлучио/ла.

1. Ауторство

2. Ауторство - некомерцијално

3. Ауторство – некомерцијално – без прераде

4. Ауторство – некомерцијално – делити под истим условима

5. Ауторство – без прераде

6. Ауторство – делити под истим условима

(Молимо да заокружите само једну од шест понуђених лиценци, кратак опис лиценци дат је на полеђини листа).

Потпис докторанда

У Београду, 19.11 .2013. _____

1. Ауторство - Дозвољавате умножавање, дистрибуцију и јавно саопштавање дела, и прераде, ако се наведе име аутора на начин одређен од стране аутора или даваоца лиценце, чак и у комерцијалне сврхе. Ово је најслободнија од свих лиценци.

2. Ауторство – некомерцијално. Дозвољавате умножавање, дистрибуцију и јавно саопштавање дела, и прераде, ако се наведе име аутора на начин одређен од стране аутора или даваоца лиценце. Ова лиценца не дозвољава комерцијалну употребу дела.

3. Ауторство - некомерцијално – без прераде. Дозвољавате умножавање, дистрибуцију и јавно саопштавање дела, без промена, преобликовања или употребе дела у свом делу, ако се наведе име аутора на начин одређен од стране аутора или даваоца лиценце. Ова лиценца не дозвољава комерцијалну употребу дела. У односу на све остале лиценце, овом лиценцом се ограничава највећи обим права коришћења дела.

4. Ауторство - некомерцијално – делити под истим условима. Дозвољавате умножавање, дистрибуцију и јавно саопштавање дела, и прераде, ако се наведе име аутора на начин одређен од стране аутора или даваоца лиценце и ако се прерада дистрибуира под истом или сличном лиценцом. Ова лиценца не дозвољава комерцијалну употребу дела и прерада.

5. Ауторство – без прераде. Дозвољавате умножавање, дистрибуцију и јавно саопштавање дела, без промена, преобликовања или употребе дела у свом делу, ако се наведе име аутора на начин одређен од стране аутора или даваоца лиценце. Ова лиценца дозвољава комерцијалну употребу дела.

6. Ауторство - делити под истим условима. Дозвољавате умножавање, дистрибуцију и јавно саопштавање дела, и прераде, ако се наведе име аутора на начин одређен од стране аутора или даваоца лиценце и ако се прерада дистрибуира под истом или сличном лиценцом. Ова лиценца дозвољава комерцијалну употребу дела и прерада. Слична је софтверским лиценцама, односно лиценцама отвореног кода.